Experimental Study on Geocell-Reinforced Recycled Asphalt Pavement (RAP) Bases under Static and Cyclic Loading

By

Jitendra Kumar Thakur

B.E., Tribhuvan University, Nepal, 2007

Submitted to the Graduate Degree Program in Civil, Environmental, and Architectural
Engineering and the Graduate Faculty of the University of Kansas School of Engineering
in partial fulfillment of the requirements for the degree of
Master of Science

Committee members

Dr. Jie Han, Chairperson

Dr. Anil Misra

Dr. Robert L. Parsons

Date defended: 01/07/2010

The Thesis Committee for Jitendra Kumar Thakur certifies that this is the approved version of the following thesis:

Experimental Study on Geocell-Reinforced Recycled Asphalt Pavement (RAP) Bases under Static and Cyclic Loading

Dr. Jie Han, Chairperson

Committee members

Dr. Anil Misra

Dr. Robert L. Parsons

Date approved: 01/07/2011

ABSTRACT

Recycled Asphalt Pavement (RAP) is a removed and reprocessed pavement material containing asphalt and aggregates which can be used as a base course material for pavement applications. Geocells are a three-dimensional interconnected honeycomb type of geosynthetics used to reinforce weak soils and base courses of roads and are ideal for soil confinement. The objectives of this study are to evaluate characteristics of milled recycled asphalt pavement (RAP) collected from a city street in Lawrence, Kansas and to investigate the creep and cyclic behavior of geocell-reinforced RAP bases over rigid subgrade under static loading and over weak subgrade under cyclic loading through laboratory testing respectively.

The compaction and CBR curves were obtained for the RAP. The Mohr-Coulomb failure envelopes for RAP and RAP/geocell interface were obtained by direct shear tests. The asphalt binder and the aggregates were extracted from RAP. The extracted aggregates were tested for their properties including gradation, specific gravity, and fine aggregate angularity (FAA). The viscosity of the extracted asphalt binder was also determined. The results indicated that the asphalt content obtained by the ignition method was slightly higher than that by the centrifuge method. Gradation results indicated that the compaction did not change the gradation of the RAP.

Fourteen medium-scale laboratory static plate loading tests were conducted on RAP samples under two vertical stresses at different confining conditions to investigate the creep deformation behavior of geocell-reinforced RAP bases. The creep axial strains at different time were estimated for RAP at different confining conditions and vertical stresses. The results indicated that the geocell confinement significantly reduced the initial deformation and the rate of creep of the RAP bases. Six medium-scale plate loading tests at different confining conditions and one unconfined compression test were conducted on RAP samples by applying static loads in increment to understand the pressure-displacement response and evaluate the bearing capacity and stiffness of the unreinforced and geocell-reinforced RAP bases. The results indicated that geocell significantly increased the bearing capacity and stiffness of RAP bases.

Nine large-scale laboratory cyclic plate loading tests were conducted on RAP base sections with three different base course thicknesses. The novel polymeric alloy (NPA) geocells were used to reinforce the RAP bases. The behavior of unpaved RAP bases, such as permanent deformation, percentage of elastic deformation, stress distribution, and strains in the geocell walls was investigated. The results indicated that the geocell effectively reduced permanent deformation, and vertical stress at the interface of base and subgrade and increased the stress distribution angle and increased percentage of elastic deformation. The strain measurements demonstrated that the geocell-reinforced RAP bases behaved as a slab.

DEDICATION

The author dedicates this work to his parents,
Mr. Ram Swarth Thakur and Mrs. Kamalesh Devi

ACKNOWLEDGEMENT

First of all, I would like to express my heartfelt gratitude to my advisor, Prof. Jie Han, for his excellent guidance, caring, infectious enthusiasm, unlimited zeal, and providing me with an excellent environment for doing research. Besides advising my study, he always looked for every opportunity for me to develop useful skills for my future careers. His instructions and illustrations to help/support individuals with his best capacity are highly impressive. I also wish to thank Prof. Anil Misra and Prof. Robert L. Parsons for their valuable advices and also for participating as members of my graduate advisory committee. I would never have been able to finish my thesis without the guidance of my committee members.

The geocell material used in this study was provided by PRS Mediterranean, Inc. in Israel. The financial support by the Mid-American Transportation Center and PRS Mediterranean, Inc. are greatly appreciated. I am also grateful to R.D. Johnson Excavating, Co., Lawrence, Kansas for providing the RAP material for this research.

I am indebted to the members of KUGS (Kansas University Geotechnical Society) especially Dr. Sanat Pokharel (Post-doc research associate), Subhash Chandra Thakur, Dr. Xiaoming Yang, Kahle Loveless, Aj Rahman, Dr. Matthew Pierson, Dr. Anil Bhandari, Milad Jowkar, Cheng Lin, Deep Khatri, and Bhagaban Acharya for their great cooperation, advices, and help during the entire process of this study.

It is my pleasure to thank the laboratory supervisor, Mr. Howard J. Weaver and the laboratory Technician, Mr. Matthew Maksimowicz for their help.

The gratitude is extended to my elder brother (Ajay Thakur), elder sisters (Anju, Indu, Rinku), brother in laws (Ashok, Santosh and Arun), and sister in law (Sadhna Thakur). Last but not least, my very special thanks go to my parents, Mr. Ram Swarth Thakur and Mrs. Kamalesh Devi, whom I owe everything as I am today. They always support me and encourage me with their best wishes.

TABLE OF CONTENTS

LIST OF TABLES

LIST OF FIGURES

CHAPTER 1

INTRODUCTION

1.1 Overview

Recycled Asphalt Pavement (RAP) is a removed and reprocessed pavement material containing asphalt binder and aggregates. The use of Recycled Asphalt Pavement (RAP) has been in practice since 1930s and is necessary to reduce the cost of construction materials; to reduce waste of petroleum based products; and to conserve natural resources by requiring less virgin aggregate and asphalt in road construction projects. The U.S. Federal Highway Administration estimated that 100.1 million tons of asphalt pavements are milled off each year during resurfacing and widening projects (Missouri Asphalt Pavement Association, 2010). Of that, 80.3 million tons are reclaimed and reused for roadbeds, shoulders, and embankments (Missouri Asphalt Pavement Association, 2010). More than 73 million tons of RAPs are processed each year in the United States with much of them re-used in pavement construction (Kelly, 1998). According to the User Guidelines for Byproducts and Secondary Use Materials in Pavement Construction (FHWA-RD-97-148, 2008), RAP can be used as a granular base material in paved and unpaved roadways, parking areas, bicycle paths, gravel road rehabilitation, shoulders, residential driveways, trench backfill, engineered fill, and culvert backfill. This study considered RAP used as a base course material in unpaved roads.

Geosynthetics have been widely used as construction materials for soil reinforcement in civil engineering projects such as slopes, retaining walls, landfills, foundations, embankments, earth retaining structures, reservoirs, canals, dams, bank and coastal protection, airfields, railroads, subgrade improvement, and reinforcement to base courses of road sections etc. since the 1970s. Today, there are many types of geosynthetic products (e.g., geogrid, geotextile, geocell, geomembrane, geonet, geopipe, geofoam, and geocomposite etc.) available in the market. Each product is designed for solving a specific type of civil engineering problems. Geocells are a three-dimensional interconnected honeycomb type of geosynthetics used to confine soil. Geocell was used in this study to confine the RAP bases of unpaved road sections. The pictures of RAP materials and geocell are shown in Figures 1.1.1 and 1.1.2, respectively.

Figure 1.1.1 Recycled asphalt pavement (RAP) material

Figure 1.1.2 Bundled NPA geocell easy for transportation

1.2 Problem Statement

Currently, great emphasis is placed on sustainable construction and infrastructure with green technology because the demand for sustainable and environmental friendly roads is increasing day by day. More technologies for sustainable roadway construction are needed. One way to construct environmentally sound roads is through the use of recycled asphalt pavement materials. Recycled Asphalt Pavement (RAP) is a removed and reprocessed pavement material containing asphalt binder and aggregates. Historically, RAP has been used with new bituminous materials by either a hot-mix or cold-mix recycling process. However, a large quantity of waste asphalt remains unused. Recent investigations have shown that the waste problems can be reduced by combining RAPs with base and subbase aggregate materials using the cold in-place recycling technique. Using RAP as a base course material would preserve non-renewable aggregate as well as reduce the amount of space needed to store millions of tons of RAP created each year. RAP has been used as granular bases by at least 13 state agencies in the United States in the past decade. Peter Stephanos, the director of the FHWA Office of Pavement Technology stated that recently, most State DOTs are seriously considering the economic and environmental benefits of using RAP in greater proportions and facing challenges to maintain high-quality pavement infrastructures (Copeland et al., 2010).

However, limited research has been done to quantify its structural capacity with fundamental engineering properties. Rutting has been observed in some projects a few years after construction (Mamlouk and Ayoub, 1983). A typical unreinforced road and rutting problems in unpaved roads are shown in Figures 1.2.1 and 1.2.2, respectively.

Figure 1.2.1 Picture of unpaved road

(Courtesy of Dr. Han)

Figure 1.2.2 Rutting in unpaved road

(Courtesy of Dr. Han)

It is the author's belief that RAP base courses may have excessive deformation under traffic loading due to the existence of asphalt in RAP. It is believed geocell confinement can reduce the rutting potential and improve the performance of RAP bases. Hence geocell was used in this study to confine the RAP bases to achieve improved performance by reducing creep deformation and increasing percentage of elastic deformation. The typical sections of unreinforced and geocell-reinforced RAP bases are shown in Figures 1.2.3 and 1.2.4, respectively.

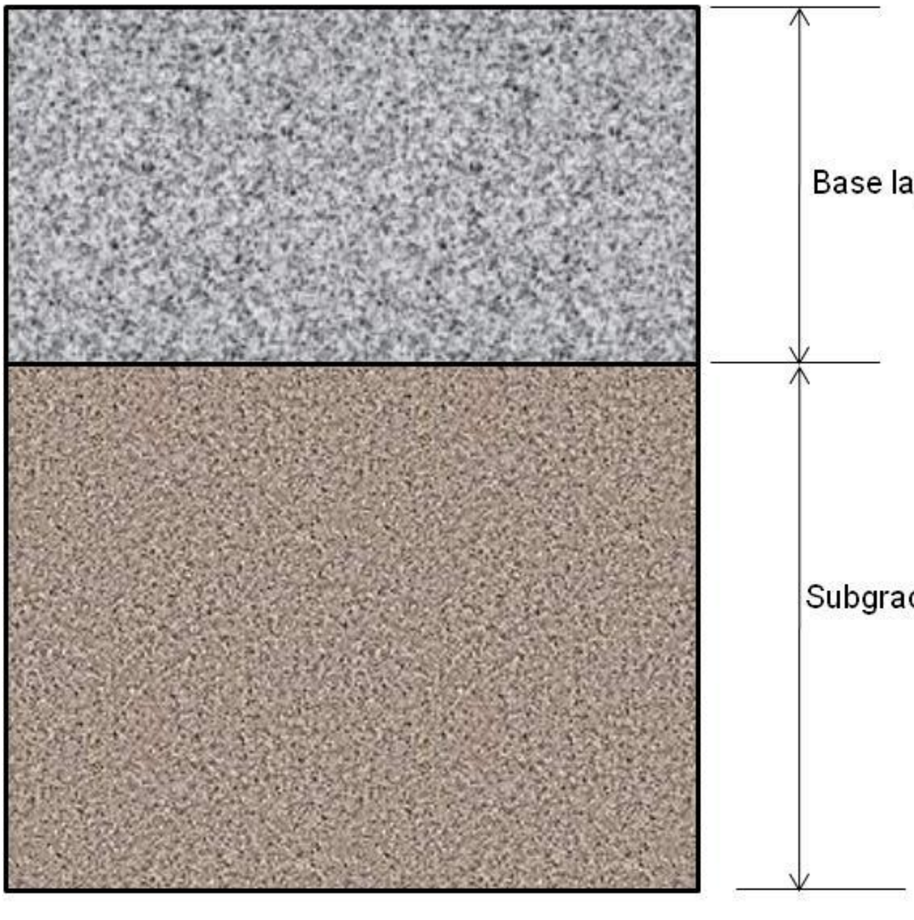

Figure 1.2.3 Typical section of an unreinforced unpaved road

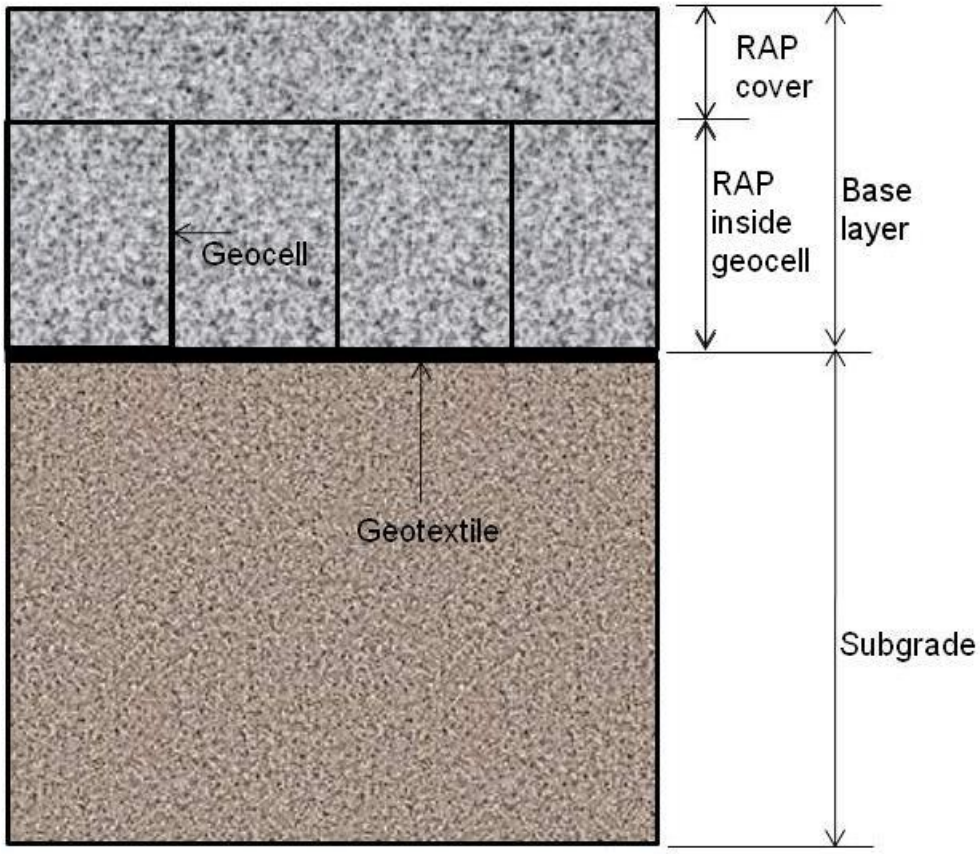

Figure 1.2.4 Typical section of a geocell-reinforced unpaved road

1.3 Objectives

The objectives of this study are to evaluate characteristics of recycled asphalt pavement (RAP) collected from a city street in Lawrence, Kansas and to investigate the creep and cyclic behavior of geocell-reinforced bases over rigid subgrade under static loading and over weak subgrade under cyclic loading.

The characteristics of RAP included compaction curve, CBR curve, cohesion and friction angle, asphalt binder content, viscosity of asphalt binder, gradation, specific gravity, and angularity of aggregates extracted from RAP. The creep behavior included axial deformations and rates of axial deformations of reinforced and unreinforced RAP bases under different confining conditions at two different static vertical stresses for about 7 to 10 days. The cyclic behavior included permanent deformations, elastic deformations, vertical stresses at the interface between base and subgrade, and maximum strains in geocell walls of reinforced and unreinforced RAP bases under cyclic loading.

1.4 Research Methodology

The research was executed using the following methodologies: (1) an extensive literature review on recycled asphalt pavement and geocell reinforced unpaved roads; (2) evaluation of characteristics of recycled asphalt pavement; (3) creep study by performing medium-scale laboratory static plate load tests; and (4) cyclic behavior of RAP bases by performing large-scale laboratory cyclic plate load tests.

1.5 Organization

This thesis consists of six chapters.

Chapter 1 Introduction: This chapter provides introduction which includes overview, problem statement, objectives, and research methodology.

Chapter 2 Literature review: This chapter includes review of past studies relevant to this research. These studies were focused on the recycled asphalt pavement (RAP) and geocell.

Chapter 3 Laboratory evaluation of characteristics of recycled asphalt pavement (RAP): This chapter describes the test equipments and procedures and analyzes the test results obtained from different laboratory tests.

Chapter 4 Creep tests of geocell-reinforced bases: This chapter describes the test equipments and procedures, and analyzes the results obtained from medium-scale laboratory plate load tests under static loading.

Chapter 5 Large-scale cyclic plate load tests: This chapter describes the test equipments and procedures, and analyzes the results obtained from large-scale laboratory plate load tests under cyclic loading.

Chapter 6 Conclusions and recommendations: This chapter presents the conclusions from this study and the recommendations for future study.

CHAPTER 2

LITERATURE REVIEW

2.1 Introduction

This chapter provides a literature review of recycled asphalt pavement (RAP), uses of RAP, properties of RAP, geocell and its function, past studies for behavior of recycled asphalt pavement bases, and geocell-reinforced roads.

2.2 Background of Recycled Asphalt Pavement (RAP)

Recycled Asphalt Pavement is a removed and reprocessed pavement material containing asphalt binder and aggregates produced when asphalt pavements are removed for resurfacing or reconstruction. It is obtained either by milling or a full depth recovery method. Milling involves the mechanical removal of up to 50 mm thick of pavement in a single pass whereas a pneumatic pavement breaker or rhino horn on a bulldozer is used for full-depth removal of pavement (Viyanant et al., 2007). RAP is stockpiled at HMA plants. According to the National Asphalt Pavement Association (NAPA), more than 90% of U.S. roads and highways are paved with hot-mix asphalt (HMA) (Copeland et al., 2010). The federal, state, and local transportation agencies are facing an increasing demand of raw materials needed for new and rehabilitation road projects. HMA producers and different transportation agencies are suggesting RAP as an alternative to virgin aggregate and asphalt to respond the shrinking supply of raw materials and rising costs of aggregates and binders (Copeland et al., 2010). The Federal Highway Administration (FHWA) supports and promotes the use of recycled asphalt pavement materials in pavement construction. RAP can be recycled into virgin asphalt mixtures by three most common methods: (i) hot mix recycling at plant, (ii) hot in-place recycling, and (iii) cold in-place recycling.

2.2.1 Advantages

The following are the advantages of using RAP (From http://www.fhwa.dot.gov/pavement/recycling/rap/index.cfm, retrieved December 13, 2010):

(i) It preserves the natural environment.

(ii) It reduces the amount waste disposal.

(iii) It reduces demand for aggregate and bituminous binder.

(iv) It reduces energy and transportation costs in getting construction materials (aggregate and asphalt binder).

(v) It provides cost effective material for highway construction.

(vi) It demonstrates reasonable life cycle cost and good engineering performance.

2.2.2 Disadvantages

There are a few minor drawbacks of using RAP (Peploe, 2006):

(i) Potential for fuming in the production of recycled hot mix (RHM): This issue can be solved by the use of appropriate plants and procedure in the production of RHM.

(ii) Leaching of carcinogens from the bituminous components of millings while the RAP material is stockpiled or in service: It was reported by the New Jersey Department of Environmental Protection Asphalt Millings Guidance Document (NJDEP, 2001) that asphalt millings could have very high concentration of toxic compound named polycyclic aromatic hydrocarbons (PAHs). When RAP is used in an unsealed road application, the PAHs can migrate from the road pavement and contaminate adjacent soils and water courses (peploe, 2006). However, Vercoe (personal communication with peploe, 2006) suggested that the toxic compounds from milling are rarely released, unless the binder is comprised of coal tar. Hence leaching is not a big problem in today's recycling process as coal tar is not generally used as binder these days. Townsend and Brantley (1998) also investigated the leaching behavior of RAP through laboratory testing and concluded that RAP poses minimal risk to groundwater as a result of pollutant leaching under land disposal or beneficial reuse. The pollutants investigated were volatile organic compounds (VOCs), polycyclic aromatic hydrocarbons (PAHs), and some heavy metals (Ba, Ca, Cr, Cu, Pb, Ni, and Zn) (Cosentino et al., 2003).

2.2.3 Applications

According to the User Guidelines for Byproducts and Secondary Use Materials in Pavement Construction (FHWA-RD-97-148, 2008), RAP can be used as a granular base material in paved and unpaved roadways, parking areas, bicycle paths, gravel road rehabilitation, shoulders, residential driveways, trench backfill, engineered fill, and culvert backfill.

According to FHWA, RAP can be used as granular base or subase aggregate, embankment or fill material, or used with hot-mix asphalt, cold-mix asphalt, and cold in-place asphalt.

2.2.4 Progress in production and uses

RAPs are produced by removal of asphalt pavements during resurfacing and rehabilitations of roads. More than 73 million tons of RAPs are processed each year in the United States with much of them re-used in pavement construction (Kelly, 1998). According to NAPA 2007, about 100 million tons of RAP are used by different transportation agencies of the United States each year, compared to 72 million tons used annually in the early 1990s (Copeland et al., 2010). The Federal Highway Administration estimated that 100.1 million tons of asphalt pavements are milled off each year during resurfacing and widening projects and about 80.3 million tons are reused in the construction of roads, roadbeds, shoulders, and embankments (Missouri Asphalt Pavement Association, 2010).

The transportation agencies separate RAP materials into finer and coarse particles by processing it at asphalt concrete production plants for use in different construction projects. The processing and stockpiling of RAP at an asphalt concrete production plant is presented in Figure 2.2.1.

Figure 2.2.1 Processing and stockpiling of RAP (http://www.fhwa.dot.gov/PAVEMENT/recycling/rap/index.cfm)

A survey conducted by the North Carolina Department of Transportation (NCDOT) on behalf of FHWA and the American Association of State Highway and Transportation Officials (AASHTO) in 2007 and 2009 showed that use of RAP are increasing across the nation. The survey results are presented in the maps in Figures 2.2.2 a, 2.2.2 b, and 2.2.2 c (Copeland et al, 2010).

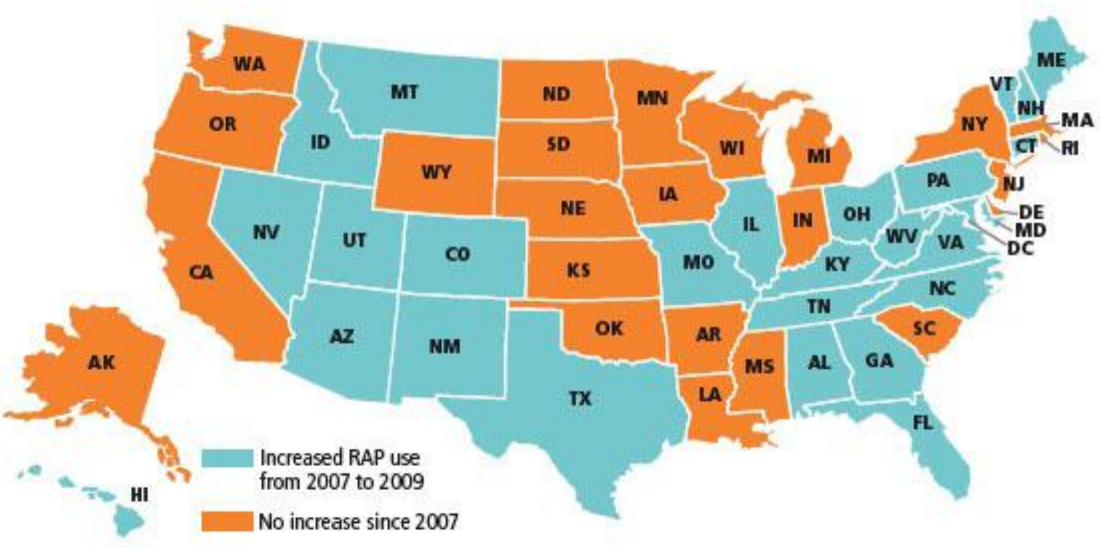

Fig 2.2.2a Map showing states that have increased RAP use since 2007 (From Copeland et al., 2010)

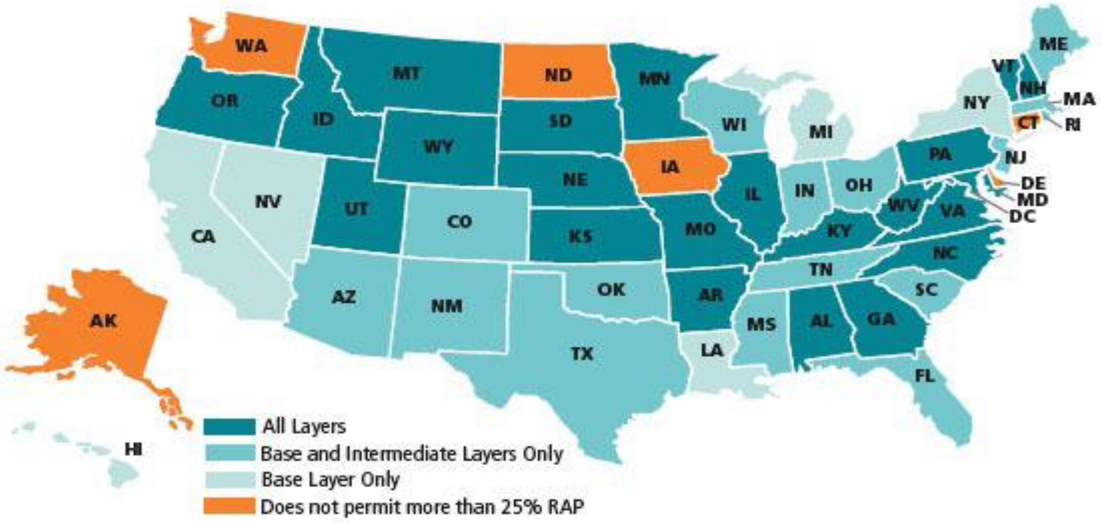

Fig 2.2.2b Map showing states that permit more than 25 % RAP in 2009 (From Copeland et al., 2010)

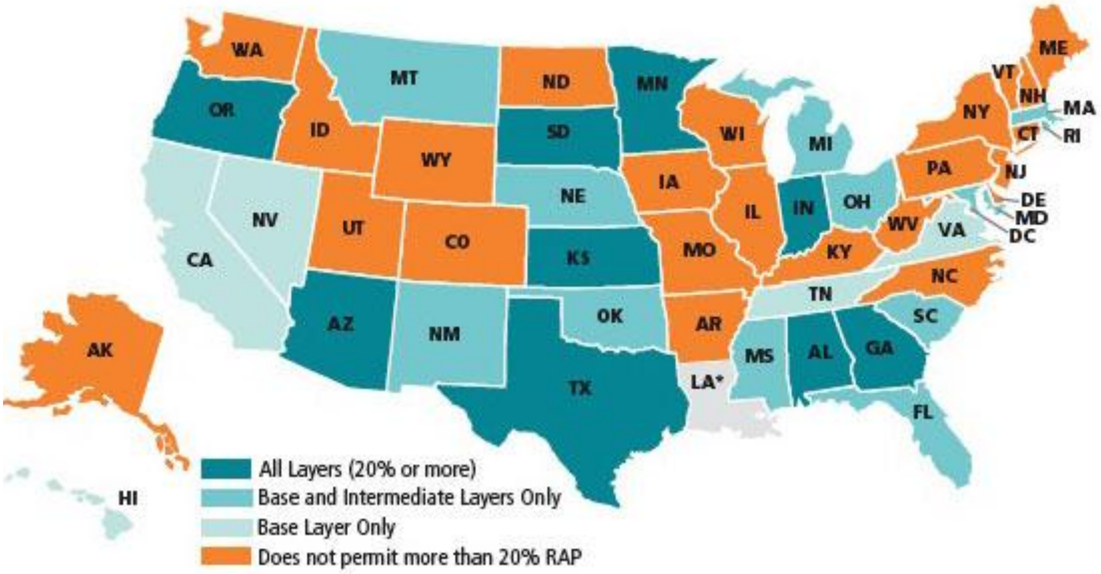

Source: FHWA
* Lousiana did not respond to this question

Fig 2.2.2c Map showing states that use more than 20% RAP in 2009. (From Copeland et al., 2010)

Several states have used high percentage of RAP as listed in Table 2.2.1

Table 2.2.1 Locations, % RAP used, and dates of construction

(From http://www.fhwa.dot.gov/PAVEMENT/recycling/rap/index.cfm)

Location	% RAP	Dates of Construction
North Carolina	40	Sep-07
South Carolina	30 and 50	Oct-07
Wisconsin	25	Nov-07
Florida	45	Dec-07
Kansas	30 to 40	May-08
Delaware	35	Summer 2008
Minnesota	30	2008
Illinois	10 to 50 allowed	2008

Based on extensive literature review by McGarrah (2007), practices of different DOTs regarding the use of base course materials are presented in Table 2.2.2. McGarrah (2007) contacted State material engineers to generate this table. State material engineers from California, New Mexico, Rhode Island, South Dakota, and Texas were not contacted due to lack of contact information or the states were unresponsive. Information for these states was obtained through their respective standard specifications. New Jersey and Colorado DOTs used 100% RAP as base course materials in 2007. However, these two material departments modified these values, which are presented in Table 2.2.2. For Minnesota and Utah DOTs, the maximum percentages given in the table are the maximum asphalt contents allowed in the RAP blend.

Table 2.2.2 Practices of DOTs regarding use of RAP as base material (From McGarrah, 2007)

State	RAP allowed	Maximum % by weight	Processed before use	Type of quality assurance (QA) testing required
Florida	No	N/A	N/A	N/A
Illinois	No	N/A	N/A	N/A
Montana	Yes	50-60	No	Corrected nuclear gauge
New Jersey	Yes	50	Yes-Gradation	Corrected nuclear gauge + sample
Minnesota	Yes	3	Yes-Gradation	Dynamic cone penetrometer
Colorado	Yes	50	Yes-Maximum Aggregate Size	Roller compaction Strip
Utah	Yes	2	Yes-Gradation	Nuclear gauge or breakdown curve
Texas	Yes	20	Unknown	Various (including nuclear gauge)
California	Yes	50	Unknown	No special testing procedure listed
New Mexico	Yes	Unknown	Unknown	Corrected nuclear gauge
Rhode Island	Yes	Unknown	Yes-Gradation	Unknown
South Dakota	No	N/A	N/A	N/A

The publication FHWA-HRT-10-001 reported the top 10 requirements for greater use of RAP (Copeland et al., 2010):

(i) Performance tests for evaluating RAP mixtures

(ii) Best practices of mix design and constructions.

(iii) Ability to characterize RAP without harmful solvents.

(iv) Determination of necessary changes in binder performance grade.

(v) Determination of amount of RAP mixed with virgin HMA.

(vi) Field performance data on high-RAP mixtures.

(vii) Ability to replicate plant heating in labs for virgin and RAP binder blending

(viii) Assistance to States RAP specifications and current practices

(ix) Improved understanding of variability of RAP.

(x) Implementation of best practices for processing RAP, including evaluating the need for fractionation.

2.3 Properties of RAP

The past studies showed there is lack of understanding of variability of RAP. Hence the properties of RAPs obtained from different sites need to be determined before their use in the real construction works. The User Guidelines for Waste and Byproduct Materials in Pavement Construction (FHWA-RD-97-148, 2008) suggested that the following physical, chemical and mechanical properties of RAP need to be determined prior to its use in real construction projects (http://www.fhwa.dot.gov/publications/research/infrastructure/ structures/97148/rap131.cfm):

2.3.1 Physical properties

(i) Gradation: The particle size distribution of milled or crushed RAP depends on the type of equipment used to generate RAP, the type of aggregate used in the pavement etc. Milling, crushing, and screening processes control the gradation of RAP. Degradation of RAP is caused more by milling than crushing. Gradation of milled

RAP is generally finer than crushed RAP whose gradation is finer than that of virgin aggregates crushed with the same type of crushing equipment. Typical range of particle size distribution for RAP is shown in Table 2.3.1.

Table 2.3.1 Typical range of particle size distribution for RAP (From http://www.fhwa.dot.gov/publications/research/infrastructure/structures/97148/rap131.cfm)

Sieve size (mm)	Percent finer after processing or milling
37.5	100
25	95-100
19	84-100
12.5	70-100
9.5	58-95
75	38-75
2.36	25-60
1.18	17-40
0.60	10-35
0.30	5-25
0.15	3-20
0.075	2-15

(ii) Unit weight: The unit weight of RAP depends on the type of aggregate in RAP and the moisture content of RAP in the stockpiles. The unit weight of RAP has been found to be 1.94 to 2.30 g/cm^3, which is slightly lower than that of natural aggregate.

(iii) Specific gravity: Specific gravity is used in calculating void content of aggregate and also used in volume-weight conversion.

(iv) Aggregate angularity: Aggregate angularity is the measure of uncompacted void content of aggregates. Uncompacted void content indicates the stability of the base course aggregate.

(v) Moisture content: Limited information available regarding moisture content of RAP stockpile shows that moisture content of RAP will increase during storage. Average moisture content of stored crushed RAP has been found up to 5% which further increases to a value as high as 7 to 8% during a rainy season.

(vi) Asphalt content: The asphalt recovered from the RAP is harder than virgin asphalt due to exposure of pavement to air during use and weathering. The asphalt content has been found in the range of 3 to 7% by weight.

(vii) Asphalt penetration: Asphalt penetration value is used as a measure of consistency. Higher values of asphalt penetration indicate softer consistency. Penetration values of asphalt extracted from RAP at 25°C range from 10 to 80.

(viii) Asphalt viscosity: Asphalt is a viscous material. Lower viscosity of asphalt indicates higher flowability and deformability and vice versa. Absolute viscosity of asphalt binder extracted from RAP is expected in the range of 4,000 to 25,000 poises at 60°C.

(ix) Permeability: Permeability of RAP is considered similar to that its constituent aggregate. Consentino et al. (2003) conducted falling head permeability tests on RAP and obtained average permeability of RAP of 2×10^{-4} cm/sec.

(x) Drainage characteristics: RAP is considered nonplastic, free draining, and not frost susceptible.

2.3.2 Chemical properties

RAP consists of about 93 to 97% aggregates and 3 to 7% asphalt. Hence, the overall composition of RAP is similar to that of constituent aggregate as aggregate is its major component. Asphalt consists of high molecular weight aliphatic hydrocarbons as principal constituent and other materials such as sulfur, nitrogen, and polycyclic hydrocarbons of very low chemical reactivity as minor constituents. Asphalt is composed of asphaltenes and maltenes (resins and oils). Asphaltenes are more viscous than maltenes and play a major role in determining asphalt viscosity. The oils are reconverted to resins and resins to asphaltenes by the oxidation of aged asphalt resulting in age hardening and higher viscosity binder.

2.3.3 Mechanical properties

The mechanical properties of RAP depend on the original asphalt pavement type, the methods used to recover RAP, and the degree of processing necessary to prepare the RAP for a particular application. Following are the major mechanical properties of RAP:

(i) Compacted unit weight: Senior et al. (1994) reported the maximum dry density of RAP in the range of 1.6 to 2.0 g/cm^3 which is somewhat lower than that of soil or rock. RAP containing more fine particles has higher compacted density.

(ii) California bearing ratio (CBR): Bearing strength of RAP material is determined based on a CBR value of RAP. Hanks and Magni (1989) reported that CBR values of 100% RAP were in the range of 20 to 25 % while those of 40% RAP mixed with 60% natural aggregate after strengthening for 1 week were 150% or higher.

(iii) Shear strength: Shear strength is a function of normal stress, friction angle, and cohesion of particular material. Doig (2000), Bennert et al. (2000) and Garg and Thompson (1996) reported friction angles of 44°, 44°, and 45° and cohesion of 2.3 psi (15.9 kPa), 2.3 psi (15.9 kPa), and 1.9 psi (13.1 kPa) for three different RAPs, respectively (Cosentino et al., 2003).

(iv) Consolidation characteristics: The consolidation characteristics of RAP-soil mix is expected to be in the range of granular soil depending on the gradation, moisture content, and amount of soil added to the RAP. The compressibility of coarsely graded RAP, or RAP-aggregate mix should be neglected for all practical purposes.

2.4 Previous Experimental Studies on RAP

2.4.1 Falling and constant head permeability tests

Bennert and Maher (2005) presented the permeability test results of RAP, RAP-dense graded aggregate base course (DGABC) blend, and RAP-recycled concrete aggregate (RCA) blend based on the falling and constant head permeability tests conducted by the New Jersey Department of Transportation (NJDOT) in Table 2.4.1.

Table 2.4.1 Permeability of different types of RAP blends
(Modified from Bennert and Maher, 2005)

Material type	Permeability test type	
	Constant head (cm/day)	Falling head (cm/day)
100% RAP	515.1	423.7
75% RAP +25% DGABC	51.8	64.0
50% RAP + 50% DGABC	3465.6	1188.7
25% RAP + 75% DGABC	3700.3	847.3
100% RCA	0	9.1
75% RCA +25% RAP	30.48	36.6
50% RCA +50% RAP	164.6	121.9
25% RCA +75% RAP	21.3	24.4

The data shows that the permeability values measured by constant head permeability tests exceed 3048 cm/day, which deviate from the values of permeability obtained from falling head tests. This difference may be due to the falling head not being able to provide laminar flow through the material.

2.4.2 California Bearing Ratio (CBR) test

Bennert and Maher (2005) presented the CBR results of RAP, RAP-DGABC blend, and RAP-RCA blend based on the tests conducted by the New Jersey Department of Transportation (NJDOT) in Table 2.4.2. The CBR curves were corrected for concavity following the AASHTO T 193 method.

Table 2.4.2 California bearing ratio of different types of RAP blends (From Bennert and Maher, 2005)

Material type	CBR value (%)	
	0.1’’ (2.5 mm) penetration	0.2” (5.0 mm) penetration
100% RAP	18	20
75% RAP +25% DGABC	37	41
75% RAP +25% RCA	29	37
50% RAP+ 50% DGABC	83	94
50% RAP + 50% RCA	68	87
25% RAP +75% DGABC	87	96
25% RAP + 75% RCA	106	137
100% DGABC	182	195
100% RCA	169	205

2.4.3 Triaxial shear strength test

Triaxial shear strength of the 100% RAP was evaluated by NJDOT using the triaxial tests under static loading conditions at confining pressures of 34.5, 69, and 103.4 kPa. Mohr circle diagrams were constructed based on maximum deviatoric stresses from each confining pressure to determine the friction angle (φ) and the cohesion (c). Shear strength of the RAP was determined by using Equation 2.4.1:

$$\tau = c + \sigma_n \tan\varphi \qquad (2.4.1)$$

where τ = shear strength, c=cohesion, and φ = friction angle.

Bennert and Maher (2005) reported the friction angle and cohesion of the RAP as 44.5° and 17.2 kPa respectively based on the NJDOT experiment.

2.4.4 Resilient modulus test

Resilient modulus test is used to characterize base, subbase and subgrade materials for the design of pavement systems. There could be different resilient modulus values for a single material at different stress conditions. The NJDOT conducted repeated load triaxial tests on different RAP blends and resilient moduli (M_R) were evaluated under the following pavement stress scenario:

HMA layer: thickness = 12.7 cm, E = 3,102,640 kPa
Base course: thickness = 30 cm, M_R =206,843 kPa
Subgrade: E = 68,947 kPa

Bennert and Maher (2005) presented the resilient moduli of the RAP blended samples in Table 2.4.3 based on NJDOT experiments and concluded that addition of RAP increased the resilient modulus properties of DGABC.

Table 2.4.3 Resilient moduli of different types of RAP blends

(Modified from Bennert and Maher, 2005)

Sample type	Resilient modulus (M_R), kPa
100 % RAP	267,089
75% RAP + 25% DGABC	208,987
50% RAP + 50% DGABC	225,727
25% RAP + 75% DGABC	193,239
0% RAP (100% DGABC)	138,185

2.4.5 Permanent deformation test

Thompson and Smith (1990) reported permanent deformation as a key factor for pavement failure. The NJDOT conducted permanent deformation tests on RAP blended samples using an MTS closed loop hydraulic testing equipment by applying a 310 kPa haversine stress waveform under 103 kPa confining pressure. All samples were loaded to 100,000 cycles. Bennert and Maher (2005) presented the permanent deformation results of RAP blended samples as shown in Figure 2.4.1.

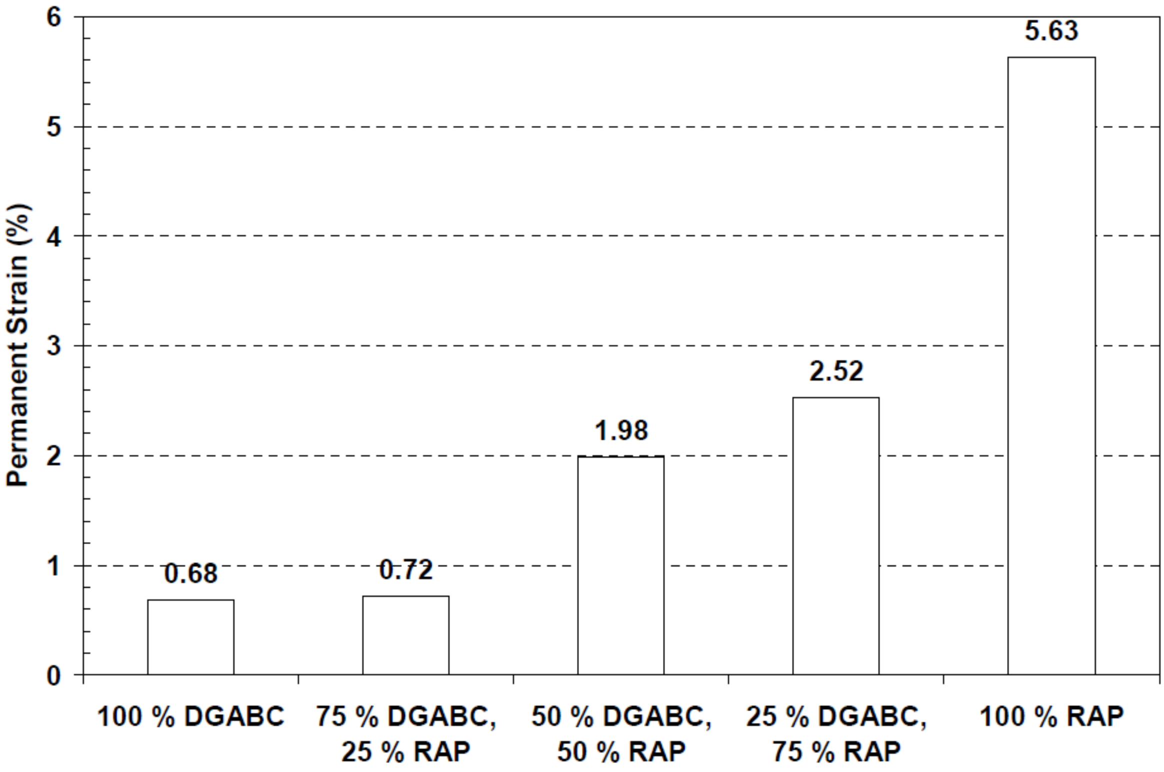

Figure 2.4.1 Permanent deformation results for RAP blended samples (From Thompson and Smith, 1990)

2.4.6 Triaxial compression test

Cosentino et al. (2003) conducted triaxial compression tests to determine strengths of RAP and RAP-soil mixtures. Stress-strain characteristics of RAP and RAP-soil mixtures at different confining stresses were developed as shown in Figure 2.4.2a and 2.4.2b. The fine sand used for mixing with RAP was processed from muck obtained from a spoil storage/dewatering area located at the intersection of US1 and Conlan Blvd. in Melbourne, Florida.

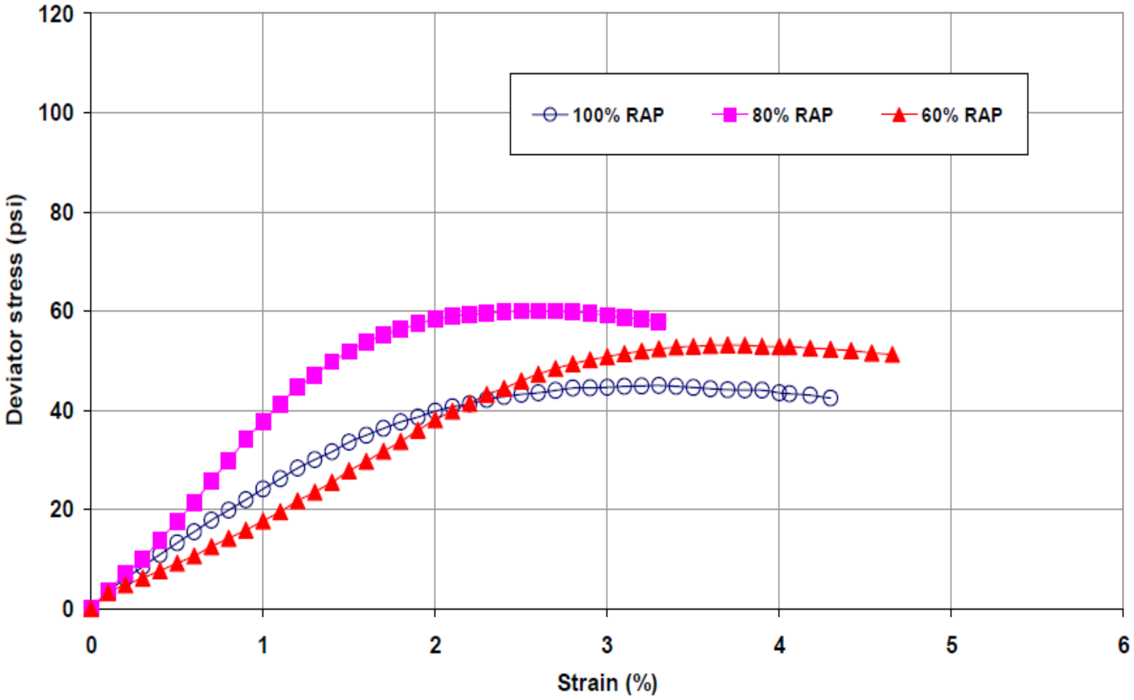

Figure 2.4.2a Stress-strain characteristics of RAP blends at effective confining pressure of 5 psi (From Cosentino et al., 2003)

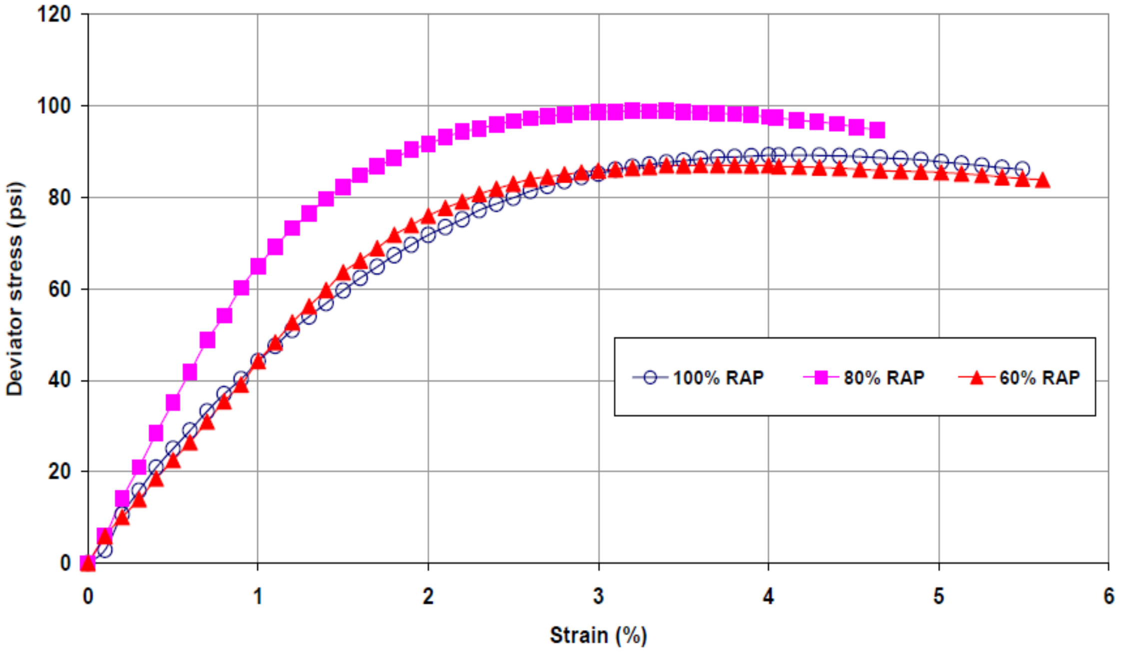

Figure 2.4.2b Stress-strain characteristics of RAP blends at effective confining pressure of 15 psi (From Cosentino et al., 2003)

Cosentino et al. (2003) presented the following properties of RAP-soil mixtures based on the stress-strain characteristics in Table 2.4.4.

Table 2.4.4 Properties of RAP-soil mixture obtained from triaxial compression tests (Cosentino et al., 2003)

Properties	100% RAP		80% RAP		60% RAP	
	σ_3 = 5 psi	σ_3 = 15 psi	σ_3 = 5 psi	σ_3 = 15 psi	σ_3 = 5 psi	σ_3 = 15 psi
σ_1 at failure (psi)	50	104.3	65	113.9	58.2	102.1
$E_{initial}$ (psi)	2357	4400	3780	6957	1470	4245
E_{secant} (psi)	2400	4450	3780	6957	1810	4420
Friction angle (°)	44		41		39	
Cohesion (psi)	4.9		9.2		8.7	

where σ_1 = deviator stress and σ_3 = confining pressure

2.4.7 Creep behavior

RAP is characterized as a time, temperature, and stress-dependent material. According to Bartenov and Zuyev (1969), static fatigue and dynamic fatigue are two interrelated thermally activated processes for a viscoelastic material like RAP. The material subjected to static fatigue is regarded as one subjected to creep. The creep tests showed that the creep of RAP is sensitive to mixture variables including asphalt grade, binder content, aggregate type, air void content, testing temperature, and testing stress (Little et al., 1993). Cosentino et al. (2003) conducted creep tests on compacted RAP, RAP-soil mix, and soil samples under a fully confined condition at different vertical static stresses using the Brainard Kilman Terraload Consolidation Load Frame and confirmed that RAP creeps under static loading. The creep deformation behavior from Cosentino et al. (2003) is shown in Figure 2.4.3. In this figure, RAP100_33.5psi stands for the 100% RAP sample tested under 33.5 psi applied vertical pressure, RAP80_33.5psi stands for RAP-soil (80%-20%) mix sample tested under 33.5 psi applied vertical pressure, and A3_33.5psi stands for 100% A3 soil sample tested under 33.5 psi vertical stress. A3 refers to a fine sand-trace of organics that was processed from muck obtained from a local dredging project in Florida.

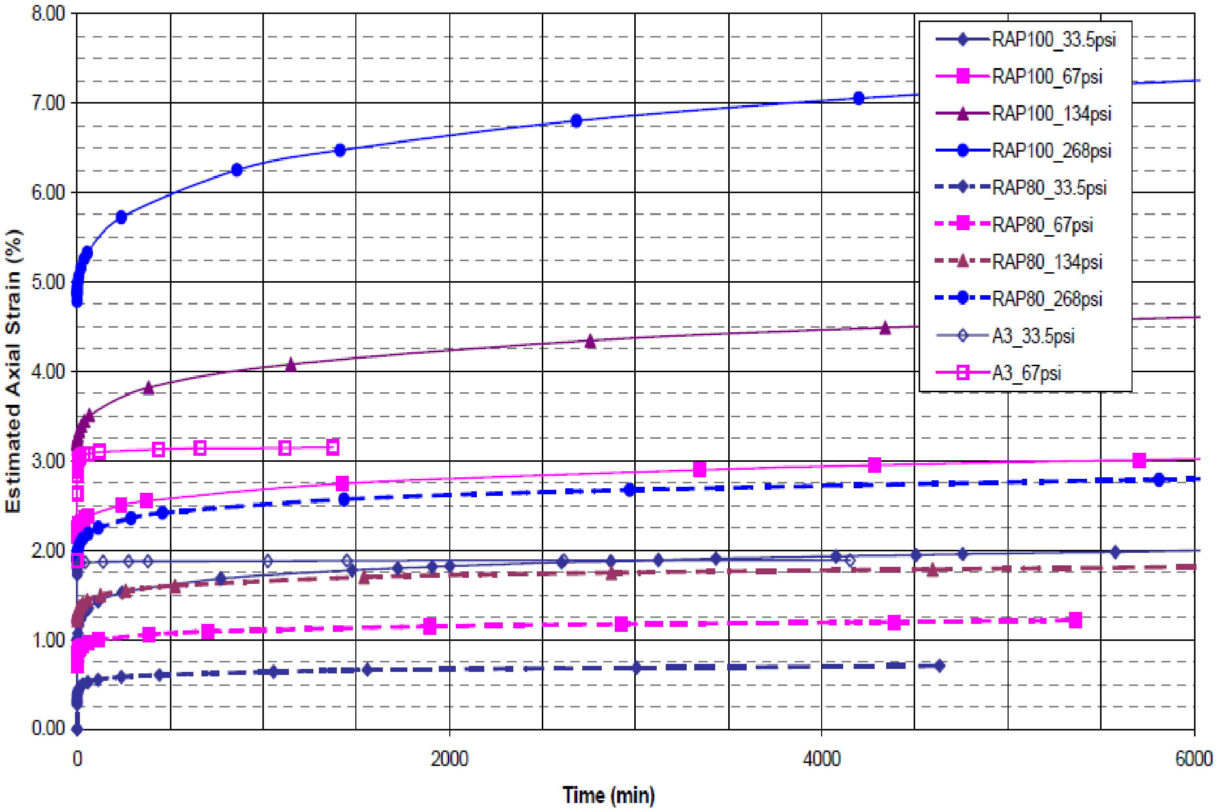

Figure 2.4.3 Axial strain versus time curve (From Cosentino et al., 2003) (1 psi = 6.9 kPa)

Cosentino et al. (2003) further evaluated the long-term characteristics of RAP by calculating the slope of each curve between 1000 and 4000 minutes. The slopes of all ten curves are presented in Table 2.4.5.

Table 2.4.5 Slope of axial strain versus time curve (Cosentino et al., 2003)

Stress level (psi / kPa)	Soil type	Slope of curve (%/minute)
33.5 / 231.2	100% RAP	$7.2\mathrm{x}10^{-5}$
	80% RAP	2.1x10-5
	A-3 soil	2.2x10-6
67 / 462.3	100% RAP	9.0x10-5
	80% RAP	1.4x10-5
	A-3 soil	2.0x10-6
134 / 924.6	100% RAP	1.4x10-4
	80% RAP	4.3x10-5
	A-3 soil	N/A
268 / 1849.2	100% RAP	2.4x10-4
	80% RAP	7.1x10-5
	A-3 soil	N/A

Viyanant et al. (2007) performed consolidated-drained triaxial tests on compacted RAP samples at effective confining stresses (σ’3) between 34 and 340 kPa and at varying deviatoric stresses to quantify creep responses of RAP. Each creep test lasted for 1 week or until the sample failed. They suggested that creep should be taken into account when RAP is used in geotechnical applications and pointed out the most critical situation which occurs under large stress levels. In addition, their results predicted potential creep deformations of RAP with time.

2.5 Geocell-reinforced soil

Geosynthetics have been widely used as construction materials for soil reinforcement in civil engineering projects such as slopes, retaining walls, roads, landfills, foundations, subgrade improvement and reinforcement to base courses of road sections etc. since the 1970s. Geosynthetics are used to improve the performance of unpaved and paved roads for over 40 years (Giroud and Han, 2004a, b). Based on a comprehensive literature review by Yuu et al. (2008), theories and design methods are far behind the applications of geocells in the field, especially for roadway applications because the mechanisms of geocell reinforcement have not been well understood. Most of the published research has focused on planar reinforcement and has resulted in several design methods for geotextile or geogrid-reinforced unpaved roads (for example, Giroud and Han, 2004a, b; Steward et al. 1977 etc.). Only limited research has been done to develop design methods for the geocell reinforcement, for example, Yang (2010) and Pokharel (2010). Such a gap between theory and application limited the usage of geocell. Yang (2010) proposed a mechanistic-empirical design model for geocell-reinforced unpaved roads if subgrade and bases are stable. Pokharel (2010) obtained a simplified design method for geocell-reinforced unpaved roads if subgrade is unstable. However, more research is needed to develop such a design method for three-dimensional interconnected geocells infilled with RAPs.

2.5.1 Design methods for geosynthetic-reinforced roads

Barenberg et al. (1975)

Barenberg et al. (1975) presented a method that utilizes different bearing capacity factors for the unpaved road application with or without a geotextile. “Lateral restraint theory” is the core of this method. This method was developed based on the following assumptions: (1) soft, cohesive soil subgrade, (2) load repetitions less than 100, (3) a crushed-rock aggregate surface course, (4) a circular contact area, and (5) stresses at a depth determined using the Boussinesq method. Based on small-scale laboratory tests, Barenberg et al. (1975) showed that bearing capacity factors (N_c) of 6 and 3.3 were appropriate for sections with and without a geotextile placed upon the subgrade, respectively. Rodin (1965) indicated that at the onset of bearing failure, N_c= 6.2 is for a rigid footing and N_c= 3.1 for a flexible footing.

Apparently, the addition of the geotextile upon the subgrade causes the section to fail in a similar way to that of a rigid footing (i.e., a general failure rather than a local failure). Currently, the United States Army utilizes this method for construction of low-volume unpaved roads with minor design improvements suggested by Steward et al. (1977) and Henry (1999). The Barenberg et al. (1975) method was extended to address a slightly greater number of load repetitions by Steward et al. (1977) through further reductions of the recommended bearing capacity factors. The Barenberg et al. (1975) design method does not consider the modulus or tensile strength of the geotextile for any purposes.

Steward et al. (1977)

Steward et al. (1977) drew similar conclusions as Barenberg at al. (1975) from the field observations on the Quinault test road. Stress levels expressed in N_c-values were found corresponding to road performance. Design charts were developed by the US Forest Service based on this study to provide assistance for engineers to estimate the required aggregate thickness as a function of a chosen c_uN_c-value (c_u, undrained cohesion of subgrade) for a particular combination of wheel loads and tire pressure (see the FHWA Geotextile Engineering Manual, 1984).

Kinney (1979)

Kinney (1979) developed a so-called fabric tension model, which considers the behavior of the geotextile in a soil-fabric-aggregate system including induced shear and normal stresses and strain energy stored in the geotextile. This model was based on the concept that the outward movement of aggregate and clay under loading causes outward shear stresses on the fabric, creating tension in the fabric. When the fabric is stretched over a curved surface, higher normal stresses are generated in the aggregate above the fabric than in the subgrade below the fabric under the loading area. The fabric resists stretching, causing inward-directed shear stresses on the gravel and the clay. Expressions were developed for calculating the induced shear and normal stresses knowing the tension in the geotextile and the deformed shape of the geotextile. The sum of the shear stresses on both sides of the fabric was set equal to the rate of change in the tension-per-unit-width of the fabric along its length. The geotextile-induced shear stresses could only be determined if the fabric is assumed to be slipping with respect to one or both of the surrounding materials. If the slip is assumed, the shear stress on the slipping side can be set equal to the maximum shear strength available, which is governed by the friction and adhesion between the fabric and the adjoining material and by the normal stress on the interface. The geotextile-induced normal stress was set equal to the tension in the geotextile per unit width divided by the radius of curvature.

Barenberg et al. (1980)

Based on the theoretical and experimental work by Kinney and Barenberg (1978) and Kinney (1979), Barenberg et al. (1980) modified the originally proposed design procedure (1975) in order to include the profound effect of the modulus of the fabric on the strains within the granular layer. This model includes the membrane effect and was termed as the fabric tension model. In this method, the allowable subgrade stress is expressed as a function of subgrade cohesion with due consideration of the presence of the fabric. For a given aggregate thickness and rut geometry, the strain and the stress in the fabric are calculated. An equivalent vertical support provided by the fabric is computed as the differential stress across the fabric. The permissible stress on the fabric is the sum of the permissible subgrade stress and the differential stress across the fabric. The actual stress, calculated according to the Boussinesq solution for a given surface load, is equal to the permissible stress and the resulting equation is solved for the cohesion of the subgrade.

Giroud and Noiray (1981)

Giroud and Noiray (1981) simplified the formula for the required thickness of granular base over soft subgrade under an unreinforced condition in terms of the number of repetitions proposed by the Army Corps. They used a stress distribution method with a fixed distribution angle ($\tan\theta=0.6$) to calculate the stress at the interface between base and subgrade under a static load applied on a rectangular contact area. This stress depends on the thickness of the base and is limited by the bearing capacity of a unreinforced or reinforced base with a bearing capacity factor N_c = 3.14 or 5.14, respectively. Due to different bearing capacity factors for unreinforced and reinforced bases, the required base thickness for the unreinforced or reinforced base is different. The difference in the base thickness between unreinforced and reinforced bases is the reduction in base thickness due to geosynthetic reinforcement. The same reduction in base thickness by the geosynthetic was assumed under either static or repeated loading. Giroud and Noiray (1981) did consider the tensile contribution of the geosynthetic to the reduction of the vertical stress at the interface between base and subgrade using a tensioned membrane theory, however, this contribution is minimal unless the rut depth is excessive (> 100 mm.). Giroud and Noiray (1981) assumed a soft, saturated clay subgrade that is undrained and a granular base having a California Bearing Ratio (CBR) of at least 80. They adopted the ESAL concept used in the AASHTO Design Guide (1993) to account for axle loads at different intensities. Giroud and Noiray (1981) also obtained an empirical relationship to account for the effect of rut depth different from 3 in (75 mm).

Haliburton and Barron (1983)

A design method which emphasizes the benefit of lateral restraint of the aggregate was developed by the Haliburton Associates based on the research conducted for the US Air Force and the Nicolon Corporation. This method is described in the FHWA Geotextile Engineering

Manual (1984), referring to a paper by Haliburton and Barron (1983). Plate load tests showed that an ‘optimum’ depth exists, at which the maximum reinforcing effect of the cohesionless cover is obtained. This optimum depth was found to lie between 0.33 and 0.4 times the width B of the loaded area. In their initial tests using dense sand subgrade, the bearing capacity of the unreinforced aggregate was increased more than twice and the modulus increased three- to fivefold at the optimum placement of a fabric. In addition, strain-hardening of the cover material was observed after initial shear failure. This method thus emphasized the importance of the fabric location in the soil-aggregate system. Haliburton and Barron (1983) concluded that almost any permeable conventional engineering fabric is adequate for separation, provided it does not have holes or is not torn during construction. According to the FHWA Manual, Holtz and Harr (1983) reviewed Haliburton’s ‘optimum depth’ concept and concluded that this method appears to be non-conservative.

Giroud et al. (1985)

Giroud et al. (1985) developed a design method for geogrid-reinforced unpaved roads to take into account the mechanism of geogrid/base interlocking. The design method included several mechanisms by which the geogrid can improve unpaved road behavior, in particular the load distribution capability of the base layer. Giroud et al. (1985) developed design charts relating the required base thickness to the undrained shear strength of subgrade, tensile stiffness of geogrid, traffic, and allowable rut depth of the unpaved road.

Holtz and Sivakugan (1987)

Holtz and Sivakugan (1987) used the Giroud and Noiray (1981) design procedure to develop design charts for rut depths of 75, 100, 150, 200, and 300 mm. The modulus of the geotextile was found not that important for smaller rut depths as compared with larger rut depths (300 mm or larger). It was explained that at smaller rut depths the membrane resistance assumed in the Giroud and Noiray (1981) design procedure is not well developed. Holtz and Sivakugan (1987) found that a rapid increase in the aggregate thickness is required for the subgrade with avery low undrained shear strength, irrespective of the rut depth and the geotextile modulus. Thus, a slight increase in the shear strength of the subgrade used for design could result in a significant reduction in the required aggregate thickness.

Milligan et al. (1989)

Milligan et al. (1989) presented a design method for unreinforced and reinforced unpaved roads. In their model, an outward shear stress is induced on top of the subgrade by a vertical load without a geosynthetic while an inward shear stress is induced on top of the subgrade due to the existence of a geosynthetic layer. The outward shear stress reduces the bearing capacity of the subgrade while the inward shear stress increases the bearing capacity.

Burd (1995)

Burd (1995) proposed a model considering membrane action in reinforced unpaved roads. Detailed consideration was given how to determine the width of reinforcement within which the tension is nonzero. This analytical model only deals with the case with a single application of a monotonic load. In the analysis, stresses acting on the reinforcement are first assumed. Membrane equations are solved to obtain a deformed reinforcement shape. A compatibility condition, similar to that proposed by Bourdeau (1989), is used to obtain the width of reinforcement within which the tension is nonzero. The main differences from that described by Bourdeau (1989) are the load-spread model for the fill and the rigid-cohesive model for the subgrade. This method resulted in a reasonable comparison with model test data and numerical results.

Tingle and Webster (2003)

Tingle and Webster (2003) modified the Steward et al. (1977) method for geogrid reinforcement. The proposed modification is adopted in the COE method for design of geotextile- and geogrid-reinforced unpaved roads (USCOE, 2003). Tingle and Webster (2003) used full-scale experiments to evaluate the applicability of their design procedure for geogrid-reinforced unpaved roads and further validated the bearing capacity for geotextile-reinforced unpaved roads. Their analysis recommended that the bearing capacity factor (N_c) for unreinforced unpaved roads proposed by Steward et al. (1977) and adopted by the COE should continue to be used. The bearing capacity factor (N_c) currently used by the COE design method for unpaved roads reinforced with geotextiles of 5.0 should be used until additional conclusive evidence is developed for its revision. A bearing capacity factor (N_c) of 5.8 should be used for the design of unpaved roads reinforced with both a geotextile and a geogrid under soft cohesive subgrade conditions. These bearing capacity factors for geotextile-reinforced and composite (geotextile and geogrid) reinforced unpaved roads were obtained based on experimental study. Additional field tests should be conducted at different subgrade strengths and loading conditions to further validate the COE design method. Ideally, a comprehensive test program should be conducted to develop a mechanistic-empirical design procedure.

Giroud and Han (2004)

Giroud and Han (2004) developed a theoretically based design method for the thickness of the base course of unpaved roads which considers distribution of stress, strength and modulus of base course material, interlock between geosynthetic and base course material, and geosynthetic stiffness in addition to design parameters considered in earlier methods (Giroud and Noiray 1981; Giroud et al. 1985), such as traffic volume, wheel load, tire pressure, subgrade strength, rut depth, and influence of a reinforcing geosynthetic (geotextile or geogrid) on the failure mode of the unpaved road or area. Giroud and Han (2004) used the stress distribution method to calculate the stress at the interface between the base and the subgrade and assumed the stress distribution angle changing with the number of repetitions. Different bearing capacity factors were proposed for geotextile and geogrid considering the interface roughness between the geosynthetic and the subgarde. Their method was calibrated against full-scale field test data for unreinforced unpaved roads and laboratory test data for reinforced unpaved roads. It was also verified by field test data for reinforced unpaved roads. It calculates the required base course thickness for a reinforced unpaved road using a unique equation.

Yang (2010)

Yang (2010) developed three-dimensional numerical models to simulate the behavior of geocell-reinforced soil under static and repeated loadings. A non-linear elastoplastic model was used to model infill soil where as a linear elastic plate model was used to model geocell for novel polymer alloy (NPA) geocell-reinforced soil under static loadings. In addition, a mechanistic-empirical model was developed for NPA geocell-reinforced soil under repeated loadings with some modifications in the stress-dependent response model of current mechanistic-empirical pavement design guide (MEPDG) to consider the three-dimensional constitutive equation of tangent resilient modulus, the compaction-induced initial horizontal stress in the soil, and the residual stress increase due to the accumulated permanent deformation of geocell with the number of load passes. A parametric study was also performed based on the calibrated numerical models to investigate the effects of following factors: (i) thickness of the geocell-reinforced layer, (ii) geocell modulus, (iii) subgrade stiffness and strength, (iv) interface shear modulus, and (v) infill material modulus. Yang

(2010) concluded that the developed numerical model well simulated the experimental results from the geocell-reinforced soils.

Pokharel (2010)

Pokharel (2010) developed a design method for NPA geocell-reinforced unpaved road by modifying the method developed by Giroud and Han (2004) which is discussed above. He introduced a modulus improvement factor (I_f) which was proposed by Han et al. (2007) to account for modulus increase of the base course by geocell confinement and set the maximum limit of the modulus ratio to 7.6 for NPA geocell-reinforced unpaved roads. The factor (k') depending on the geocell reinforcement was introduced and calibrated based on large-scale laboratory cyclic plate loading tests and full-scale moving wheel tests on NPA geocell-reinforced granular bases over weak subgrdae. The design formula was verified by the test data. This method can also be used for other geocell-reinforced unpaved roads by calibrating the k' value for other geocell products using cyclic plate loading tests and/or moving wheel tests.

2.5.2 Experimental study on geocell-reinforced soil

Triaxial compression test

Bathurst and Karpurapu (1993) conducted a series of large-scale triaxial tests on a 200 mm high isolated geocell-reinforced soil and unreinforced soil specimens. The reinforced specimens were tested with a height-to-diameter ratio of unity to match the dimensions of a typical base-reinforced system. Frictional resistance of soil infill was found same for both unreinforced and reinforced soil samples. A simple elastic membrane model was used to estimate the additional apparent cohesion present in the reinforced soil sample. Bathrust and Karpurapu (1993) concluded the following: (i) the stiffness and strength of reinforced soil increased because of the confining effect of geocell as shown in Figure 2.5.1; (ii) apparent cohesion increased with the degree of geocell confinement as shown in Figure 2.5.2; (iii) the proposed elastic membrane model can be used to determine the strength parameters of geocell-reinforced granular soil without conducting large-scale triaxial compression tests.

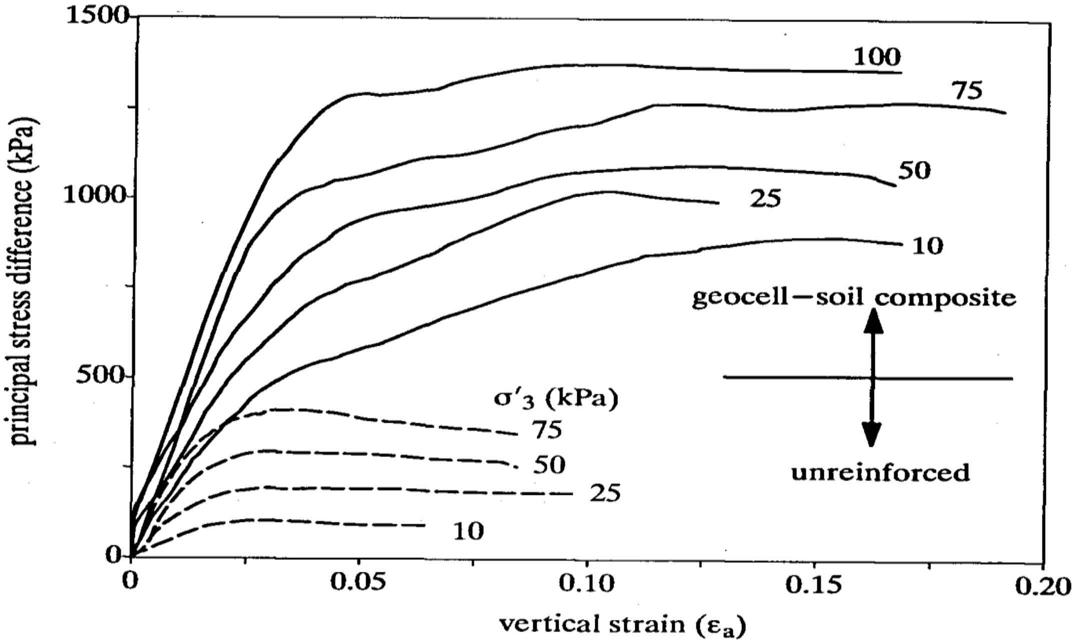

Figure 2.5.1 Principal stress differences versus axial strain (From Bathurst and Karpurapu, 1993)

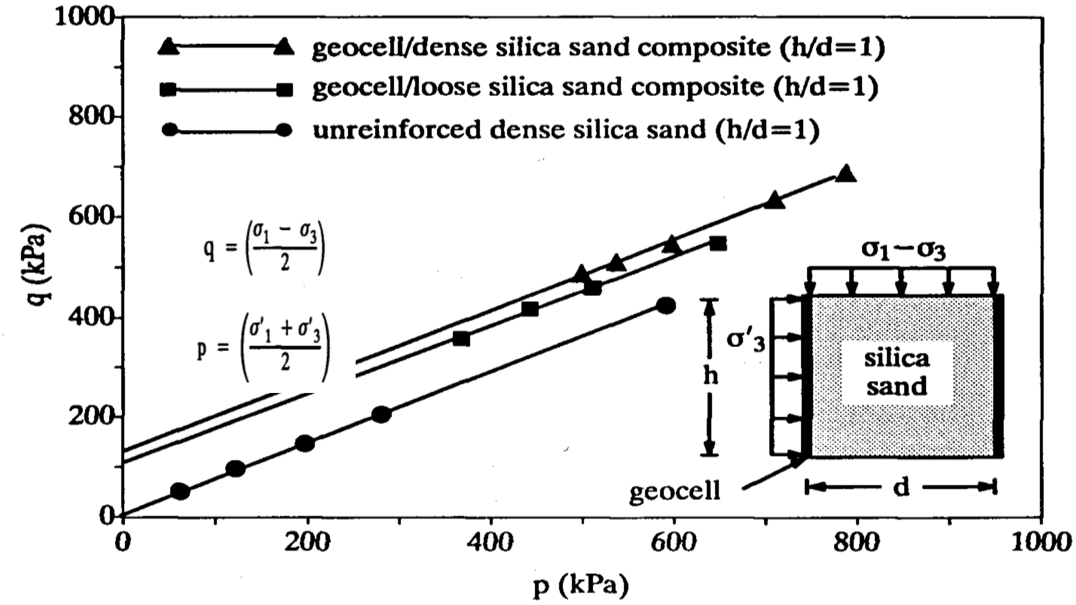

Figure 2.5.2 Failure strength envelope for goecell-reinforced and unreinforced triaxial test specimens (From Bathurst and Karpurapu, 1993)

Rajagopal et al. (1999) conducted a series of triaxial compression tests on unreinforced, single geocell-renforced, and multi geocell-reinforced granular soils. Geocells used for the research were made using woven and non woven geotextiles. They found significant amount of apparent cohesion and an increase in stiffness for the geocell-reinforced granular soils. They came to the following conclusions: (i) the frictional strength of granular soil is independent of geocell reinforcement; (ii) the induced apparent cohesion is a function of tensile modulus of geosynthetics used to make geocells; (iii) at least three interconnected geocells should be used to simulate the performance of many interconnected geocells; and (iv) the membrane correction procedure developed by Henkel and Gilbert (1952) can be used to determine the induced apparent cohesion in the geocell-reinforced soils.

Direct shear test

Wang et al. (2008) performed a series of direct shear tests using large-scale direct shear equipment with shear box dimensions of 500mm x 500mm x 400mm on three types of specimens (i.e. silty gravel soil, geocell-reinforced silty gravel soil, and geocell-reinforced cement stabilizing silty gravel soil). They observed the shear stress-displacement behavior and the strengthening mechanism of geocell reinforced soils. The following conclusions were made by Wang et al. (2008): (i) unreinforced and geocell-reinforced soils showed similar nonlinear shear stress and displacement behavior whereas geocell-reinforced cement stabilizing soil showed quasi-elastic behavior; (ii) the friction angle remained almost same for all three specimens; (iii) cohesion was found to increase by 2.44 and 10 times for the geocell-reinforced silty gravel soil and geocell-reinforced cement stabilizing silty gravel soil compared to the unreinforced sample respectively.

Plate load tests

Mandal and Gupta (1994) also conducted a series of plate loading tests to investigate the load-settlement behavior of geocell-reinforced sand with different cell height to width ratios over soft clay under static loading. Test results showed that the geocell-reinforced sand exhibited a beam action at lower settlement ratios (i.e. up to 5 to 10%) and a tensioned membrane effect at higher settlement ratios (i.e. over 20%). The settlement ratio was defined as the ratio of settlement to width of plate. Geocell with a larger width and a larger thickness had a higher bearing capacity. The settlement ratio increased with increasing the geocell width but decreased with increasing the geocell depth.

Mhaiskar and Mandal (1992a, b, 1996) conducted a series of loading tests to investigate the effect of geometric ratio of geocell, strength of geocell, infill soil density, etc. under static and cyclic loading conditions. A general purpose finite element package ANSYS was used to simulate experimental results with the help of a three dimensional analysis. They concluded that the geocell-reinforced base performed better when the geocells had a higher ratio of the height to width, higher density of infill, and higher modulus of geocell material. In addition, geocell-reinforced soil had a greater bearing capacity than horizontal geotextile-reinforced soil. The geocell-reinforced soil with the geocell height to diameter ratio of 2.0 and dense infill had a higher bearing capacity. They further concluded that the geocell-reinforced sand layer performed better than the planar reinforcement and the unreinforced sand under cyclic loading.

Pokharel et al. (2009c) conducted laboratory plate load tests in medium-scale loading apparatus to investigate the behavior of unreinforced and geocell-reinforced bases. The loading system used consisted of 15.2 cm diameter air cylinder with a maximum air pressure of 2,100 kPa. The test box had a plan area of 60.5cm x 60.5cm. Kansas River sand and quarry waste were used as base materials. The static tests were conducted on both unreinforced and reinforced sections by increasing the load in increment of 35 kPa whereas repeated tests were conducted on reinforced sections only at an applied pressure of 345 kPa and 550 kPa for the sand and quarry waste respectively. They concluded that bearing capacity and stiffness of the Kansas River sand was improved by a factor of 1.75 and 1.5 respectively under static loading, however, stiffness of the quarry waste was improved by very marginal amount under static loading due to the existence of apparent cohesion as shown in Figure 2.5.3. In addition, the permanent deformations of geocell-reinforced quarry waste were reduced by a factor of 1.5 compared to the unreinforced base. The reinforced quarry waste showed a higher percentage of elastic deformation than the unreinforced quarry waste due to the geocell confinement whereas Kansas River sand showed a lower percentage of elastic deformation due to its poor gradation, sub-rounded particles and no apparent cohesion.

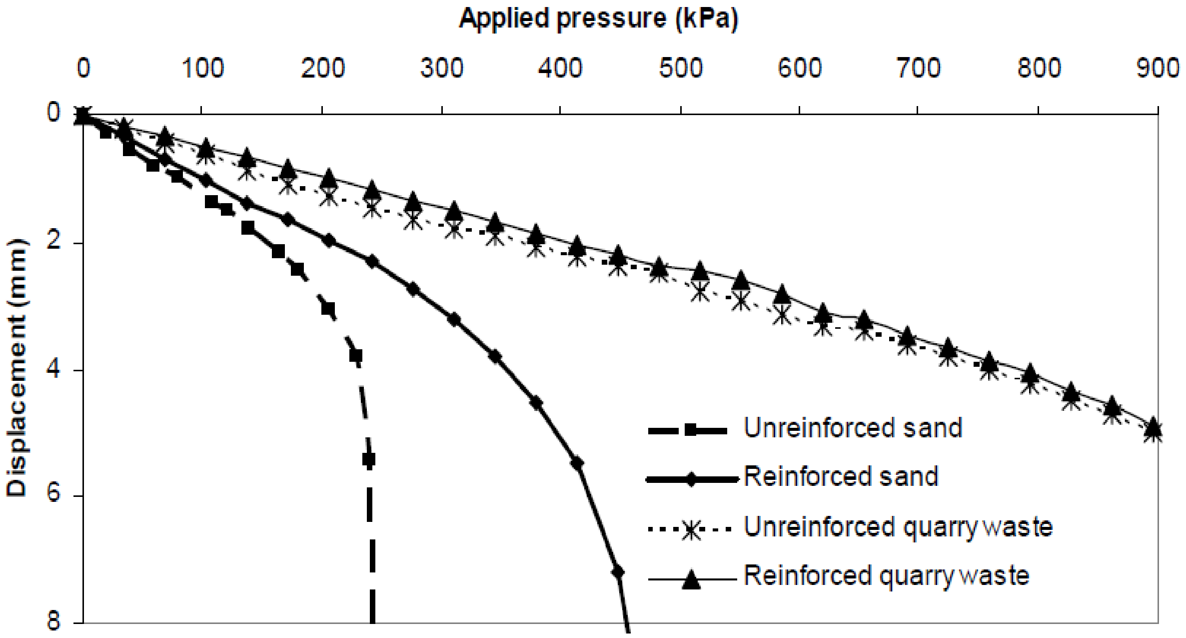

Figure 2.5.3 Pressure-displacement curve for unreinforced and geocell-reinforced bases under static loading (From Pokharel et al., 2009c)

Pokharel et al. (2010) also conducted medium-scale laboratory plate loading tests to investigate the factors affecting behavior of single geocell-reinforced bases such as shape, type, embedment, height of geocells, and quality of infill materials. They concluded as follows: (i) geocell-placed in a circular shape had higher stiffness and bearing capacity than that placed in an elliptical shape; (ii) the confined geocell had a higher stiffness but lower ultimate load capacity than the unconfined geocell; (iii) the benefit of geocell was more pronounced for the infill material without apparent cohesion than that with apparent cohesion; and (iv) the multiple geocell-reinforced bases are stiffer and bear more loads compared to single geocell-reinforced bases.

Moving wheel tests

Yang (2010) and Pokharel (2010) conducted moving wheel tests on unpaved road sections to evaluate the behavior of geocell-reinforced granular bases over the weak subgrade by using accelerated pavement testing (APT) facility at the Kansas State University. They concluded as follows: (i) the NPA geocell improved stability of unpaved road and reduced the permanent deformation; (ii) the base course layer of NPA geocell-reinforced unpaved road should be thick enough to be stable (Yang, 2010); (iii) the base course should be well compacted and enough cover to geocell should be provided in addition to geocell reinforcement to have better performance of unpaved road sections (Pokharel, 2010); and (iv) geocell-reinforced unpaved roads distributed the load to a wider area compared to unreinforced roads (Pokharel 2010).

2.6 Summary

The following conclusions can be made from the past studies:

(i) Recycled asphalt pavement material has a structural value and can be used as subbase and base course layers.

(ii) Use of RAP is considered a sustainable technology which preserves natural environment, reduces the amount of waste disposal, and provides cost effective material for highway construction.

(iii) Geocell-reinforced roads perform better than planner geosynthetic-reinforced roads and unreinforced roads.

(iv) Geocell provides confinement and tension membrane effects which result in an increase in stiffness and bearing capacity of base courses.

(v) Properties of geocell, shape, type, embedment, height of geocell, and quality of infill materials play important roles in the effectiveness of the geocell-reinforced bases.

CHAPTER 3

LABORATORY EVALUATION OF CHARACTERISTICS OF RECYCLED ASPHALT PAVEMENT (RAP)

This chapter describes the test equipments and procedures used to evaluate characteristics of RAP and its constituents and presents the test results obtained from different laboratory tests.

3.1 Material

The RAP material was provided by R.D. Johnson Excavating, Co., Lawrence, Kansas, which was milled off from a city street in Lawrence, Kansas.

3.2 Test Methodology

3.2.1 Binder content of RAP

The RAPs were sampled by quartering the sample in accordance with ASTM C702-98 Method B. Eleven samples were taken for ignition testing and three for centrifuge testing. The ignition and centrifuge tests were performed following ASTM D6307 and ASTM D2172, respectively. In the ignition test, the oven-dried RAP was burned in an ignition oven at 540**°C**, and the asphalt binder content was determined from the difference between the masses of the RAP before and after burning. In the centrifuge test of extraction, a loose RAP was placed into a bowl and covered with trichloroethylene for disintegration of the sample and the aggregate and asphalt were then separated by applying a centrifuge force. The asphalt binder content was calculated by the difference from the masses of the extracted aggregate, moisture content, and mineral matter in the extract. Minerals in the washing of centrifuge were obtained by the ashing method. The ignition furnace and centrifuge testing machine are shown in Figures 3.2.1 and 3.2.2 respectively. The aggregates extracted from the RAP by the ignition method were also tested for their properties including gradation before and after compaction, specific gravity, and uncompacted void content of fine aggregate while the asphalt extracted by the centrifuge method was tested for viscosity.

Figure 3.2.1 NCAT Ignition Furnace

Figure 3.2.2 Centrifuge testing machine

Table 3.2.1 shows the binder contents obtained by the centrifuge and ignition methods of extraction. A correction factor of 0.25% was determined based on the mass difference of centrifuge-extracted aggregates before and after burning and then applied to the test data from the ignition method. Table 3.2.1 shows that the corrected binder content by the ignition method was slightly higher than that by the centrifuge method. This finding is in an agreement with that obtained by Thakur et al. (2011).

Table 3.2.1 Binder contents (%) of RAP samples extracted by centrifuge and ignition methods

Sample No.	Centrifuge method	Ignition method	Mineral correction factor (%)	Corrected binder content (%)
1	6.62	6.95	0.25	6.70
2	6.80	7.11		6.86
3	6.71	7.22		6.97
4		7.09		6.84
5		7.03		6.78
6		7.20		6.95
7		7.14		6.89
8		7.20		6.95
9		7.26		7.01
10		7.02		6.77
11		7.09		6.84
Average	6.71	7.12		6.87

3.2.2 Gradation of aggregate

The aggregates extracted from the RAP by the ignition method (Figure 3.2.3) before and after compaction were washed (Figure 3.2.4) through a 0.075-mm sieve, and a sieve analysis was conducted on three samples of aggregates extracted from RAP before compaction and three of those after compaction to obtain the gradation of the aggregate (Figure 3.2.5) in accordance with the ASTM D5444 – 08.

Figure 3.2.3 Aggregate extracted from RAP by ignition method

Figure 3.2.4 Aggregate retained after washing fines through the 0.075 mm sieve.

Figure 3.2.5 Fractions of aggregates obtained by sieve analysis

Table 3.2.2 and Figure 3.2.6 show the gradation data and the gradation curves for the aggregates extracted by the ignition method before and after compaction respectively. It is shown that compaction did not change the gradation of the aggregates. The maximum size, mean size (d_{50}), coefficient of curvature (C_c), and coefficient of uniformity (C_u) of the RAP aggregate were found to be 12.5 mm, 2.0 mm, 0.85, and 8.33, respectively.

It is believed that a maximum density of aggregate can be obtained at an appropriate gradation. Figure 3.2.7 shows the comparison of the gradation of the aggregate used in this study with the power gradation curve (also referred to as the maximum density line). It is shown that the aggregate gradation in this study is close to the maximum density line; therefore, the gradation is considered densely graded. The percentage passing (p) for the maximum power gradation curve (Table 3.2.3) was calculated using Equation 3.2.1:

$$p = \left(\frac{d}{D}\right)^{0.45} \qquad \textbf{(3.2.1)}$$

where, d = aggregate size being considered and D = maximum size of aggregate

Table 3.2.2 Gradation data for aggregates extracted from RAP by ignition method

Sieve size, mm	Before compaction				After compaction			
	Samples (% passing)			Average	Samples (% passing)			Average
	1	2	3		1	2	3	
12.5	97.2	96.2	95.7	95.4	96.0	96.5	96.9	96.5
9.5	91.3	89.9	92.0	91.0	90.7	90.6	92.2	91.2
4.75	72.1	71.8	75.8	73.2	71.7	72.8	74.6	73.0
2.36	53.9	53.1	57.7	54.9	53.1	54.4	55.4	54.3
1.18	37.0	36.2	39.8	37.7	36.5	37.4	37.4	37.1
0.6	23.6	23.2	25.5	24.1	23.9	24.4	24.2	24.2
0.3	10.6	10.4	11.2	10.7	10.8	10.9	10.5	10.7
0.15	3.5	3.4	3.4	3.4	3.5	3.5	3.2	3.4
0.075	0.6	0.4	0.3	0.4	0.4	0.3	0.3	0.3

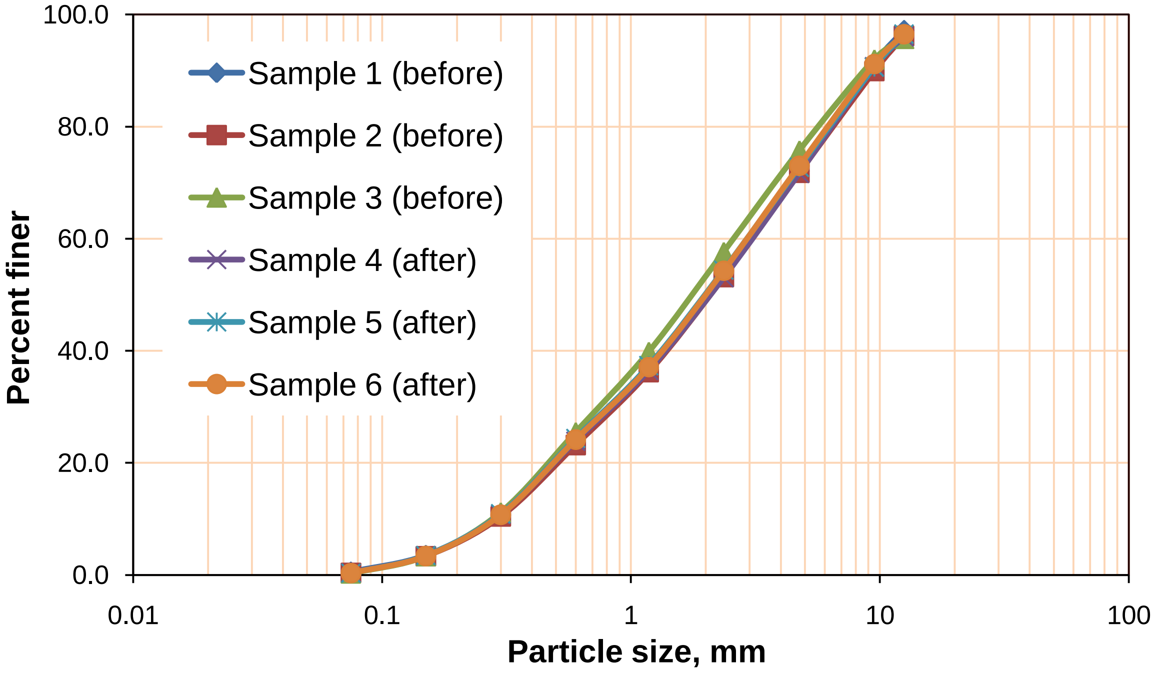

Figure 3.2.6 Gradation curves of the aggregates extracted by the ignition method before and after compaction

Table 3.2.3 Gradation data for average aggregate and power curve

Sieve size (mm)	(Sieve size)$^{0.45}$	Average percent passing		
		Before compaction	After compaction	For 0.45 power curve
12.5	3.116	96.4	96.5	100.0
9.5	2.754	91.1	91.2	88.4
4.75	2.016	73.2	73.0	64.7
2.36	1.472	54.9	54.3	47.2
1.18	1.077	37.7	37.1	34.6
0.6	0.795	24.1	24.2	25.5
0.3	0.582	10.7	10.7	18.7
0.15	0.426	3.4	3.4	13.7
0.075	0.312	0.4	0.3	10.0

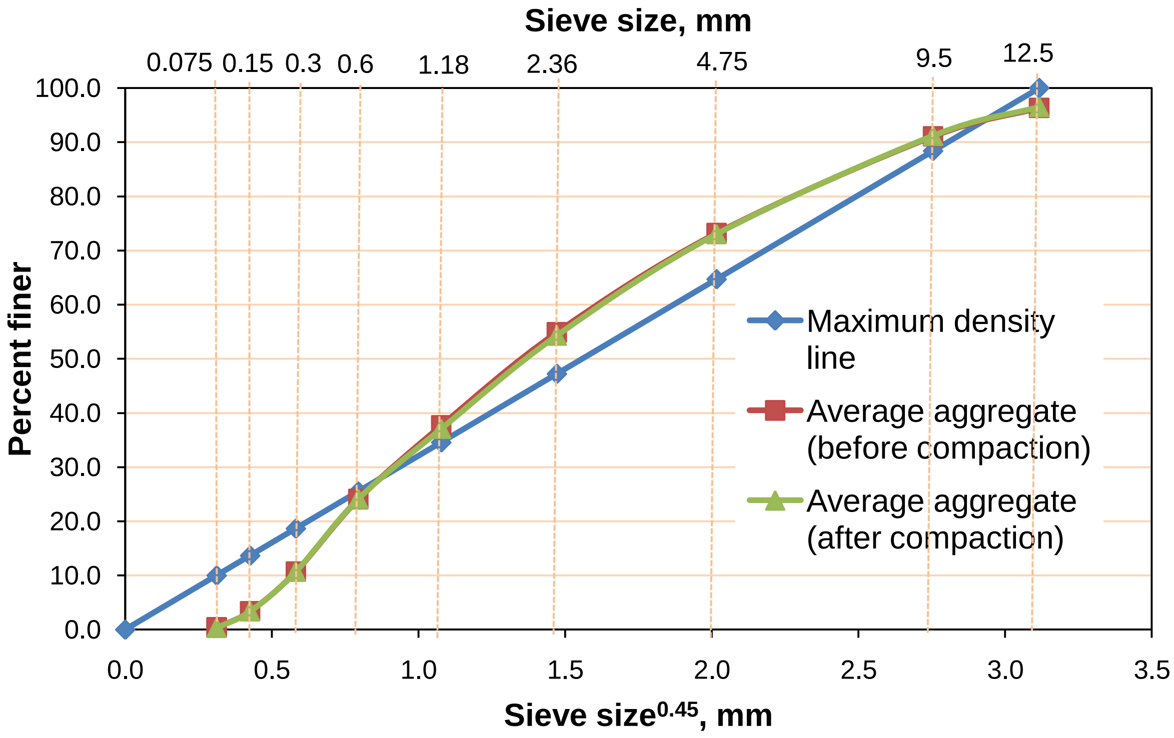

Figure 3.2.7 Power gradation curve of the aggregates extracted by the ignition method before and after compaction

3.2.3 Specific gravity of aggregate

Specific gravity is used in calculating void content of aggregate and also used in volume-weight conversion. Bulk specific gravity, SSD bulk specific gravity, and apparent specific gravity of the fine and coarse aggregates extracted by the ignition method were determined in accordance with the ASTM C128-07a and ASTM C127-07, respectively. Two samples of coarse aggregates and fine aggregates were evaluated for specific gravity. Some pictures were taken during the process of determining the specific gravity of fine aggregates which are shown in Figures 3.2.8, 3.2.9, and 3.2.10.

Figure 3.2.8 Fine aggregate in an SSD condition

Figure 3.2.9 Slump test to determine the SSD condition of fine aggregate

Figure 3.2.10 Pycnometer after removal of air bubbles

Table 3.2.4 shows the specific gravity of the aggregates extracted by the ignition method. It is shown that the fine aggregate had a higher specific gravity than the coarse aggregate.

Table 3.2.4 Specific Gravity of Aggregates Extracted by the Ignition Method

Description	**Fine aggregate**			**Coarse aggregate**		
	Sample 1	**Sample 2**	**Average**	**Sample 1**	**Sample 2**	**Average**
Bulk specific gravity	2.48	2.48	2.48	2.40	2.38	2.39
SSD Bulk specific gravity	2.55	2.55	2.55	2.49	2.49	2.49
Apparent specific gravity	2.59	2.59	2.59	2.58	2.58	2.58

3.2.4 Fine aggregate angularity

Fine aggregate angularity represents the uncompacted void content of fine aggregate. The void content indicates the angularity of the fine aggregate particles. The void content of the fine aggregate in this study was determined in accordance with ASTM C1252-06 Method B. Three samples of aggregate extracted from the ignition method were tested to evaluate the uncompacted void content of the fine aggregate. The set-up of the fine aggregate angularity test is shown in Figure 3.2.11.

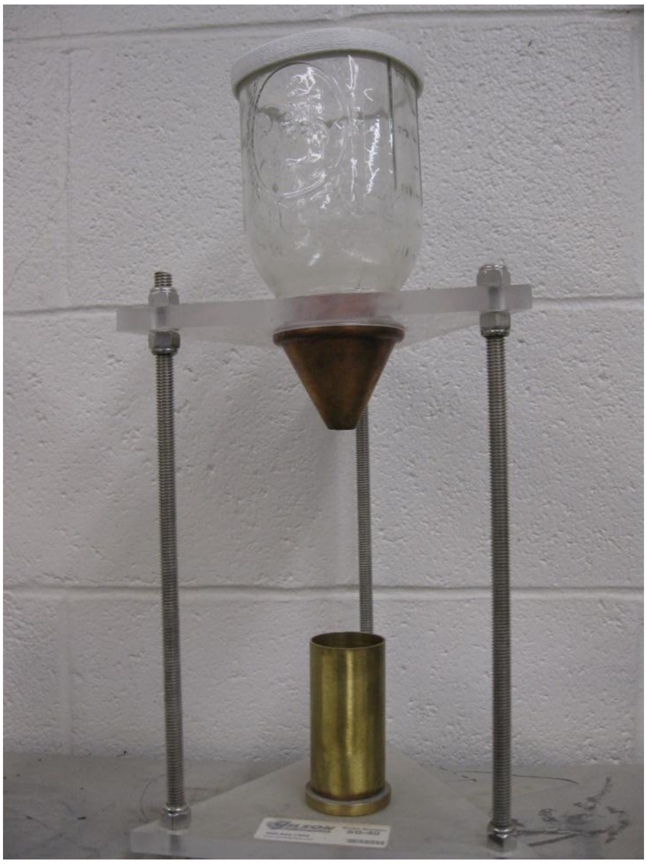

Figure 3.2.11 Fine aggregate angularity test set up

Table 3.2.5 shows the uncompacted void content of the fine aggregate extracted by the ignition method. The average void content was 39.15%.

Table 3.2.5 Uncompacted void content (%) of the fine aggregate extracted by the ignition method

Sample No.	Uncompacted void content
1	39.00
2	39.36
3	39.08
Average	39.15

3.2.5 Viscosity of asphalt binder

Asphalt was recovered in accordance with ASTM D 1856-09 from the mixture of trichloroethylene and asphalt extracted by the centrifuge method. The mixture of trichloroethylene and asphalt was distilled under a standard condition, at which time carbon dioxide was introduced into the distillation process to remove all traces of the extraction solvent. Distillation was continued until the temperature reached 135°**C**. The recovery process is commonly known as the Abson method. The recovered asphalt was tested for viscosity. The test set up of the asphalt recovery process is shown in Figure 3.2.12.

Figure 3.2.12 Set up for asphalt binder recovery by the Abson method

Asphalt is a viscous material. Hot mix asphalt (HMA) pavements are susceptible to rutting and bleeding. Lower viscosity of asphalt indicates higher flowability and deformability and vice versa. The kinematic viscosity of recovered asphalt binder at 135°**C** was determined in this study using a rotational viscometer (Figure 3.2.13) in accordance with ASTM D4402-06. The 135°**C** temperature was chosen to simulate the mixing and lay-down temperatures typically encountered in HMA pavement construction.

Figure 3.2.13 Test set-up for viscosity evaluation using a rotational viscometer

Table 3.2.6 shows the kinematic viscosity of the asphalt binder at 135°**C** recovered by using the Abson method. The average viscosity of the asphalt binder was 1.408 Pa-s.

Table 3.2.6 Kinematic viscosity (Pa-s) of asphalt binder

Sample No.	Viscosity
1	1.412
2	1.425
3	1.387
Average	1.408

3.2.6 Optimum moisture content (OMC) and maximum dry density of RAP

OMC and maximum dry density are commonly used to evaluate the compactability of subgrade, subbase, and base course materials. The OMC and maximum dry density of the

RAP were determined using the modified Proctor compaction test in accordance with ASTM D1557-09. Five modified proctor compaction tests (Table 3.2.7) were performed on RAP specimens at different moisture contents to obtain the compaction curve as shown in Figure 3.2.14. The maximum dry density of the RAP was 1.96 g/cm^3, which corresponds to the optimum moisture content (OMC) of 6.6%.

Table 3.2.7 Unit weight of RAPs at different moisture contents

Sample No.	1	2	3	4	5
Moisture content (%)	4.04	5.23	6.55	7.27	7.80
Moist unit weight, (g/cm^3)	2.00	2.02	2.08	2.06	2.07
Dry unit weight (g/cm^3)	1.92	1.92	1.95	1.92	1.92

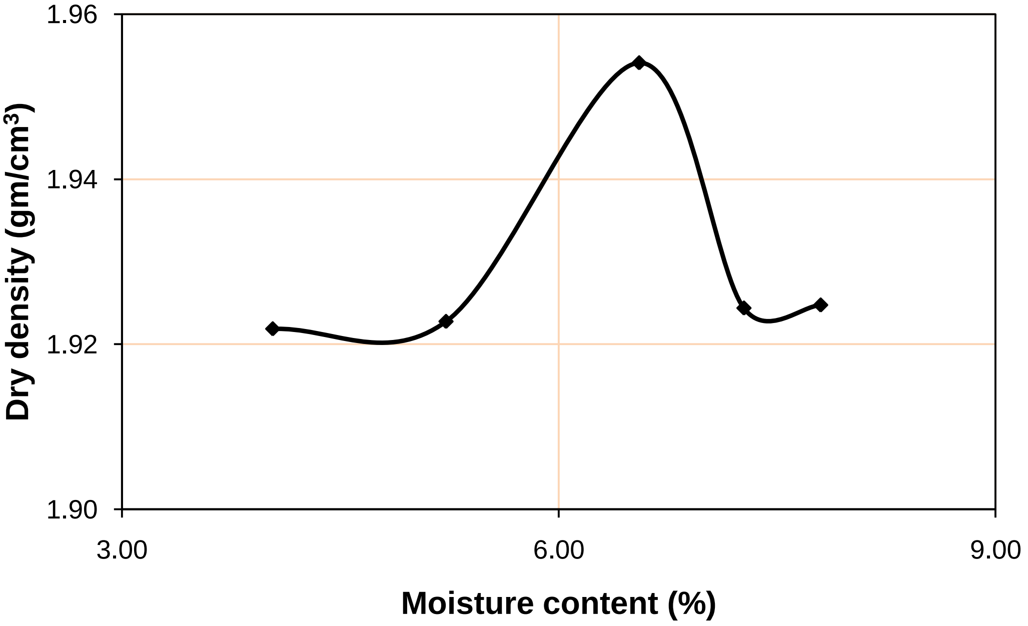

Figure 3.2.14 Modified Proctor compaction curve of RAP

3.2.7 California bearing ratio (CBR)

CBR is commonly used to evaluate the strength or stiffness of subgrade, subbase, and base course materials. The CBR values are sometimes used with empirical curves or formulae to determine the thicknesses of pavement layers. The CBR is expressed as the percentage of the unit load on the piston required to penetrate 0.1 in. (2.5 mm) and 0.2 in. (5 mm) of the test soil to the unit load required to penetrate a standard material of well-graded crushed stone. Five unsoaked California bearing ratio (CBR) tests (Table 3.2.8) were performed on laboratory compacted RAP specimens at different water contents following ASTM D 1188-07 to estimate the CBR value of the RAP in Loadtrac II instrument as shown in Figure 3.2.15.

Figure 3.2.15 CBR test in Loadtrac II

CBR values are calculated in Table 3.2.8 using Equation 3.2.2. The CBR versus moisture content curve is shown in Figure 3.2.16.

$$\textbf{CBR} = \frac{\text{Test stress}}{\text{Standard stress}} \times 100\% \qquad \textbf{(3.2.2)}$$

Standard stresses were taken as 1000 psi and 1500 psi corresponding to 0.1 inch (2.5 mm) and 0.2 inch (5.0 mm) displacement, respectively.

Table 3.2.8 CBR values of RAPs at different moisture contents

Sample No.	**1**	**2**	**3**	**4**	**5**
Moisture content (%)	4.04	5.23	6.55	7.27	7.80
CBR (%)	23.6	24.83	24.28	20.3	19.9

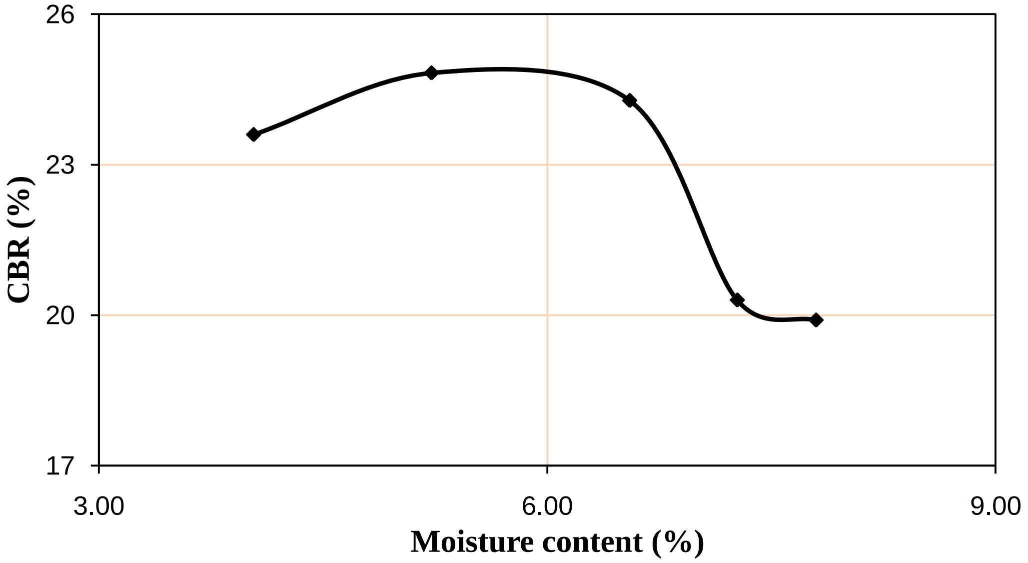

Figure 3.2.16 CBR versus moisture content curve of RAP

3.2.8 Maximum and minimum index density of RAP

The minimum index density is the density of RAP in the loosest state of compactness at which it can be placed while the maximum index density is the density of RAP in the densest state of compactness that can be attained using a standard laboratory procedure. These densities are used to determine the relative density (D_r) of the RAP in the field. From relative density, the degree of compaction i.e., relative compaction (R) can be estimated using the relation (Lee and Singh, 1971): $R = 80+0.2D_r$.

Three index density tests were conducted in the laboratory to determine the minimum and maximum densities of the RAP sample using ASTM D 4254-00 and ASTM D 4253-00 respectively. Minimum and maximum densities were calculated using Equations 3.2.3 and 3.2.4, respectively.

$$\textbf{Minimum density} = \frac{\text{Weight of dry RAP sample in loosest state}}{\text{Volume of dry sample in loosest state}} \qquad \textbf{(3.2.3)}$$

$$\textbf{Maximum density} = \frac{\text{Weight of dry RAP sample in densest state}}{\text{Volume of dry sample in densest state}} \qquad \textbf{(3.2.4)}$$

Figure 3.2.17 presents the different steps of the procedure used to determine minimum and maximum index densities of RAP samples.

(a) Placing the mold filled with loose RAP on a vibrating table and clamped at the base

(b) Placing a guide sleeve on top of the mold

(c) Placing the surcharge base plate on top of the mold

(d) Placing the surcharge weight on the surcharge base plate and then applying vibration

Figure 3.2.17 Different steps to determine minimum and maximum index densities

Table 3.2.9 presents the maximum and minimum densities of RAP samples. Average minimum and maximum index densities were found to be 1.415 g/cm^3 and 1.740 g/cm^3 respectively.

Table 3.2.9 Minimum and maximum index densities

Sample No.	1	2	3	Average
Minimum density (g/cm^3)	1.44	1.39	1.42	1.42
Maximum density (g/cm^3)	1.76	1.73	1.74	1.74

3.2.9 Geocell-RAP interface shear test

Interface shear test is used to determine the shear resistance of a geosynthetic sheet against soil or one geosynthetic sheet against another geosynthetic sheet under a constant rate of shear deformation. Peak shear strength of soil is its maximum resistance to shear stresses just before failure. Geocell infilled with soil has been used for various purposes including road applications. Hence it is necessary to evaluate the interface shear strength between geocell and infill RAP.

Five interface shear tests were performed in accordance with ASTM D 5321-02 at five different normal stresses (i.e. 35, 52, 69, 86, and 104 kPa) using a large direct shear box to determine the interface shear strength of geocell against RAP at the moisture content corresponding to 98% compaction. The lower shear box was originally bigger in plan area than the upper shear box having dimensions 30cm x 30cm x 10cm. The plan area of the lower box was made same as the upper box after placing wooden plank. The tests were performed at a shear strain rate of 0.254 mm per minute. Figure 3.2.18 presents different steps of an interface shear test performed.

(a) Lower box before RAP placed

(b) Placing RAP inside the lower box and compacting

(c) Placing geocell on the compacted RAP and then placing the upper box

(d) Placing RAP inside the upper box and then compacting

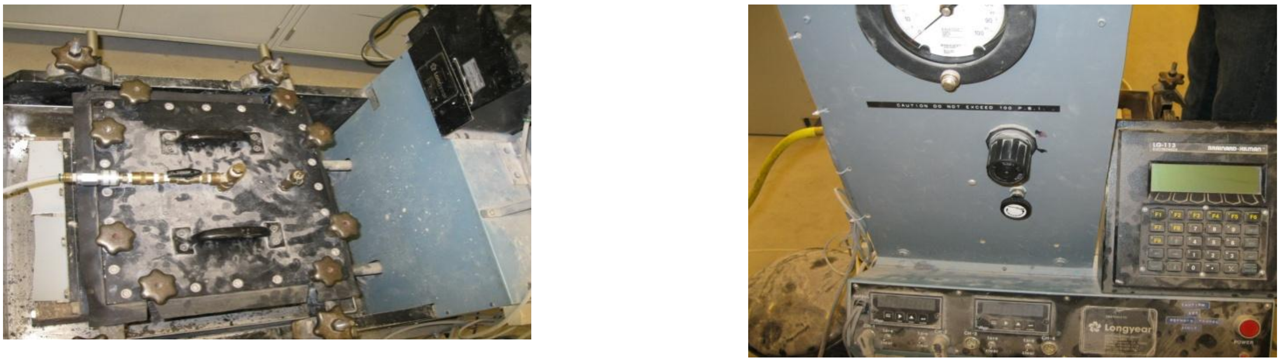

(e) Placing and tightening the top plate and connecting the air pressure hose

(f) Applying air pressure and starting the test

Figure 3.2.18 Different steps for interface shear tests

The geocell used for the interface test was made of novel polymeric alloy (NPA) having two perforations of 100 mm^2 area each on each pallet, 1.1-mm wall thickness, 150 mm height, 19.1-MPa tensile strength, and 355-MPa elastic modulus at 2% strain. The NPA is characterized by flexibility at low temperatures similar to HDPE with elastic behavior similar to engineering thermoplastic. This NPA geocell has a lower thermal expansion coefficient and higher tensile stiffness and strength than typical HDPE geocells. The creep resistance properties and other properties of NPA geocell are given in Tables 3.2.10 and 3.2.11, respectively (Pokharel, 2010).

Table 3.2.10 Creep resistance properties of the HDPE and the NPA materials (from PRS Mediterranean, Inc., Israel)

Time (Years)	Stress to create 10% strain at 23°C (N/mm)
25	5.82
50	5.65
75	5.56

Table 3.2.11 Other properties of the NPA material

(From PRS Mediterranean, Inc., Israel)

Properties		Description	Unit	Test method
Tensile strength		>20	N/mm	PRS method
Allowed strength for design of 50 yrs		>5.7	N/mm	ASTM D6992
Creep reduction factor		<3.5		ASTM D6992
Coefficient of thermal expansion (CTE)		≤80	ppm/°C	ISO 11359-2 ASTM E831
Flexural Storage Modulus at	30°C	>750	MPa	ISO 6721-1 ASTM E2254
	45°C	>650		
	60°C	>550		
	80°C	>300		
Oxidative Induction Time (OIT)		≥100	minutes	ISO 11375-6, ASTM D3895 (OIT @ 200°C, 35kPa)
Durability to UV Degradation		>400	minutes	ASTM D5885 (HPOIT @ 150°C, 3500kPa)

Figures 3.2.19 presents the shear stress-displacement curves for the geocell-RAP interface shear tests. For all the tests, shear stresses increased rapidly with increasing horizontal displacements for up to about 10 mm displacement, and then they increased marginally throughout the tests. Hence the only peak shear strength at each normal stress was observed and the residual strength was assumed equal to the peak shear strength. The observed peak shear strengths at different normal stresses are reported in Table 3.2.12 and the shear strength

envelop for interface shear tests is shown in Figure 3.2.20. The interface cohesion and friction angle were found to be 8.95 kPa and 11.06°, respectively.

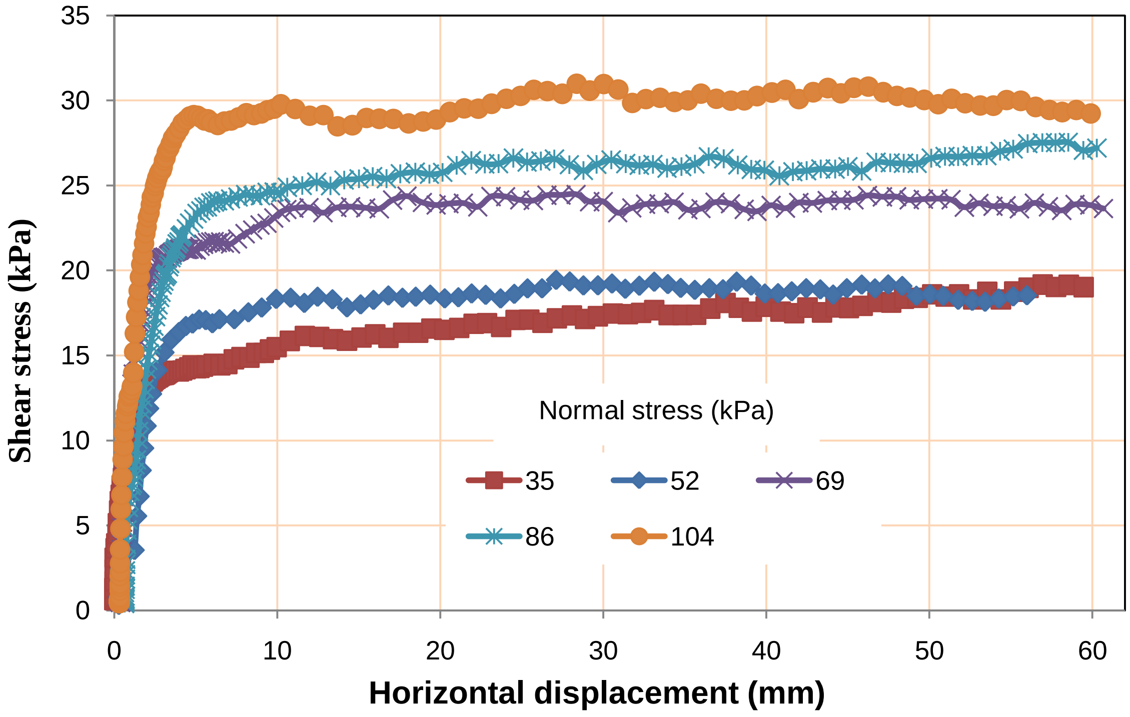

Figure 3.2.19 Shear stress-displacement behavior of geocell-RAP interface at different normal stresses

Table 3.2.12 Peak shear strengths at different normal stresses for interface shear tests

Normal stress (kPa)	Peak shear strength (kPa)
35	15.9
52	18.1
69	23.4
86	26.2
104	28.7

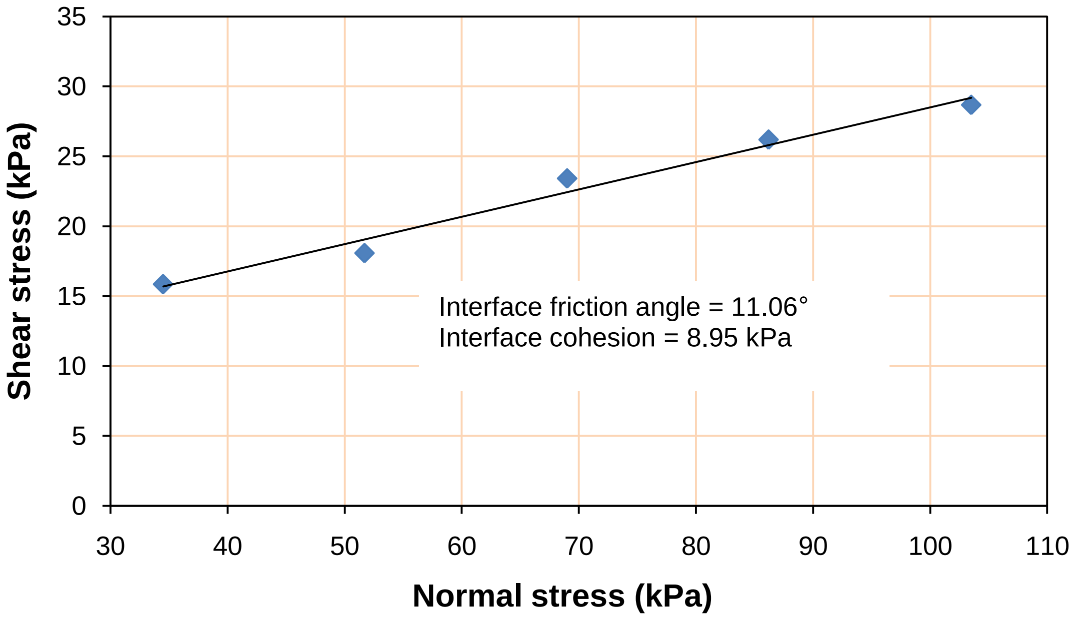

Figure 3.2.20 Shear strength envelope for interface shear tests

3.2.10 Large direct shear box test on RAP

Five direct shear tests were performed in accordance with ASTM D 5321-02 at five different normal stresses (i.e. at 35, 52, 69, 86, and 104 kPa) using the large direct shear box to determine the shear strengths of RAP at the moisture content corresponding to 98% compaction. The lower shear box was bigger in the plan area than the upper box having dimensions 30cm x 30cm x 10cm; however, the height of both boxes was equal. The tests were performed at a shear displacement rate of 0.254 mm per minute. The steps of the direct shear tests were same as those shown in Figure 3.2.18.

Figures 3.2.21 presents the shear stress-displacement curves for RAP. For all the tests, the shear stresses increased rapidly with increasing horizontal displacements for up to about 10 mm displacement, and then they increased marginally throughout the tests for some samples and for other samples they remained almost constant. Hence the only peak shear strength at each normal stress was observed and the residual strength was assumed equal to the peak shear strength. The observed peak shear strengths at different normal stresses are reported in Table 3.2.13 and the shear strength envelop for large direct shear tests is shown in Figure 3.2.22. The cohesion and friction angle of RAP were found to be 30.68 kPa and 12.90° respectively.

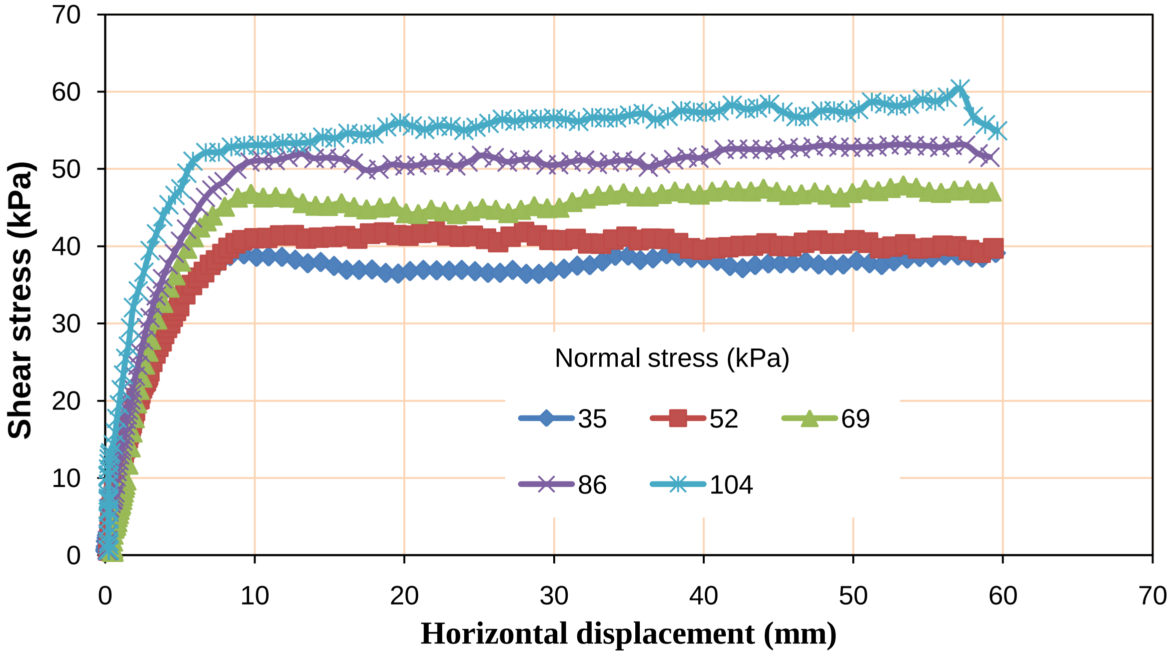

Figure 3.2.21 Shear stress-displacement behavior of RAP at different normal stresses

Table 3.2.13 Peak shear strengths at different normal stresses for direct shear tests

Normal stress (kPa)	Peak shear strength (kPa)
35	38.9
52	41.4
69	46.8
86	51.9
104	53.4

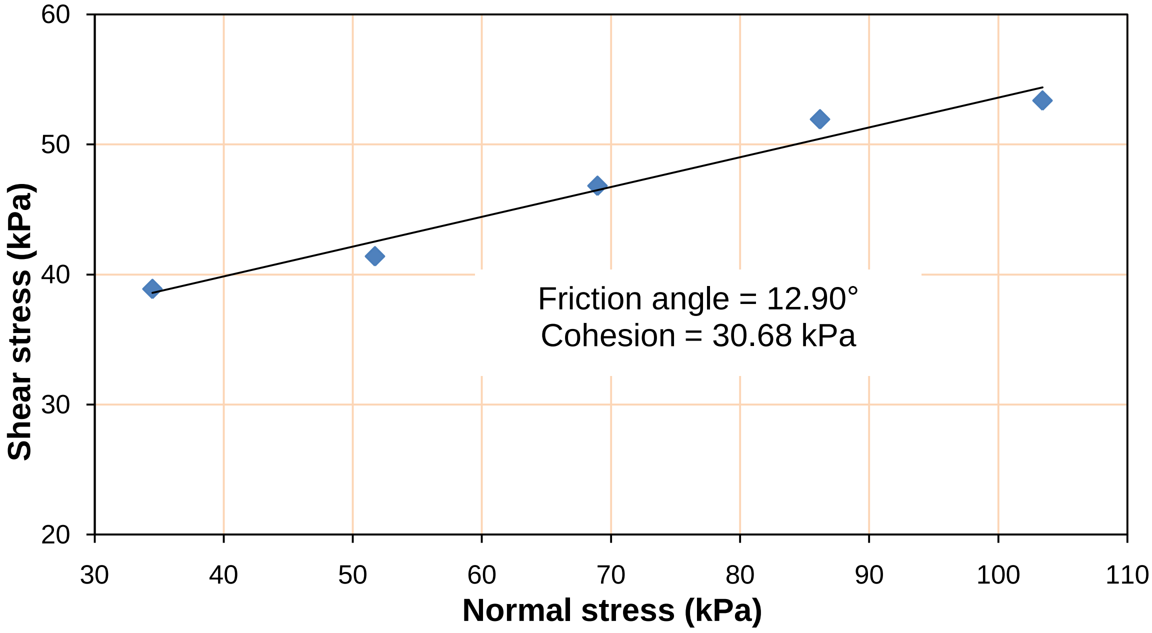

Figure 3.2.22 Shear strength envelope for direct shear tests

Interaction coefficient (C_i) between geocell and RAP and interface efficiencies of cohesion and friction angle were determined based on the results of interface and direct shear tests discussed above. Interaction coefficient and interface efficiencies of cohesion and friction angle were calculated using Equations 3.2.5, 3.2.6 and 3.2.7 respectively:

Interaction coefficient (C_i) = $\frac{\text{Interface shear strength}}{\text{RAP shear strength}}$ **(3.2.5)**

Interface efficiency on cohesion (E_c) = $\frac{\text{Interface cohesion of RAP to geocell}}{\text{Cohesion of RAP}}$ **3.2.6)**

Interface efficiency on friction angle (E_φ) = $\frac{\tan\ (\text{interface friction angle})}{\tan\ (\text{friction angle of RAP})}$ **(3.2.7)**

The interaction coefficients were calculated and are reported in Table 3.2.14.

Table 3.2.14 Interaction coefficient

Normal stress (kPa)	**Interface shear strength (kPa)**	**Shear strength of RAP (kPa)**	**Interaction coefficient (C_i)**	**Average interaction coefficient (C_i)**
35	15.9	38.9	0.41	0.48
52	18.1	41.4	0.44	
69	23.4	46.8	0.50	
86	26.2	51.9	0.50	
104	28.7	53.4	0.54	

The average interaction coefficient and interface efficiencies of cohesion and friction angle between geocell and RAP were found to be 0.477, 0.292, and 0.853, respectively.

3.3 Conclusions

Different properties of RAP and geocell were evaluated by the laboratory tests and are summarized below:

(i) The binder content of RAP was found to be 6.71% and 6.87 % by the centrifuge method and the ignition method respectively and it was found that the binder content by the ignition method was slightly higher than that by the centrifuge method

(ii) The maximum size, mean size (d_{50}), coefficient of curvature (C_c), and coefficient of uniformity (C_u) of RAP aggregate were found to be 12.5 mm, 2.0 mm, 0.85, and 8.33 respectively.

(iii) Bulk specific gravity, SSD Bulk specific gravity, and apparent specific gravity of fine aggregates were found to be 2.484, 2.557, and 2.592 respectively and those of coarse aggregates were 2.390, 2.487, and 2.585 respectively. It is shown that the fine aggregate had a higher specific gravity than the coarse aggregate.

(iv) The uncompacted void content of the fine aggregate extracted from RAP was found to be 39.15%.

(v) The kinematic viscosity of the asphalt binder at 135°**C** was found to be 1.408 Pa-s.

(vi) The maximum dry density of RAP based on the modified Proctor tests was found to be 1.96 g/cm^3, which corresponds to the optimum moisture content (OMC) of 6.6%.

(vii) The CBR of RAP at the moisture content corresponding to 98% was found to be 24.8%.

(viii) The minimum and maximum index densities were found to be 1.415 g/cm^3 and 1.740

g/cm^3 respectively.

(ix) The geocell-RAP interface cohesion and friction angle were found to be 8.95 kPa and 11.06° respectively. In addition, the cohesion and friction angle of RAP were found to be 30.68 kPa and 12.90° respectively.

(x) The average interaction coefficient between geocell and RAP and interface efficiencies of cohesion and friction angle were found to be 0.477, 0.292, and 0.853 respectively.

CHAPTER 4

CREEP TESTS OF GEOCELL-REINFORCED RAP

The chapter describes the pressure-displacement response, stiffness, and creep behavior of unreinforced and reinforced recycled asphalt pavement (RAP) bases and the various factors affecting the creep of RAP bases such as degree of confinement, applied vertical stresses, and fill cover to the RAP bases.

4.1 Materials used

The same RAP whose properties were evaluated and presented in Chapter 3 was used as the base material. The same NPA geocell described in Chapter 3 was used for confinement. The AB-3 aggregate was used as the cover material for one test section, i.e. single geocell-confined and embedded RAP. This AB-3 aggregate was obtained from Hamm Quarry Inc. located in North Lawrence, Kansas. The grain-size distribution of AB-3 is shown in Figure 4.1.1. The mean particle size (d_{50}), liquid limit, plastic limit, specific gravity at $20^{o}C$, optimum moisture content, and maximum dry density of the AB-3 aggregate were 7.0 mm, 20, 13, 2.69, 10% and 2.08 g/cm^3 respectively. The results of the standard Proctor compaction tests and the CBR tests for the AB-3 are shown in Figures 4.1.2 and 4.1.3 respectively. The CBR values were 75% at 7.1% moisture content and 46% at the optimum moisture content respectively.

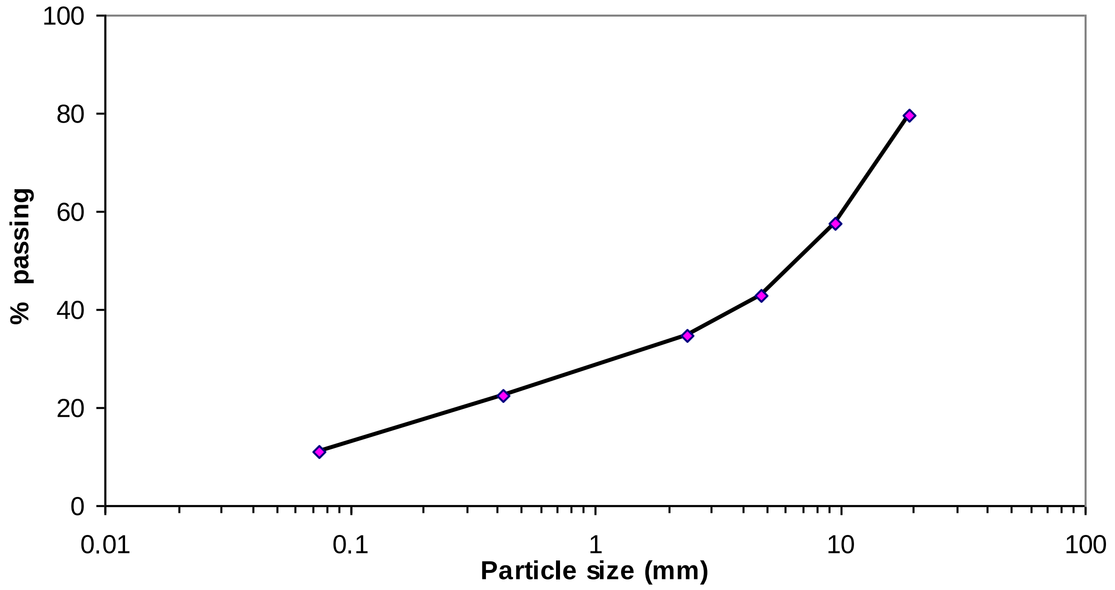

Figure 4.1.1 Grain-size distribution curve of AB-3 aggregate (From Pokharel, 2010)

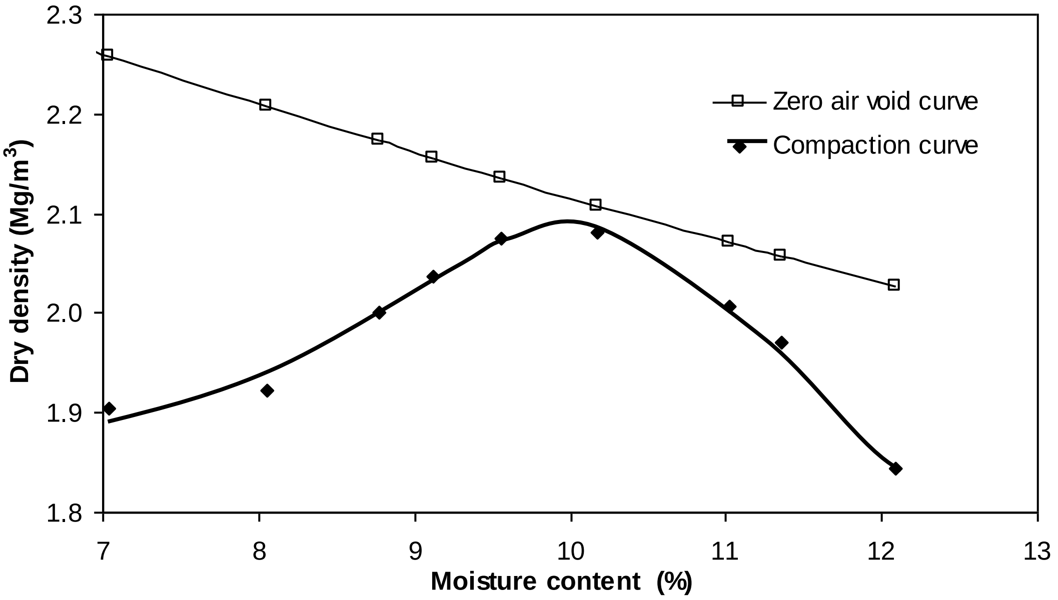

Figure 4.1.2 Standard Proctor compaction curve of AB-3 aggregate

(From Pokharel, 2010)

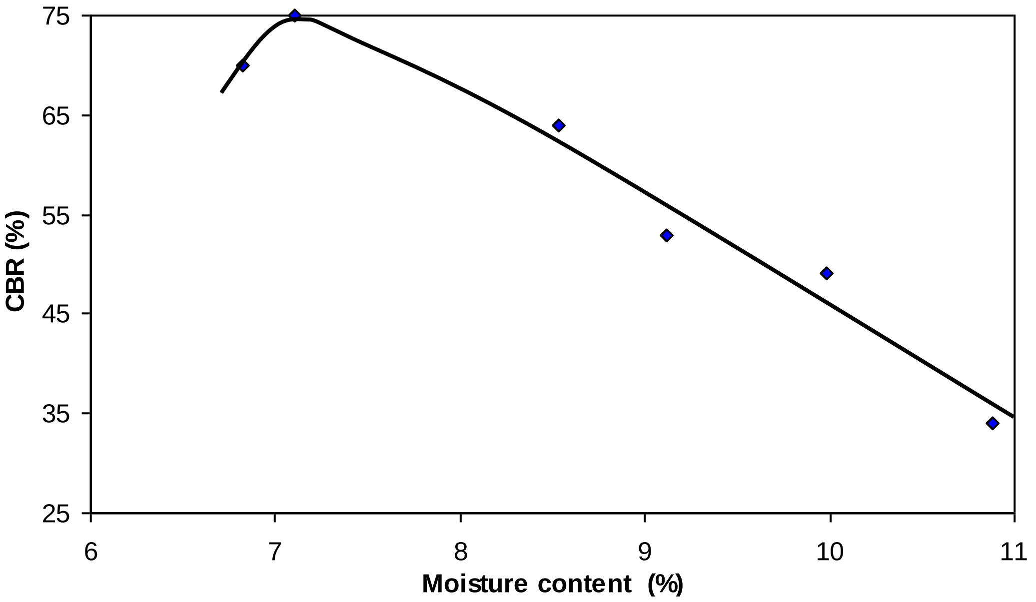

Figure 4.1.3 CBR curve of AB-3 aggregate (From Pokharel, 2010)

4.2 Static plate load tests

Nineteen plate loading tests were performed in a test box A (60.5 cm x 60.5 cm x 15 cm high), a test box B (80 cm x 80 cm x 15 cm high), and a compaction mold using a medium-size loading system to evaluate the stiffness, pressure-displacement response, and creep behavior of unreinforced and reinforced RAP bases. In addition, an unconfined compression test was conducted to determine the maximum load the RAP sample extruded from the compaction mold could sustain. Due to the low unconfined compression strength, no creep test was performed on any unreinforced unconfined RAP sample. The pressure-displacement response and the factors affecting creep of RAP bases were discussed. The novel polymeric alloy (NPA) geocells of 10 cm high were used in this study for reinforcement of RAP bases.

4.2.1 Test equipment and setup

The plate loading tests were performed in a medium size loading system designed and fabricated for the geotechnical laboratory at the Department of Civil, Environmental, and Architectural Engineering at the University of Kansas. The loading system had a 15-cm diameter air cylinder with a maximum air pressure of 900 kPa. The loading plate was 15 cm in diameter. The details of test boxes A and B are shown in Figures 4.2.1 and 4.2.2. The smaller square box (Box A) having plan area of 3660 cm^2 was used for unreinforced and single geocell reinforced RAP bases whereas the bigger square box (Box B) having plan area of 6400 cm^2 was used for multi geocell-reinforced RAP bases.

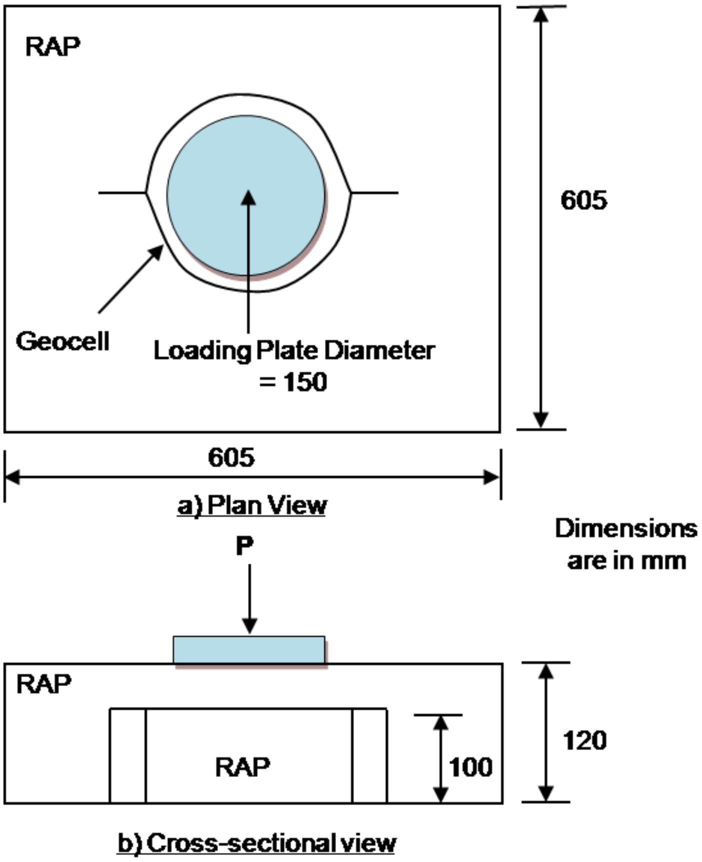

Figure 4.2.1 Set up for unreinforced and single geocell-reinforced bases

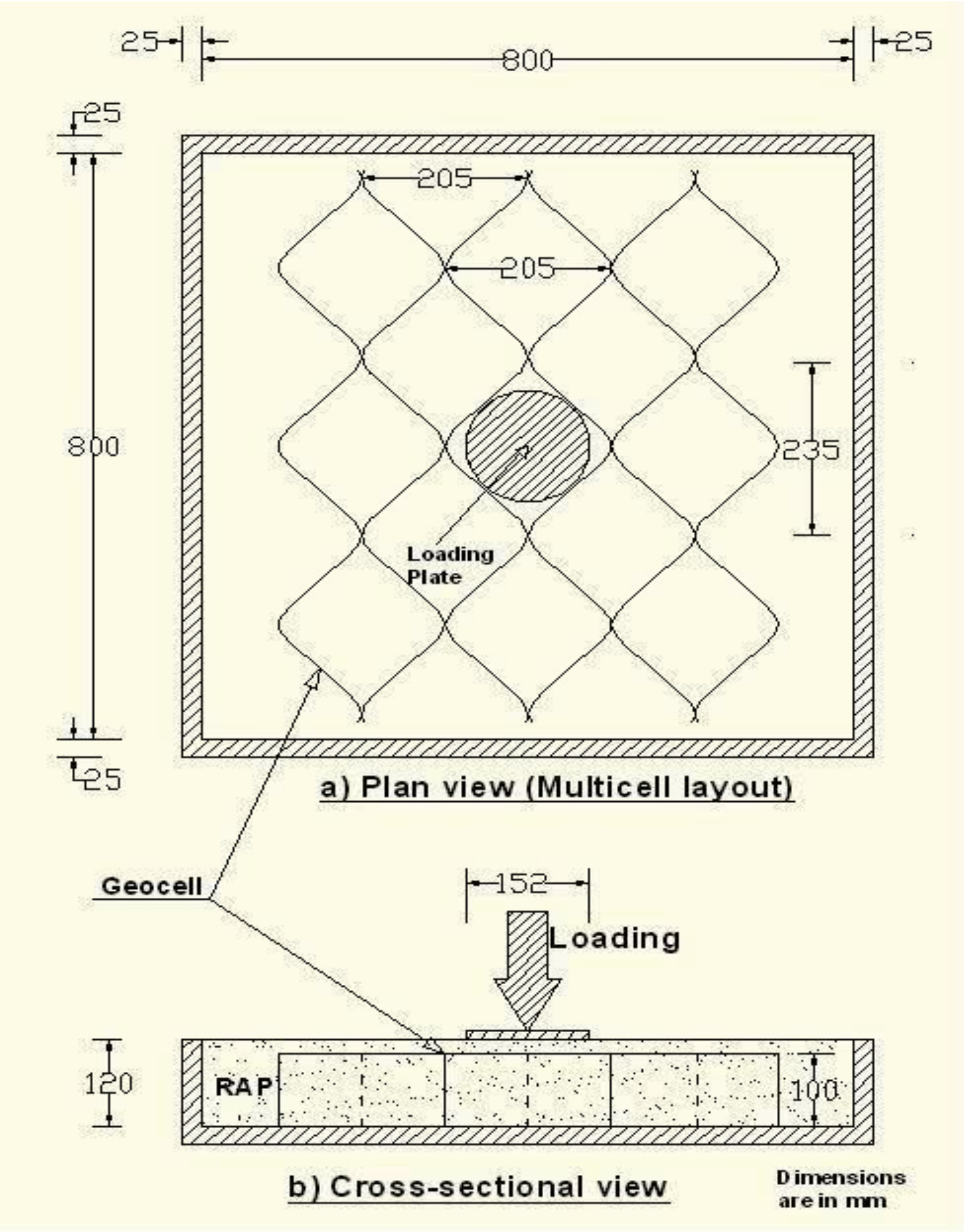

Figure 4.2.2 Set up for multi geocell-reinforced bases (Modified from Pokharel, 2010)

The plate load tests were conducted under five different confining conditions: unreinforced confined RAP, single geocell-confined but not embedded, single geocell-confined and embedded, multi geocell-confined and embedded, and fully confined RAP in a compaction mold as shown in Figures 4.2.3, 4.2.4, 4.2.5, 4.2.6, and 4.2.7 respectively. The loading system is shown in Figure 4.2.8.

Figure 4.2.3 Unreinforced confined RAP

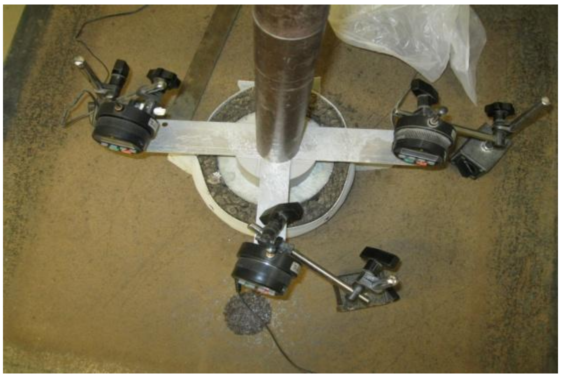

Figure 4.2.4 Single geocell-confined but not embedded

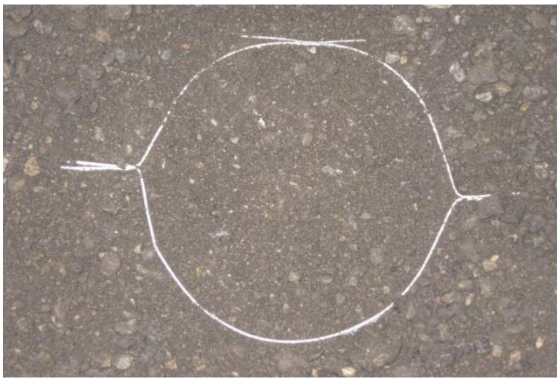

Figure 4.2.5 Single geocell-confined and embedded

Figure 4.2.6 Multi geocell-confined and embedded

Figure 4.2.7 Fully confined RAP in a compaction mold

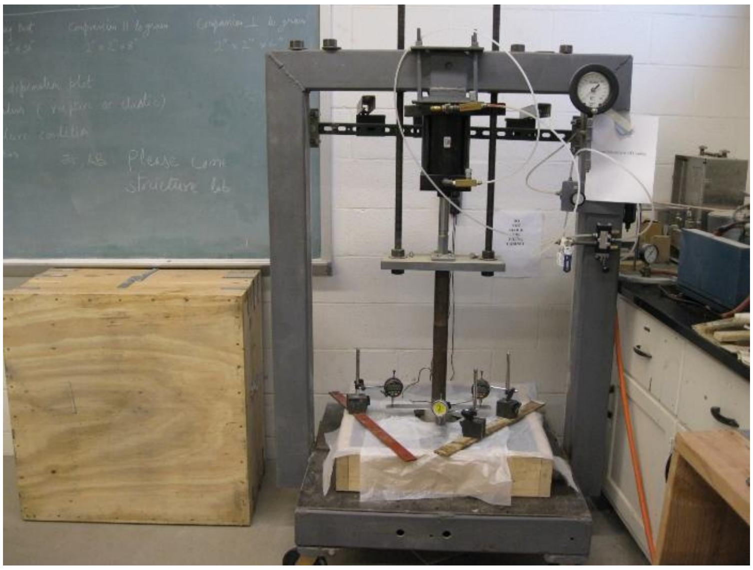

Figure 4.2.8 Loading system

For unreinforced confined RAP tests, no geocell was included. RAP was placed into the box A and compacted to 98% of the maximum density on the drier side of the compaction curve in three layers (4 cm each for the 12 cm thick RAP section) and in two layers (5 cm each for the 10 cm thick RAP section). For single geocell-confined but not embedded RAP tests, the geocell was prepared in a nearly circular shape with a diameter of 20.5 cm and RAP was placed into the geocell and compacted to 98% of the maximum density on the drier side of the compaction curve in two layers (5 cm each). For single geocell-confined and embedded RAP tests, the geocell was placed at the center of the box A in a nearly circular shape with a diameter of 20.5 cm and RAP was placed into the geocell and the box and compacted to 98% of the maximum density on the drier side of the compaction curve in two 5-cm and one 2-cm lifts for 12 cm thick sections and in two 5-cm lifts for 10 cm thick sections. For multi geocell-confined and embedded RAP tests, geocells having 13 pockets were placed at the center of Box B, each pocket in a nearly circular shape and RAP was placed into the geocells and the box and compacted to 98% of the maximum density on the drier side of the compaction curve in two 5-cm and one 2-cm lifts for 12 cm thick sections and in two 5-cm lifts for 10 cm thick sections. Desired compaction was achieved by tamping an exact amount of RAP sample calculated based on specific volume and density. For the fully confined RAP, the sample was prepared following the modified Proctor compaction test. The unreinforced unconfined RAP sample for the unconfined compression test was obtained by extruding the compacted RAP sample from the compaction mold.

4.2.2 Pressure-displacement response

An unconfined compression test was conducted to determine the maximum load the RAP sample could sustain. The RAP sample was compacted using the modified Proctor compaction hammer and was extruded from the compaction mold. The height and diameter of the sample were 120 and 150 mm, respectively. Loads were applied through a rigid metal plate on the unconfined RAP sample in increments by adjusting air pressure in the air cylinder. The deformations in two perpendicular transverse directions (Fig. 4.2.4) were measured with three digital dial gauges mounted on the loading plate and averages of three were used for calculation. The deformation of the sample corresponding to each load at every five-minute interval was recorded. The stress at which the sample failed was determined. Due to the low unconfined compression strength, no creep test was performed on any unreinforced unconfined RAP sample.

In addition, five plate loading tests were conducted by a loading system on unreinforced confined RAP, single geocell-confined and embedded RAP, and multi geocell-confined and embedded RAP bases to understand the pressure-displacement responses of the RAP bases under different confining conditions. The height of each test section was 12 cm. Loads were applied on a rigid metal plate in increments by adjusting air pressure in the air cylinder. Deformations in two perpendicular transverse directions were measured with three digital dial gauges mounted on the loading plate and averages of three were used for calculation. The deformation of the plate corresponding to each load at every five-minute interval was recorded. The pressure at which the RAP failed was determined.

The applied pressure versus displacement curves for the unconfined compression test and the plate loading tests on the RAP were shown in Figures 4.2.9 and 4.2.10 respectively. It is found that the unreinforced unconfined RAP failed at 172 kPa and other sections did not fail up to 586 kPa vertical pressure and showed linear pressure-displacement behavior. Therefore, the confinement of the RAP sample significantly increased the strength of the sample. This finding is in an agreement with that obtained by Pokharel et al. (2010).

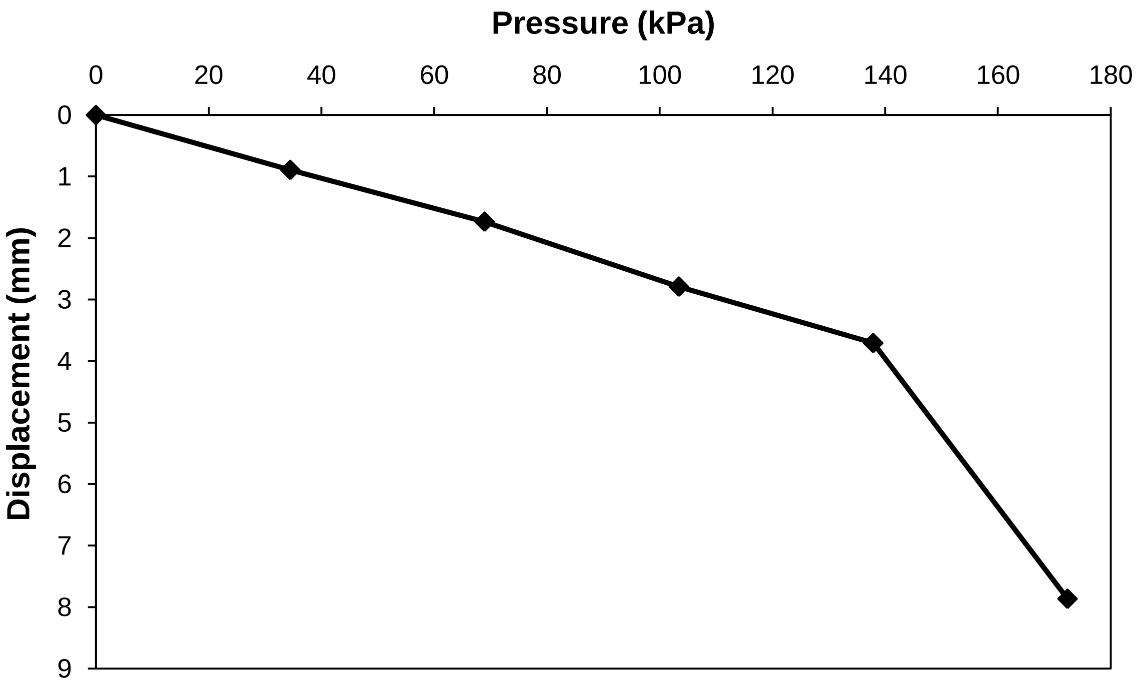

Figure 4.2.9 Pressure-displacement curve for the unconfined compression test

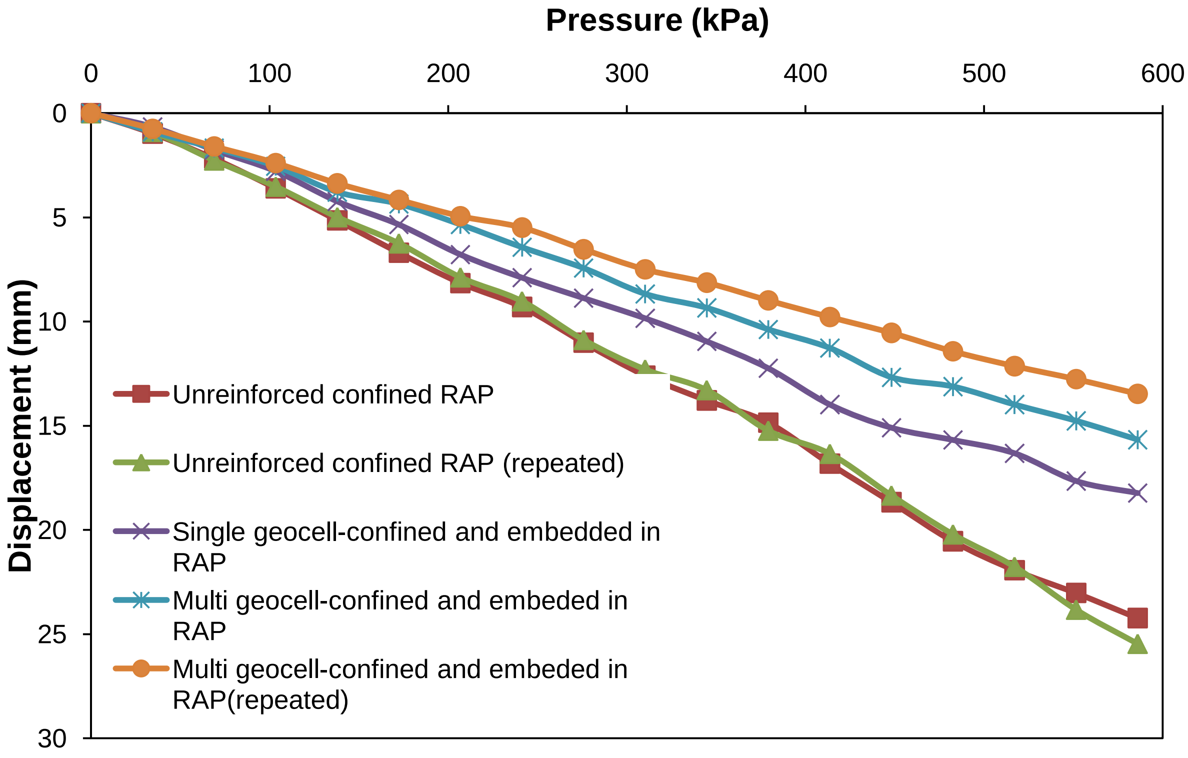

Figure 4.2.10 Pressure-displacement curves for plate load tests

The above plate load test results were further discussed in terms of stiffness improvement factor. The stiffness improvement factor is the ratio of the slope of the initial portion of the pressure-displacement curve for the reinforced confined base to that of the unreinforced confined base. The stiffness of single geocell-confined and embedded RAP and multi geocell-confined and embedded RAP bases increased by 1.2 and 1.6 times compared to unreinforced confined RAP bases respectively.

4.2.3 Creep tests

The creep tests were conducted at a room temperature of about 25°**C** on the following samples using the same loading system discussed above: unreinforced confined RAP (12 cm thick), single geocell-confined but not embedded (10 cm thick), single geocell-confined and embedded (10 cm and 12 cm thick), multi geocell-confined and embedded (10 cm thick), and fully confined RAP in a compaction mold (12 cm thick). The creep tests were performed on these samples to investigate the confinement effect in creep deformation of RAP bases. The pressures were maintained at 276 kPa (half of the typical highway truck tire pressure of 552 kPa and a typical vertical stress in base courses in paved roads under wheel loading) and at 552 kPa in the creep test for each test about 7 to 10 days to investigate the stress effect in creep behavior of RAP. The displacement with time was monitored during each test. The measured displacements were used to calculate axial strains. The axial stresses versus time curves are plotted to demonstrate different factors affecting creep behavior of RAP bases.

In order to verify the repeatability of the test method, two repeated creep tests were conducted at 276 kPa vertical stress for unreinforced confined RAP and single geocell-confined but not embedded RAP. Figure 4.2.11 demonstrates that the test method used in this study is repeatable.

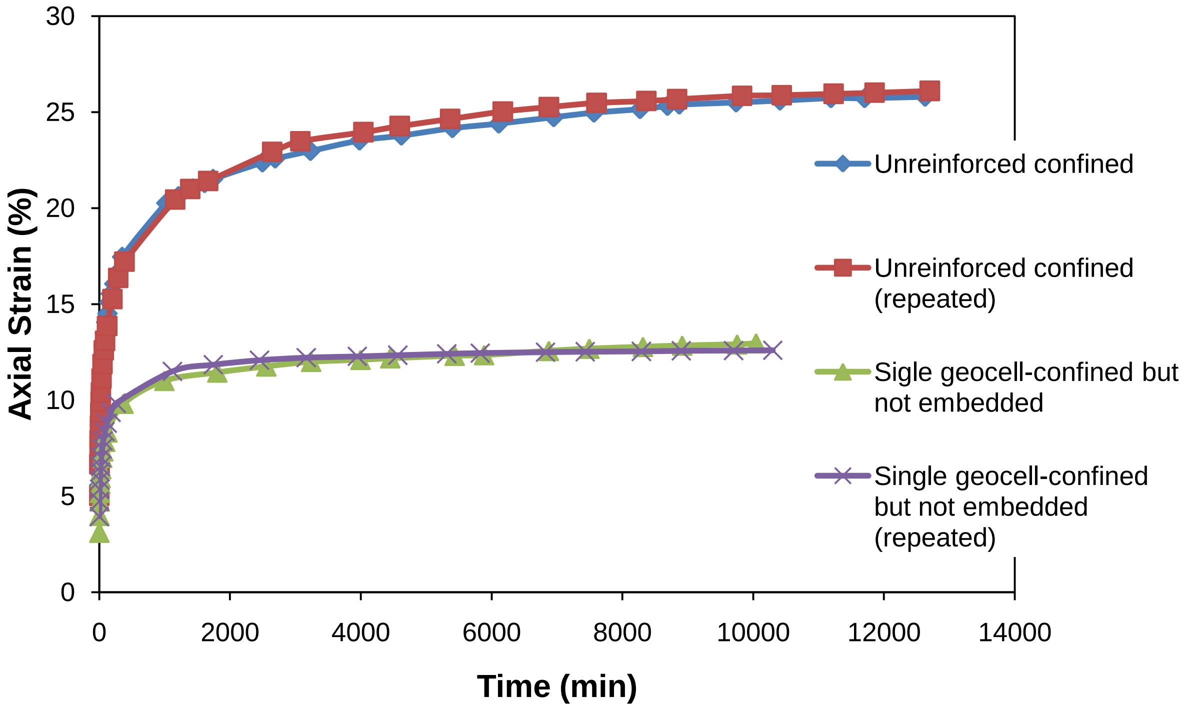

Figure 4.2.11 Repeatability of test method

The axial strain versus time curves for RAPs at five confining conditions at 276 kPa and 552 kPa vertical stresses are presented in Figures 4.2.12 and 4.2.13 respectively to demonstrate the confining and stress effects on creep behavior of RAP bases. Unreinforced confined and fully confined samples were 12 cm thick whereas all geocell-reinforced samples were 10 cm thick. It is shown that the unreinforced confined RAP had the largest initial deformation within the first few minutes. The NPA geocell-confined but not embedded RAP significantly reduced the initial deformation as compared with the unreinforced confined RAP. The creep deformations were further reduced by increasing the degree of confinement with the embedment of single geocell and multi geocell in RAP. The full confinement by the rigid compaction mold further reduced the initial deformation in the greatest amount. It was also found that the RAP bases at 552 kPa deformed more compared to 276 kPa under the same confining conditions. It was found that RAP bases crept more at higher vertical stresses and lower degree of confinement and vice versa.

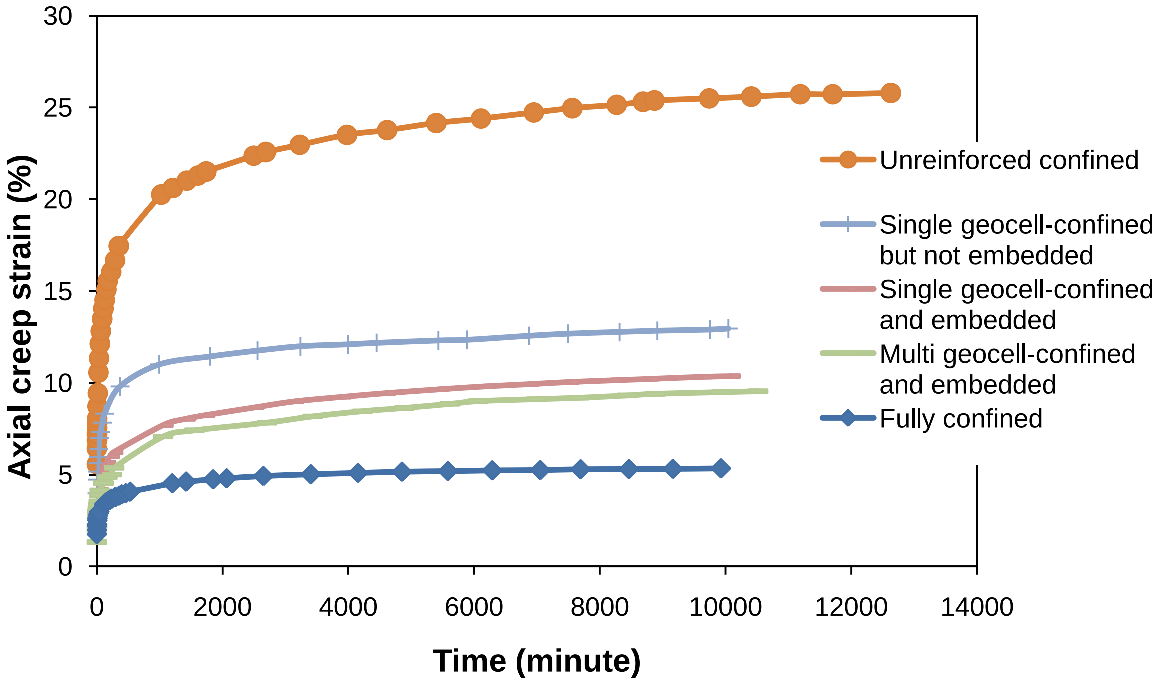

Figure 4.2.12 Creep behavior at 276 kPa vertical stress

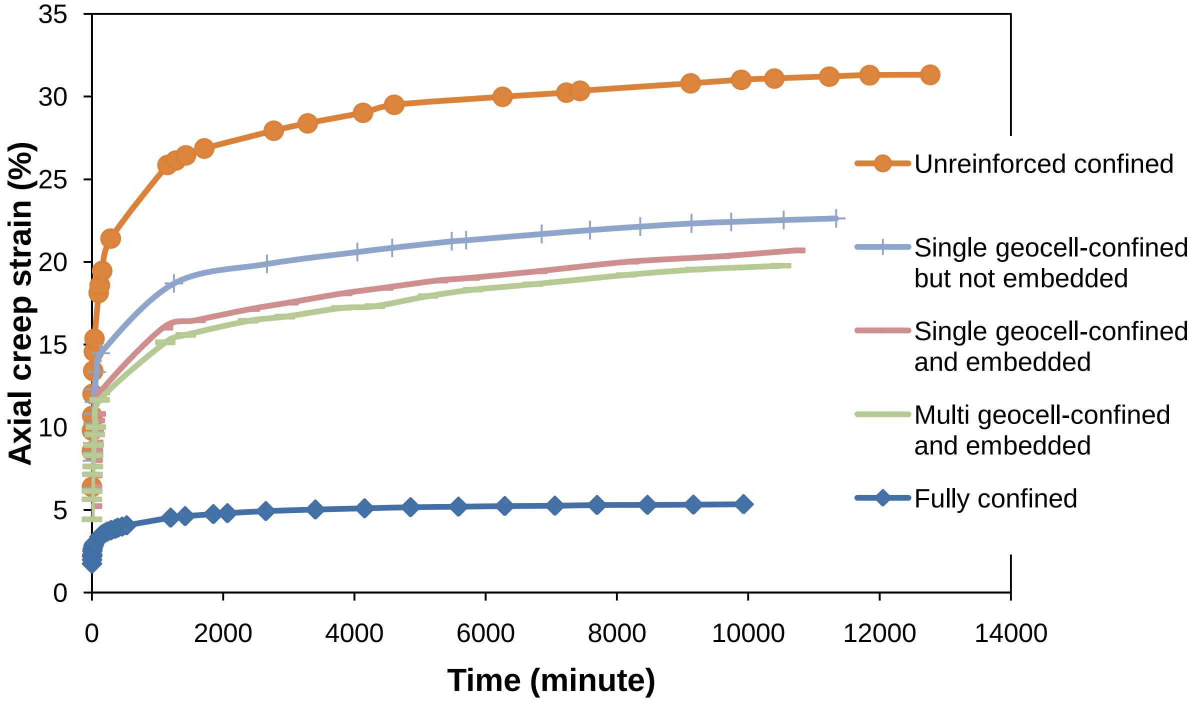

Figure 4.2.13 Creep behavior at 552 kPa vertical stress

Single geocell-confined and embedded RAP sections were tested at 276 kPa vertical stress under the following three different conditions: without cover, with 2 cm RAP cover, and with 2 cm AB-3 cover to investigate the cover effect on creep deformations of RAP bases. The total height of the section without a cover was 10 cm and that with a cover was 12 cm. The axial strain versus time curves are presented in Figure 4.2.14 to demonstrate the cover effect. The section with a RAP cover had the largest initial deformation within the first few minutes. Considering AB-3 as a rigid and low creep material, it was found that the section with the AB-3 cover had nearly the same creep deformation as that without a cover. When AB-3 was assumed to have the same deformation behavior as RAP, the axial strain was found to be the least which demonstrated that there was some deformation in AB-3 also but in lesser amount compared to RAP. The AB-3 cover significantly reduced the initial deformation as compared with the RAP cover. For practical purposes, it is necessary to provide a cover to prevent damage to the geocells, hence the AB-3 should be used as a cover material instead of RAP to reduce creep deformation of RAP bases.

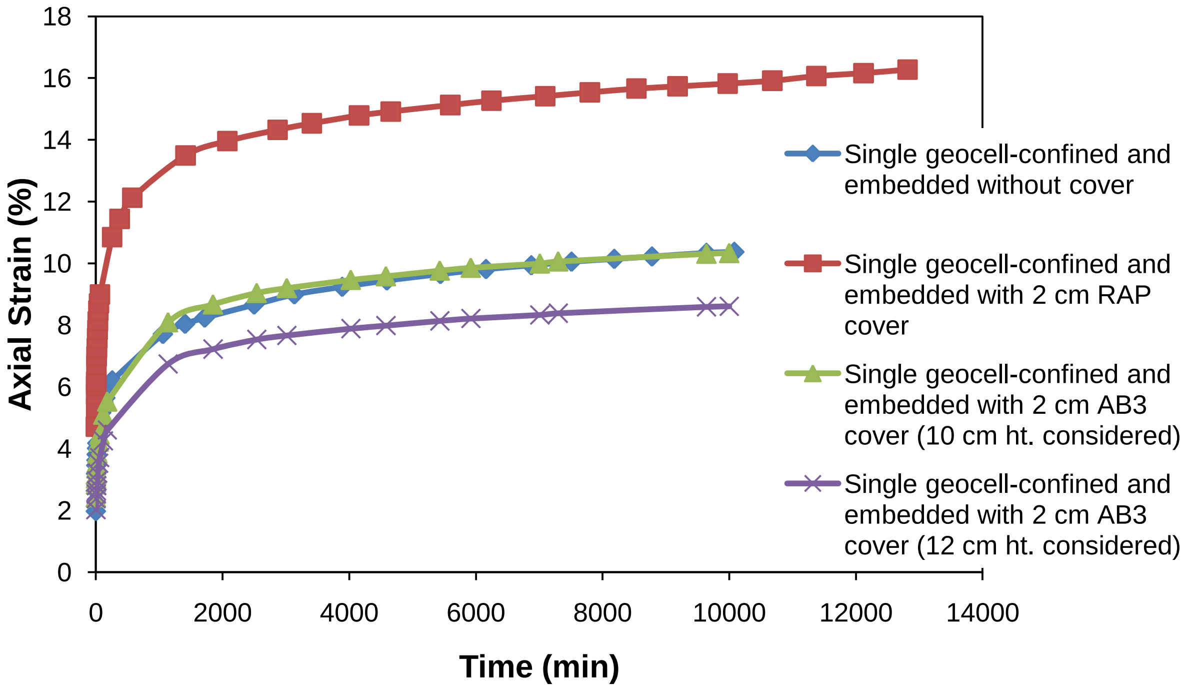

Figure 4.2.14 Cover effect in creep deformations of RAP bases

The creep behavior of the RAP can further be evaluated by calculating the slope of the curve as the rate of creep (Cosentino et al., 2003). In Cosentino et al. (2003)'s study, the slopes of the curves were calculated between 1,000 and 4,000 minutes because the curve became linear within this range. In this study, however, the curve became linear after 2,000 minutes; therefore, the slopes of the curves were calculated between 2,000 and 9,000 minutes. The slopes of the curves expressed in percent per minute, under five confining conditions at two vertical stresses, are presented in Table 4.2.1. It is clearly shown that the unreinforced confined RAP had the largest creep rate, followed by the geocell-reinforced confined RAP, and the fully confined RAP. However, the single geocell confined but not embedded sample showed a lower creep rate than other geocell confined and embedded samples. This may be due to the fact that for the geocell confined and embedded sample, when the gecocell was mobilized, the stress was transferred to the surrounding RAP through the geocell and the creep rate of RAP was higher than that of the geocell. The creep rate for the fully confined RAP is similar to that obtained by Cosentino et al. (2003).

Table 4.2.1 Slopes of axial creep strain versus time curve (between 2,000 and 9,000 minutes)

Stress Level (kPa)	Test Sample	Slope of Curve (%/min)
572	Fully confined	7.1E-5
	Multi geocell-confined and embedded	4.9E-4
	Single geocell-confined and embedded	4.9E-4
	Single geocell-confined but not embedded	4.4E-4
	Unreinforced confined	5.2E-4
276	Fully confined	7.1E-5
	Multi geocell-confined and embedded	2.6E-4
	Single geocell-confined and embedded	2.7E-4
	Single geocell-confined but not embedded	2.0E-4
	Unreinforced confined	5.0E-4

4.3 Conclusions

The following conclusions can be made from this study:

(i) The confinement of the RAP sample significantly increased the strength of the sample.

(ii) The stiffness values of single geocell-confined and embedded RAP and multi geocell-confined and embedded RAP bases were increased by 1.2 and 1.6 times compared to those of the unreinforced confined RAP bases respectively.

(iii) The novel polymeric alloy geocell significantly reduced the initial deformation and the rate of creep of the RAP and further reduction could be achieved if the RAP was fully confined.

(iv) The creep deformations decreased with an increase in the degree of confinement and a decrease in the applied vertical stress.

(v) The well-graded aggregate AB-3 cover significantly reduced the creep of geocell-confined RAP bases.

CHAPTER 5

LARGE-SCALE CYCLIC PLATE LOAD TESTS

5.1 Test Materials

5.1.1 Geosynthetics

The NPA geocells of heights at 10 cm and 15 cm were used to reinforce RAP bases and a 3.5 oz (99.65 g) non-woven geotextile was placed at the interface of subgrade and base course as a separator in all the test sections. The properties of geocells were presented in Chapter 3.

5.1.2 Base material

The same RAP, the properties of which were evaluated and presented in Chapter 3, was used as the base material. The RAP base was compacted at 5.5% moisture content to achieve 95% of the maximum dry density.

5.1.3 Subgrade material

Subgrade was prepared artificially by mixing 25% Kaolin and 75% Kansas River (KR) sand (Pokharel, 2010). The KR sand used in this study was a poorly-graded sub-rounded river sand having a mean particle size (d_{50}) = 0.54 mm, coefficient of curvature (Cc) = 0.95, coefficient of uniformity (C_u) = 3.1, and specific gravity = 2.62 (Pokharel, 2010). The grain-size distribution of KR sand is shown in Figure 5.1.1. Six standard Proctor compaction tests were performed at different moisture contents to obtain the compaction curve for this subgrade as shown in Figure 5.1.2. The maximum dry density of the mix was 2.01 g/cm^3, which corresponds to the optimum moisture content of 10.8%. Six laboratory unsoaked CBR tests were performed on the laboratory compacted subgrade at different water contents to obtain the CBR versus moisture content curve as shown in Figure 5.1.3.

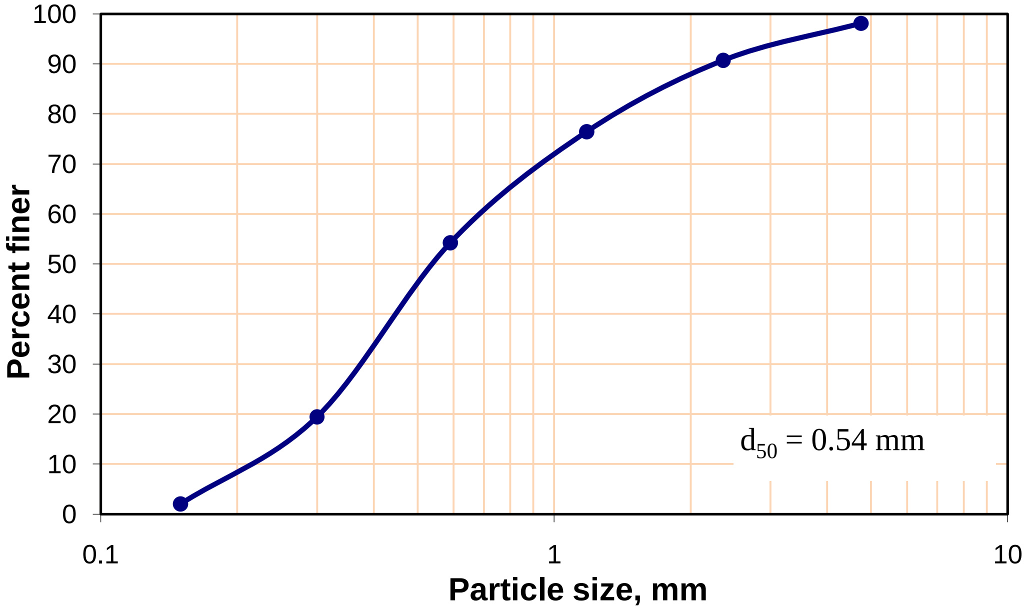

Figure 5.1.1 Gradation curve of Kansas River sand (From Pokharel, 2010)

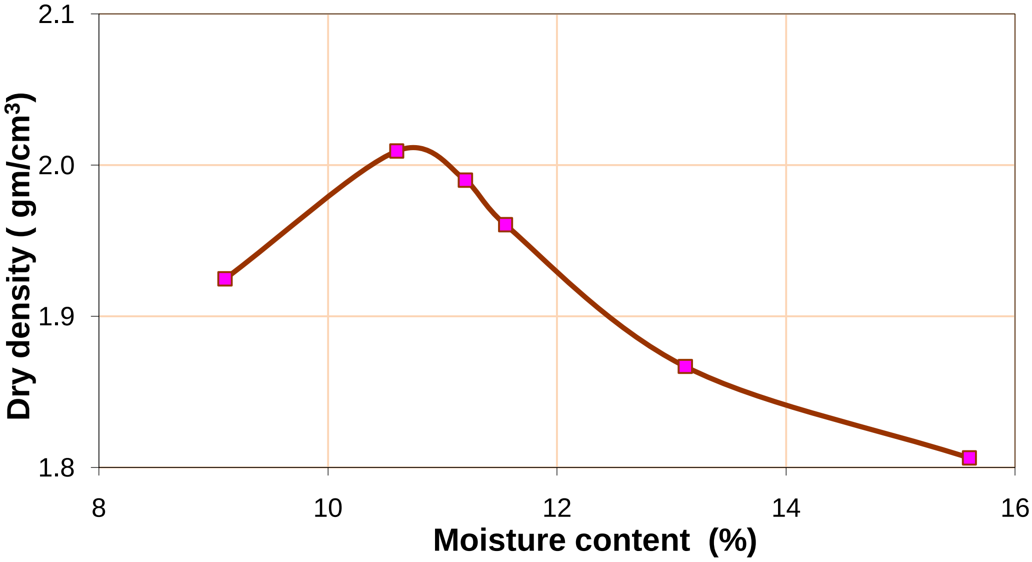

Figure 5.1.2 Standard Proctor compaction curve of subgrade (From Pokharel, 2010)

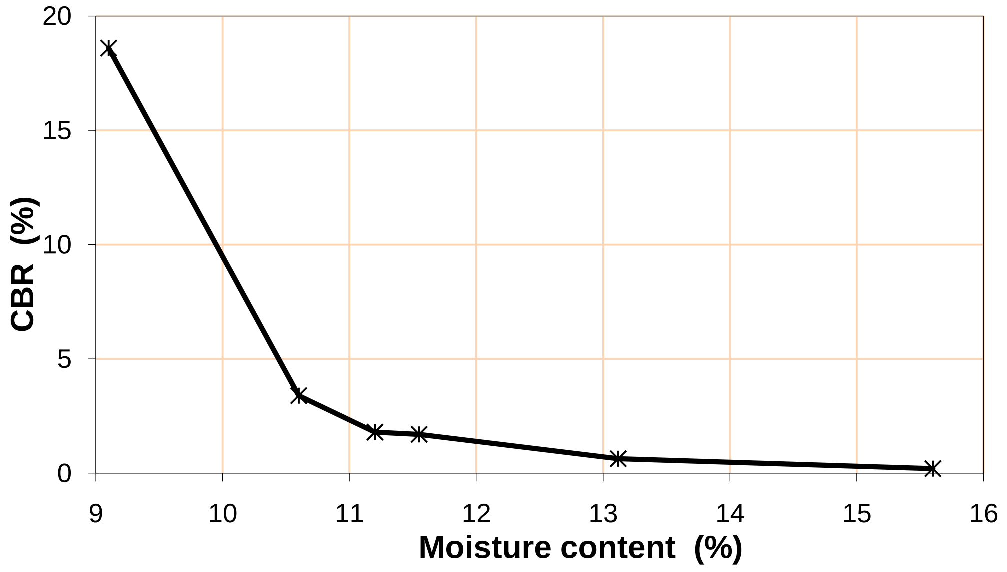

Figure 5.1.3 CBR versus moisture content curve of subgrade (From Pokharel, 2010)

5.2 Test setup and instrumentation

Nine cyclic plate loading tests were conducted in a large geotechnical test box system designed and fabricated for the geotechnical laboratory at the Department of Civil, Environmental, and Architectural Engineering at the University of Kansas. These tests were conducted on unreinforced RAP bases (15 and 30 cm thick) and reinforced bases (15, 23, and 30 cm thick) using a servo hydraulic MTS loading system. This system includes a loading actuator, a large steel box, and a data acquisition system. The instrumentation and data acquisition system included earth pressure cells, displacement transducers, and strain gages. Figure 5.2.1 shows the schematic diagram for the setup of a cyclic plate load test.

A servo hydraulic MTS loading system consists of a loading frame, a hydraulic actuator, and a servo-control unit connected to both a data acquisition system and a hydraulic control valve. The loading plate made of steel had 304 mm in diameter and 30 mm in thickness. In addition, a 10 mm thick rubber base was attached at the bottom of the loading plate to simulate rubber tire contact. The cyclic loads with a peak force of 40 kN and a trough force of 0.5 kN were applied at a wave frequency of 0.77 Hz as shown in Figure 5.2.2. The peak load was selected to simulate a single wheel load of 40 kN (equivalent to an axle load of 80kN and a tire contact pressure of 550 kPa).

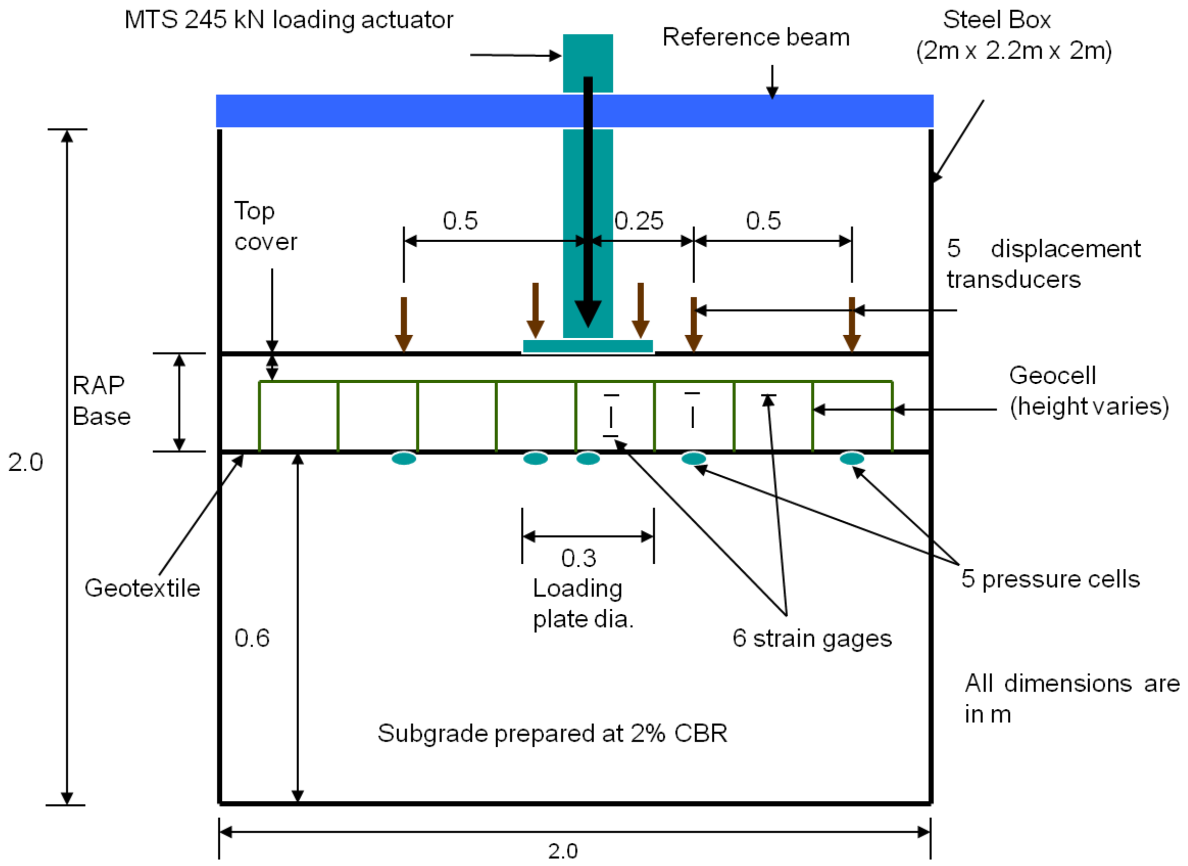

Figure 5.2.1 Schematic diagram for the set up of cyclic plate load test (From Pokharel, 2010)

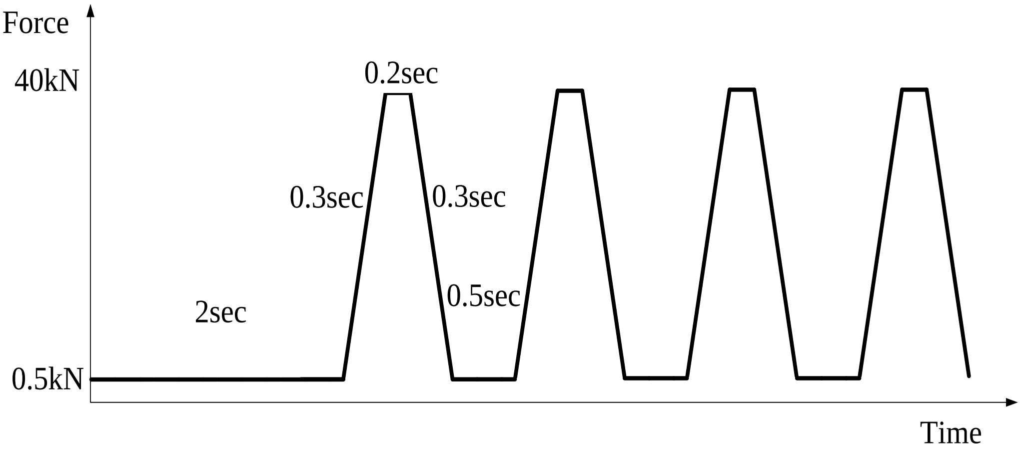

Figure 5.2.2 Cyclic loading wave (From Pokharel, 2010)

The subgrade was placed and compacted in four layers (15 cm thick for each layer) using a vibratory plate compactor at the moisture contents of 11.4% and 10.4% to obtain target CBR values of approximately 2% and 5%, respectively. The vibratory plate compactor was connected to electric supply and desired compaction was achieved by applying a number of passes until the required strength of subgrade was achieved. The required subgrade was checked by conducting vane shear tests.

A hand-operated vane shear test device was used for controlling the uniformity of the subgrade soil. The vane shear test device directly measured the undrained shear strength (C_u) of the subgrade, and then the subgrade CBR was estimated by using the correlation developed by Pokharel (2010) as follows:

$$\text{CBR} = \frac{C_u}{20.5} \qquad \textbf{(5.2.1)}$$

where, C_u = undrained shear strength of subgrade in kPa

After preparing the subgrade at a desired CBR, five strain gauge type earth pressure cells having 11.3 mm in thickness, 50 mm in outer diameter, 46 mm in sensing area diameter, and

160 g weight were installed on top of the subgrade. It was planned to install five pressure cells for each test. But due to a limited number of pressure cells available for some tests, only four pressure cells were installed. The earth pressure cells having the maximum capacity of 500 kPa and 250 kPa were installed at the center and away from the center of the loading plate, respectively.

The geotextile was placed at the interface between the subgrade and the base course in each test section and the geocell installed with strain gauges were placed on top of the geotextile for a reinforced section (Figure 5.2.3). The layout of geocell installation is shown in Figure 5.2.4. For the 15 cm thick unreinforced RAP base, RAP was placed into the box and was compacted by a vibratory plate compactor in 8 cm and 7 cm lifts. For the 30 cm thick unreinforced RAP base, RAP was placed into the box and was compacted by a vibratory plate compactor in three layers (10 cm each). For the 15 cm and 23 cm thick geocell-reinforced RAP bases, 10 cm high and 15 cm high geocells were installed respectively on top of a geotextile, filled with RAP, and then compacted by hand tamping (Figure 5.2.5). RAP covers of about 5 and 8 cm were used in 15 and 23 cm thick sections respectively for the protection of geocells. The cover materials were compacted by a vibratory plate compactor. Similarly, the 30 cm thick reinforced section was prepared in four lifts (i.e. 10 cm geocell plus 3 cm cover and 10 cm geocell plus 7 cm cover). For each base section, the RAP material of every lift was compacted at 5.5 % moisture content to obtain 95 % of the maximum density. Desired compaction was achieved by compacting an exact amount of the RAP sample calculated based on specific volume and density.

Figure 5.2.3 Geotextile and geocell installed on top of subgrade

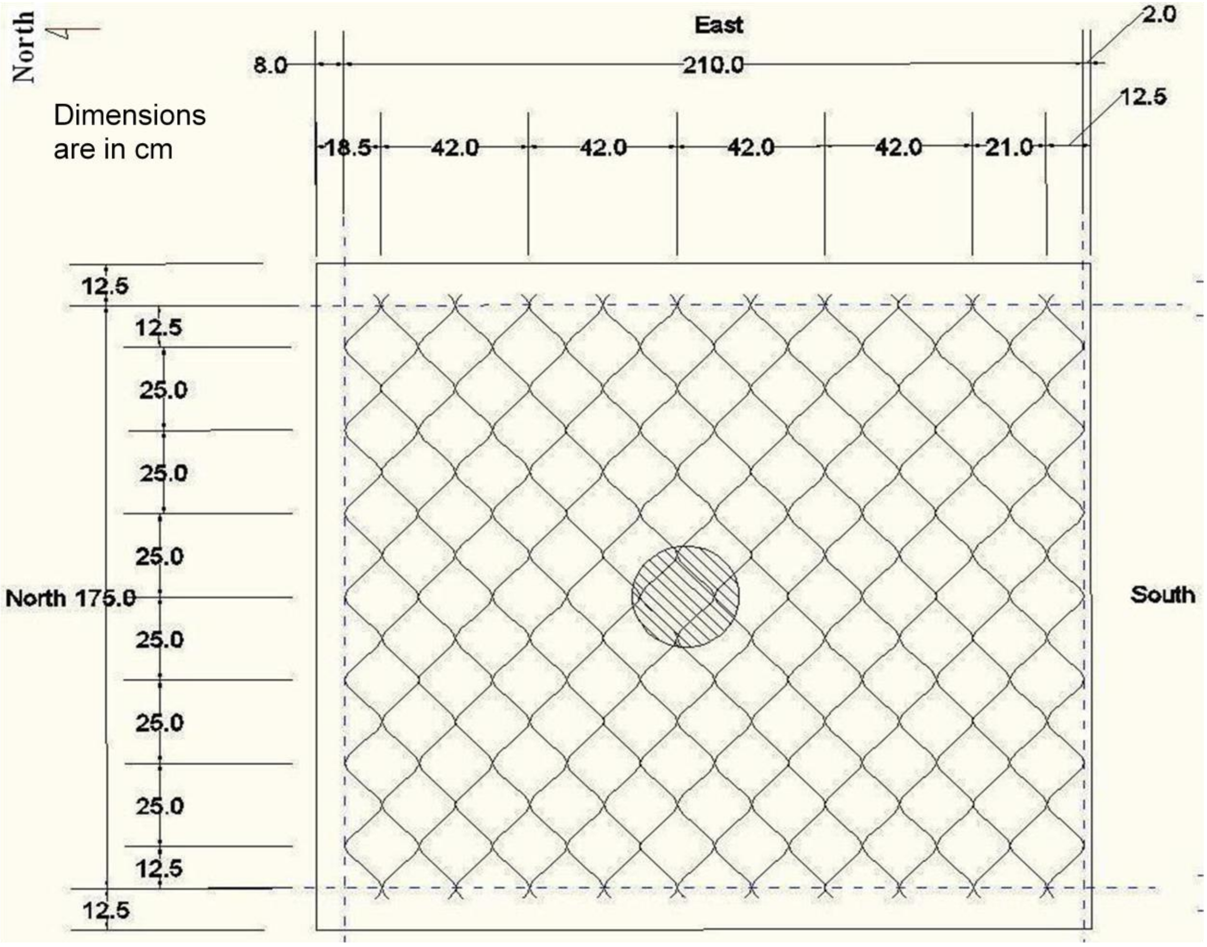

Figure 5.2.4 Layout for geocell installation inside the test box (From Pokharel, 2010)

Figure 5.2.5 Compacting RAP inside the geocell by hand tamping

Four DCP tests were conducted one day after the preparation of a base course at four different locations within the test box to verify the CBR of the subgrade and base course. Penetration indexes were determined from the DCP test data and then CBR values were estimated by the following correlation (Webster et al., 1992):

$$\mathbf{CBR} = \frac{292}{(\mathrm{PI} \times 25.4)^{1.12}} \qquad \textbf{(5.2.2)}$$

where PI = penetration index (in/blow)

The displacement transducers were installed 1 day after the preparation of each RAP base. All the displacement transducers, earth pressure cells, and strain gauges were connected to the data recorders before starting the cyclic plate load test.

Each cyclic test was planned to stop when the maximum displacement reached 85 mm. However, some tests were terminated before reaching the target maximum displacement when the problem appeared in test equipment. The displacement of each test section was taken by a ruler after the completion of the cyclic plate load test shown in Figure 5.2.6.

Figure 5.2.6 Displacement measurement at the end of a cyclic plate load test

After each cyclic plate load test, two sand cone tests in accordance with ASTM D15556-07 were conducted to evaluate the density of the compacted RAP base as shown in Figure 5.2.7.

Figure 5.2.7 Sand cone test

In addition, RAP bases were exhumed and profile measurements were taken in order to obtain the deformed shapes of the test sections after cyclic plate load tests.

5.3 Cyclic plate load test data

Four cyclic plate load tests were conducted on RAP bases over soft subgrade (target subgrade CBR = 2%) while five cyclic tests were on RAP bases over moderate subgrade (target subgrade CBR = 5%). The test data for each test presented below include vane shear test data, CBR profiles based on DCP tests, sand cone test data, permanent and the elastic deformations at the center versus the number of loading cycles, maximum vertical stresses at the interface between base and subgrade versus the number of loading cycles, and test section profiles before and after testing.

5.3.1 15 cm thick geocell-reinforced base over soft subgrade

Vane shear tests at three depths were conducted just after the preparation of subgrade at five randomly selected locations. The CBR values of subgrade were calculated using Equation (5.2.1) and are presented in Table 5.3.1. The average CBR of the subgrade was found 2.1% from the vane shear tests.

Table 5.3.1 Subgrade CBR values from vane shear tests

Depth (cm)	CBR (%) at location					Average CBR (%)
	1	2	3	4	5	
10	2.2	2.1	2.5	2.5	1.5	2.2
18	1.8	1.9	2.2	2.8	1.9	2.1
25	1.6	2.3	2.2	2.6	1.9	2.1
Average	1.9	2.1	2.3	2.6	1.8	2.1

The sand cone tests at two randomly selected locations in the RAP base were conducted after the cyclic plate load test and the average degree of compaction was found 93%.

The profiles of the calculated CBR values based on the DCP test data are shown in Figure 5.3.1. The average CBR values of the base course and subgrade were found 11.4% and 2.8% respectively by the DCP tests. Therefore, the subgrade CBR value determined by the DCP test is higher than that by the vane shear test.

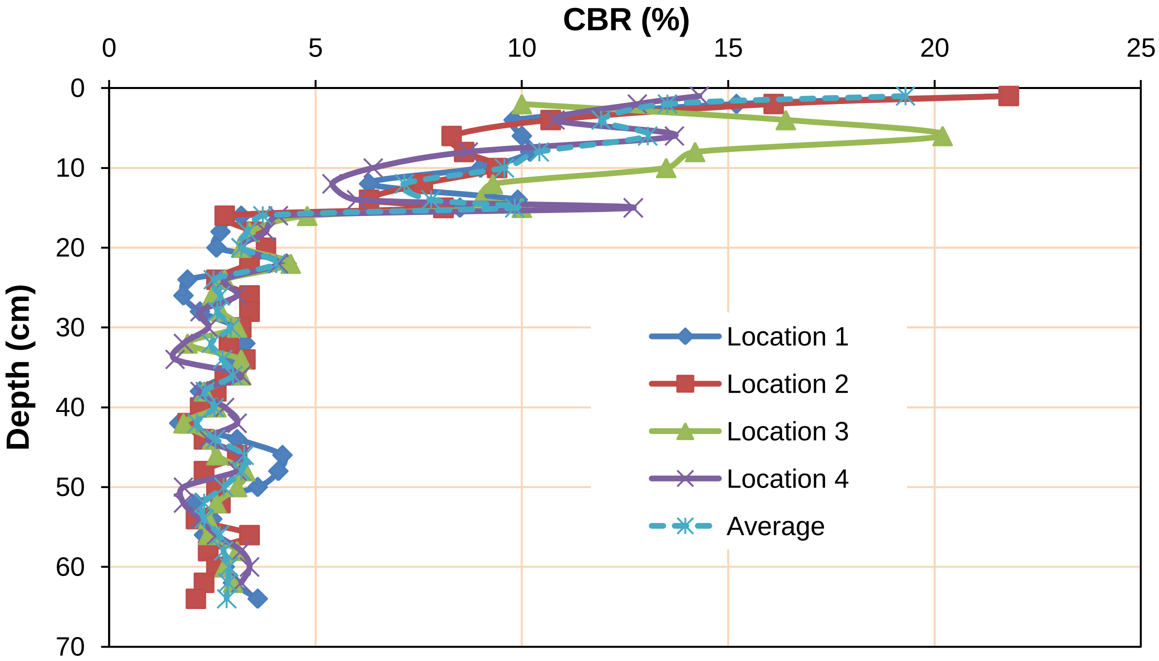

Figure 5.3.1 CBR profiles obtained from DCP tests in the 15 cm thick geocell-reinforced base over soft subgrade

Figure 5.3.2 shows the measured permanent deformations at the center of the plate versus the number of loading cycles for the 15 cm thick geocell-reinforced base over soft subgrade.

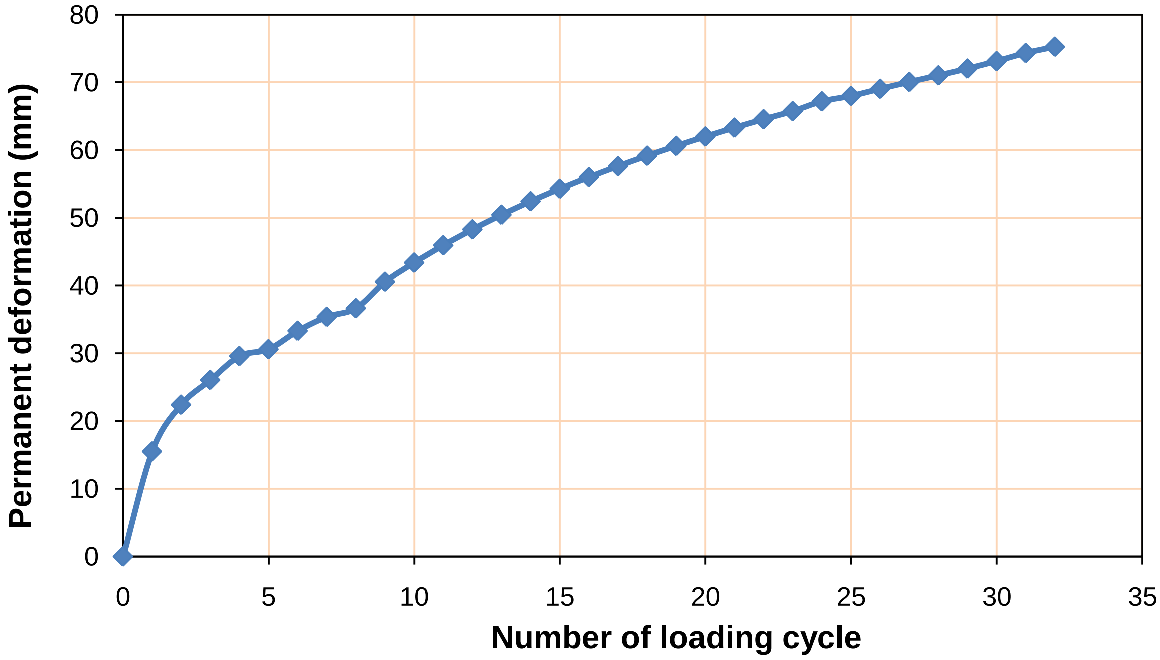

Figure 5.3.2 Permanent deformation at the center versus the number of loading cycles in the 15 cm thick geocell-reinforced base over soft subgrade

The elastic deformations at different numbers of loading cycles are presented in Figure 5.3.3. The elastic deformation is defined as the rebound of the base when unloaded from the maximum load (40kN) to the minimum load (0.5kN). The maximum elastic deformation at the center for the 15 cm thick geocell-reinforced base over soft subgrade was about 10 mm.

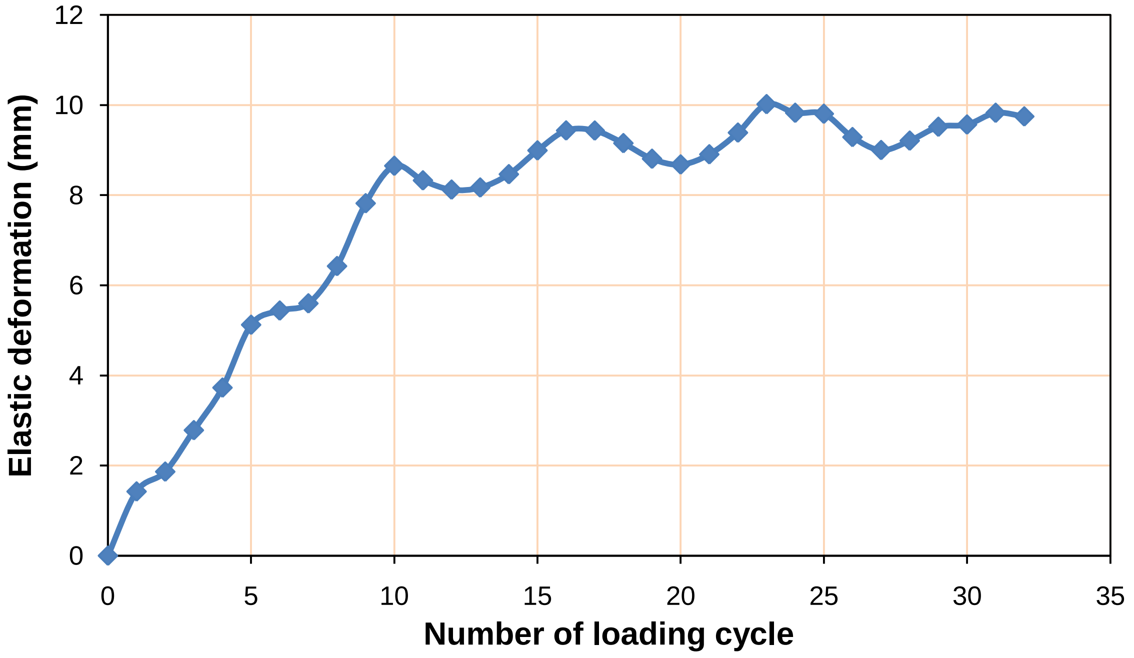

Figure 5.3.3 Elastic deformation at the center versus the number of loading cycles for the 15 cm thick geocell-reinforced base over soft subgrade

The vertical stresses at the interface of subgrade and base course were measured by the pressure cells located at 0, 12.5, 25, and 50 cm away from the center. Figure 5.3.4 shows the measured stresses at the interface of subgrade and base course versus the number of loading cycles.

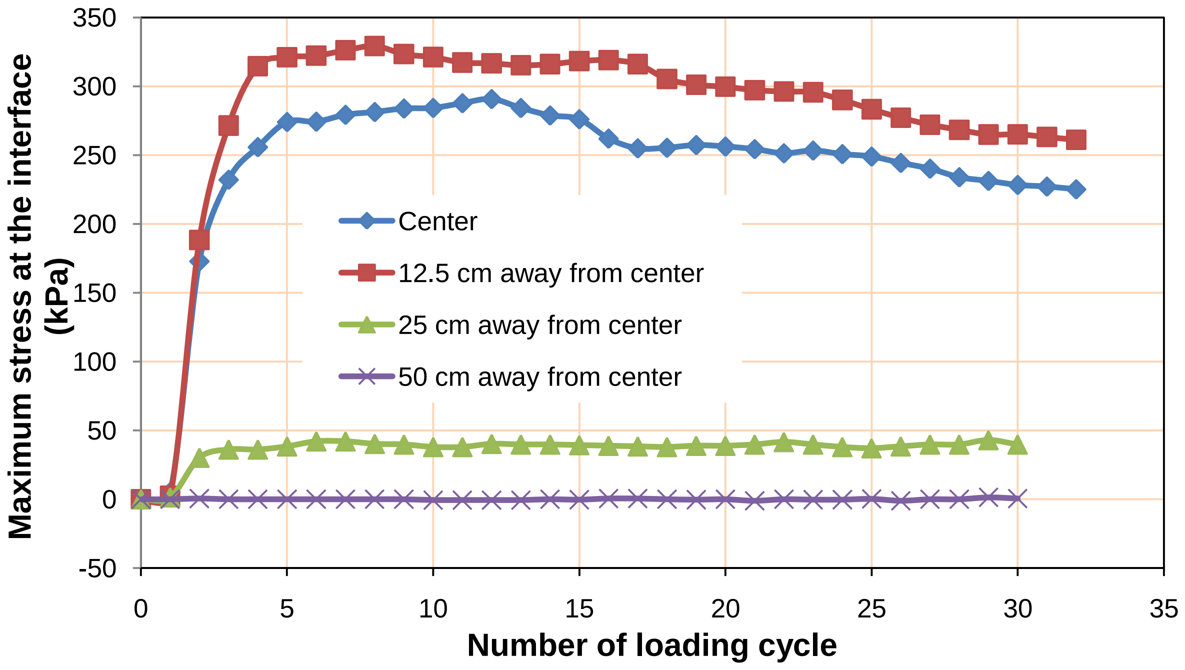

Figure 5.3.4 Measured vertical stresses at the interface of base and subgrade versus the number of loading cycles for the 15 cm thick geocell-reinforced base over soft subgrade

The profiles were manually measured before and after the test. Figure 5.3.5 shows the test section profiles for the 15 cm thick geocell-reinforced base over soft subgrade.

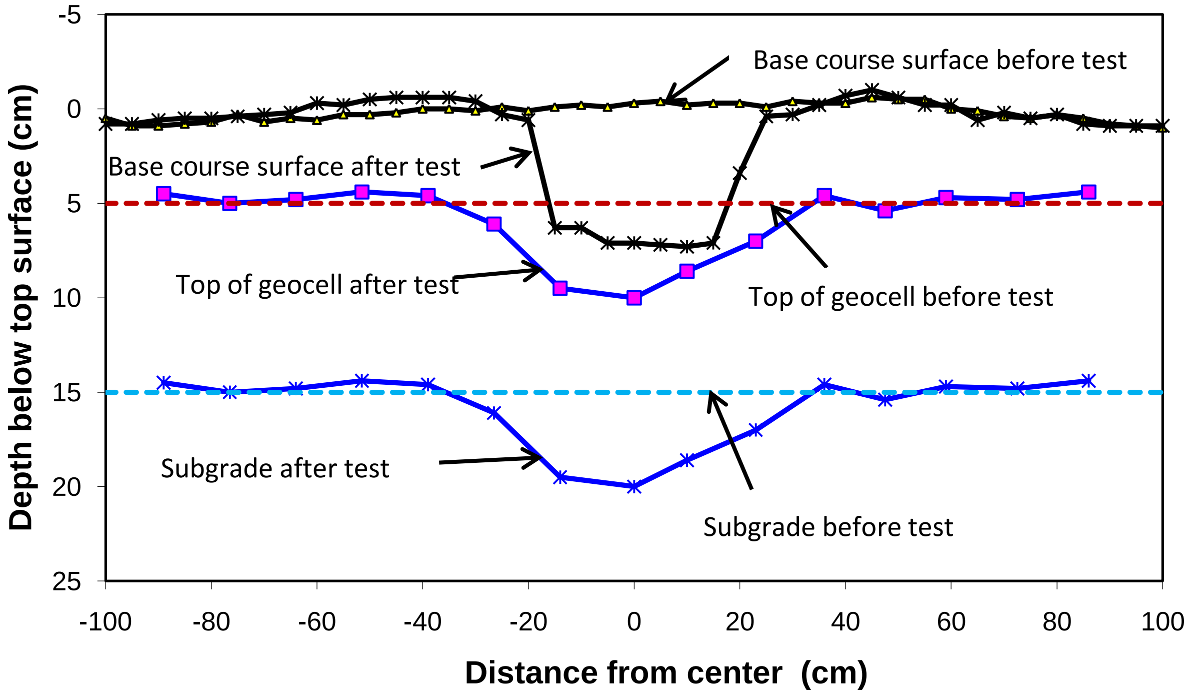

Figure 5.3.5 Profiles of 15 cm thick geocell-reinforced base over soft subgrade

5.3.2 23 cm thick geocell-reinforced base over soft subgrade

Vane shear tests at three depths were conducted just after the preparation of subgrade at five randomly selected locations. The CBR values of subgrade were calculated using Equation (5.2.1) and are presented in Table 5.3.2. The average CBR of the subgrade was found 1.9% from the vane shear tests.

Table 5.3.2 Subgrade CBR values from vane shear tests

Depth (cm)	**CBR (%) at location**					**Average CBR (%)**
	1	**2**	**3**	**4**	**5**	
10	1.8	2.0	2.0	1.8	1.5	1.8
18	2.2	1.8	1.6	1.4	2.2	1.8
25	2.0	1.9	1.8	1.8	2.2	1.9
Average	2.0	1.9	1.8	1.6	2	1.9

The sand cone tests at two randomly selected locations in the RAP base were conducted after the cyclic plate load test and the average degree of compaction was found 84%.

The profiles of the calculated CBR values based on the DCP test data are shown in Figure 5.3.6. The average CBR values of the base course and subgrade were found 6.3% and 2.1 % respectively by the DCP tests. Therefore, the subgrade CBR value determined by the DCP test is slightly higher than that by the vane shear test. The least CBR of the base was due to the inadequate compaction.

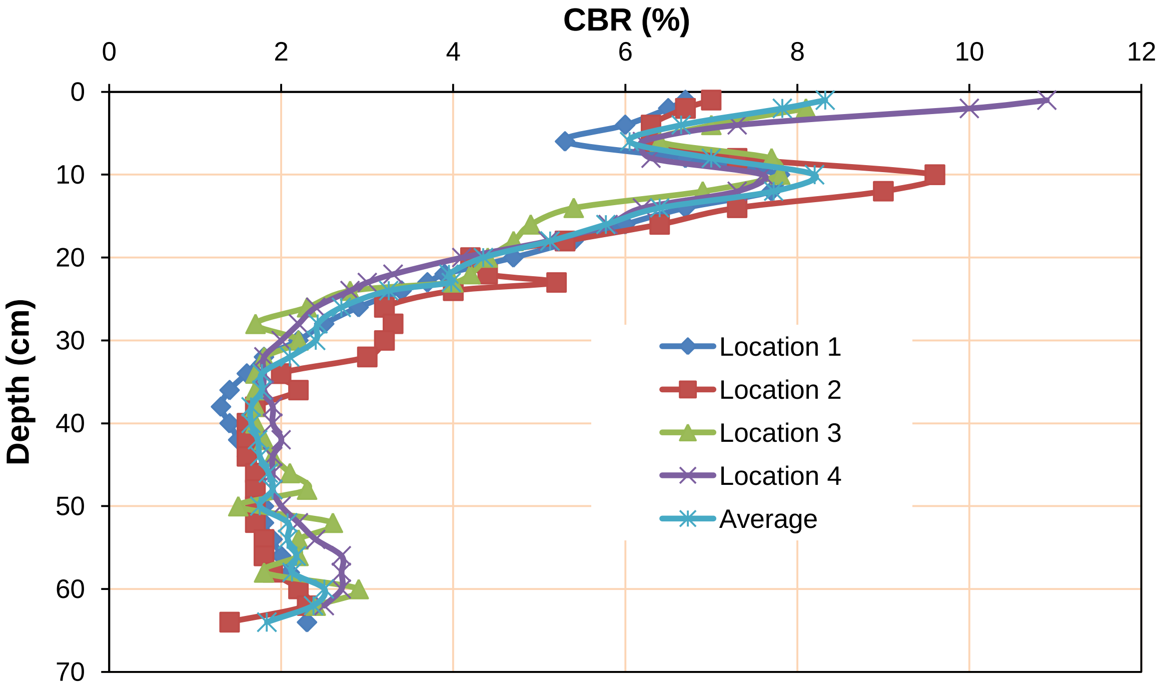

Figure 5.3.6 CBR profiles obtained from DCP tests in the 23 cm thick geocell-reinforced base over soft subgrade

Figures 5.3.7, 5.3.8, 5.3.9, and 5.3.10 show the permanent deformations at the center versus the number of loading cycles, the elastic deformations at the center versus the number of loading cycles, the maximum stresses at the interface of subgrade and base course versus the number of loading cycles, and the test section profiles for the 23 cm thick geocell-reinforced base over soft subgrade respectively.

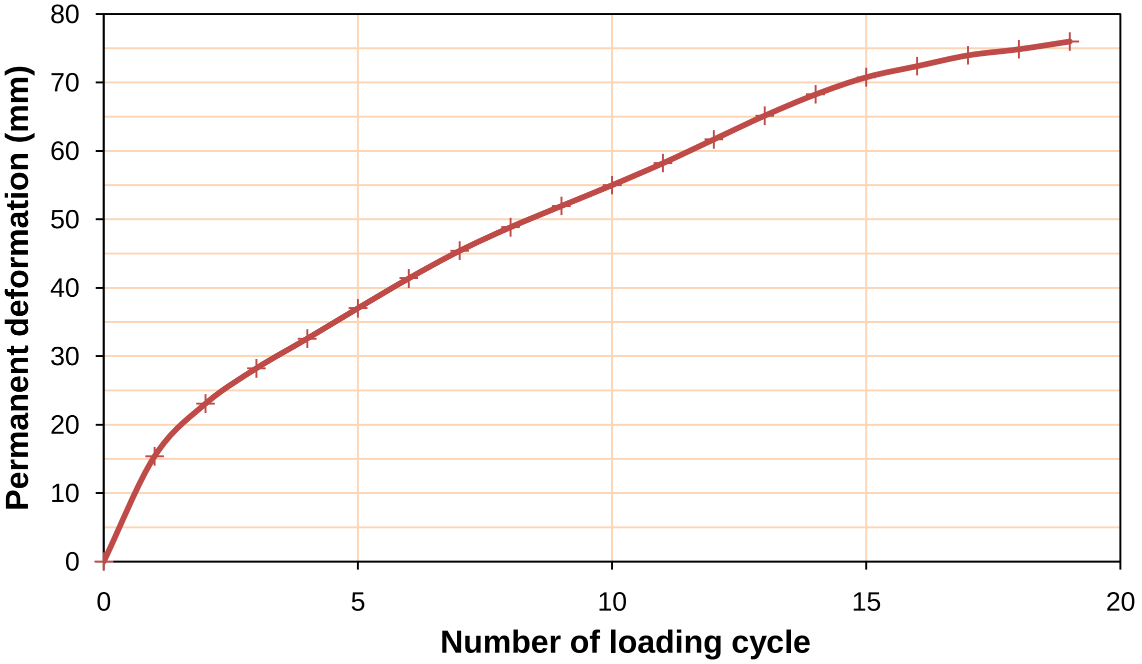

Figure 5.3.7 Permanent deformation at the center versus the number of loading cycles in the 23 cm thick geocell-reinforced base over soft subgrade

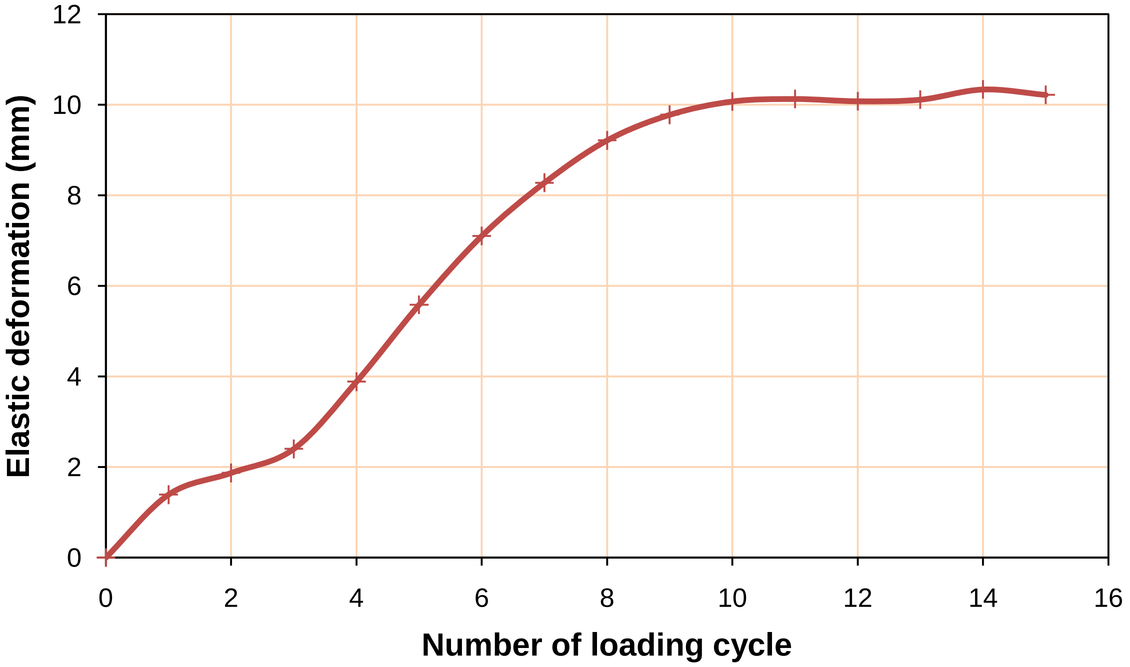

Figure 5.3.8 Elastic deformation at the center versus the number of loading cycles for the 23 cm thick geocell-reinforced base over soft subgrade

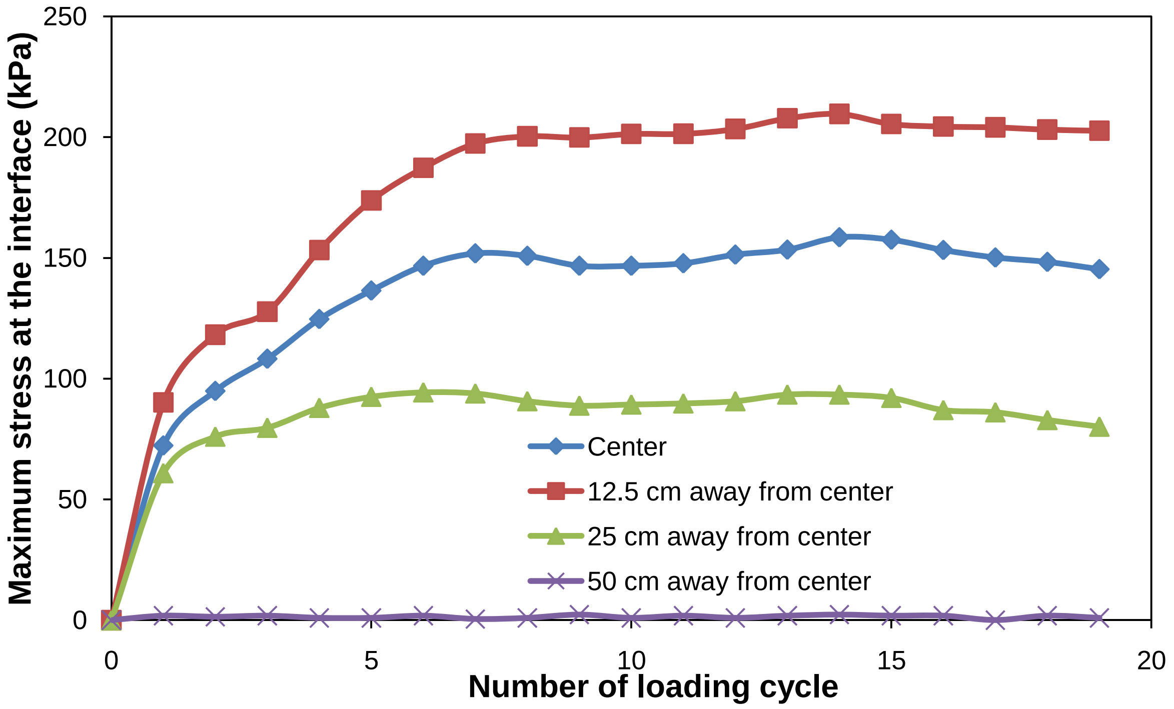

Figure 5.3.9 Measured vertical stresses at the interface of subgrade and base versus the number of loading cycles for the 23 cm geocell-reinforced base over soft subgrade

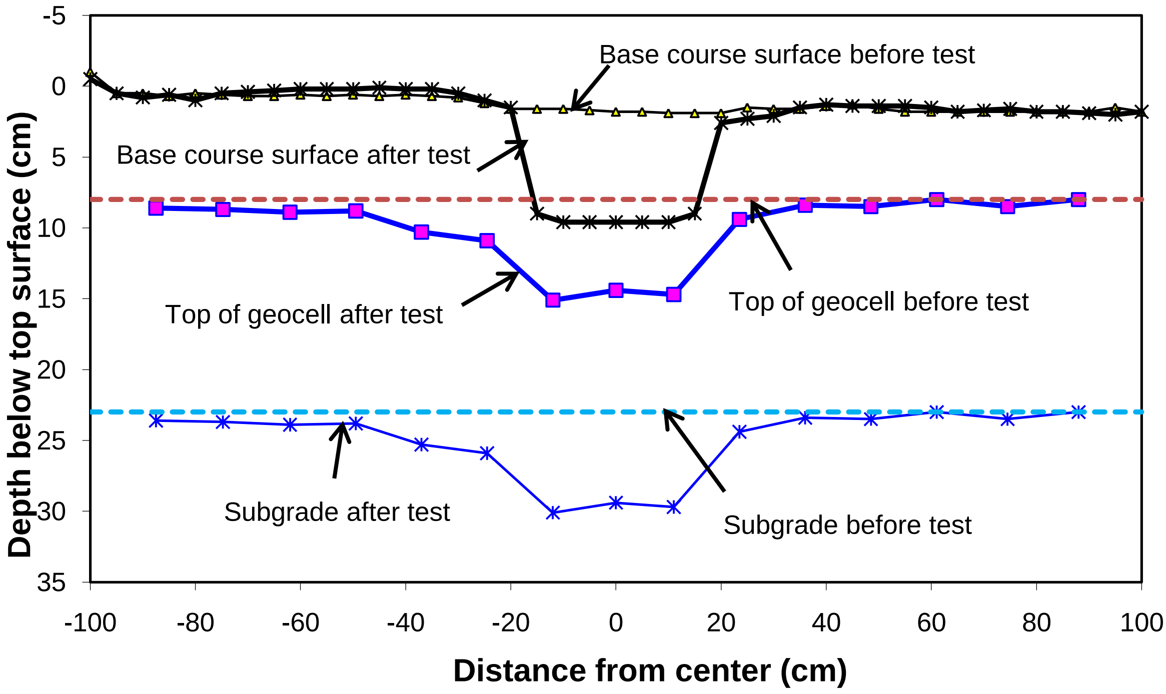

Figure 5.3.10 Profiles of 23 cm thick geocell-reinforced base over soft subgrade

5.3.3 30 cm thick geocell-reinforced base over soft subgrade

Vane shear tests at three depths were conducted just after the preparation of subgrade at five randomly selected locations. The CBR values of subgrade were calculated using Equation (5.2.1) and are presented in Table 5.3.3. The average CBR of the subgrade was found 2.0% from the vane shear tests.

Table 5.3.3 Subgrade CBR values from vane shear tests

Depth (cm)	CBR (%) at location					Average CBR (%)
	1	2	3	4	5	
10	2.2	2.2	1.5	2.1	2.2	2.1
18	1.9	2.0	2.3	2.0	1.8	2.0
25	2.2	2.0	2.2	1.6	1.8	2.0
Average	2.1	2.1	2.0	1.9	1.9	2.0

The sand cone tests at two randomly selected locations in the RAP base were conducted after the cyclic plate load test and the average degree of compaction was found 91%.

The profiles of the calculated CBR values based on the DCP test data are shown in Figure 5.3.11. The average CBR values of the base course and subgrade were found 10.2% and 2.1% respectively by the DCP tests. Therefore, the subgrade CBR value determined by the DCP test is slightly higher than that by the vane shear test.

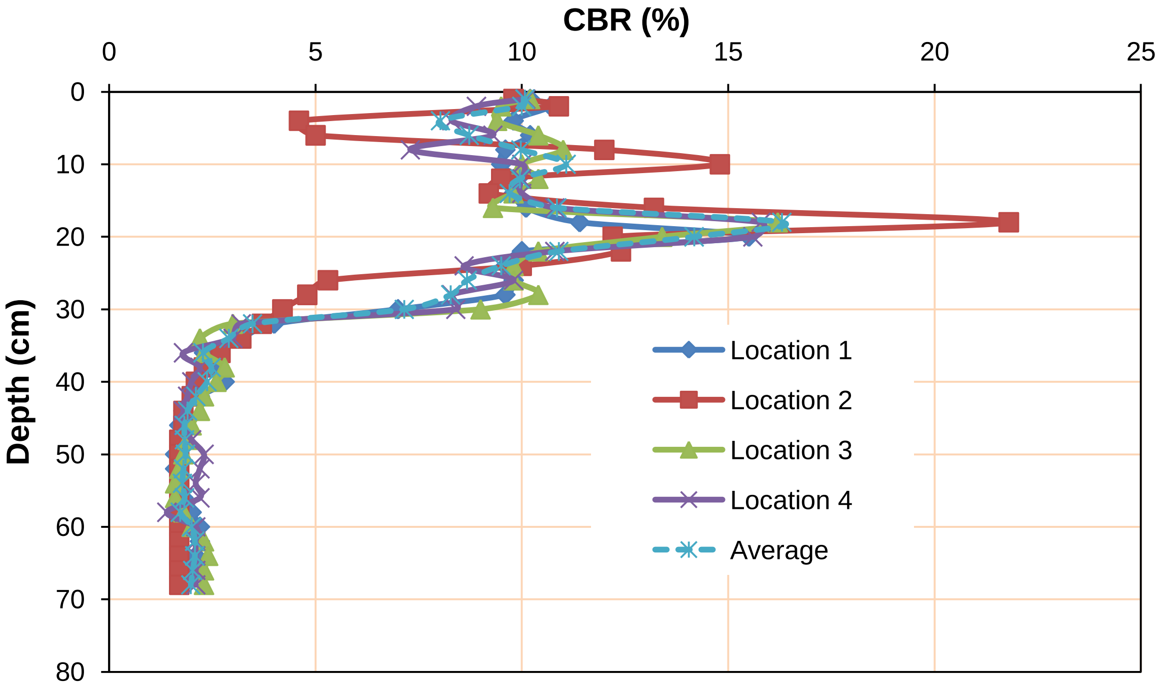

Figure 5.3.11 CBR profiles obtained from DCP tests in the 30 cm thick geocell-reinforced base over soft subgrade

Figures 5.3.12, 5.3.13, 5.3.14, and 5.3.15 show the permanent deformations at center versus the number of loading cycles, the elastic deformations at center versus the number of loading cycles, the maximum stresses at the interface of subgrade and base course versus the number of loading cycles, and the test section profiles for the 30 cm thick geocell-reinforced base over soft subgrade respectively.

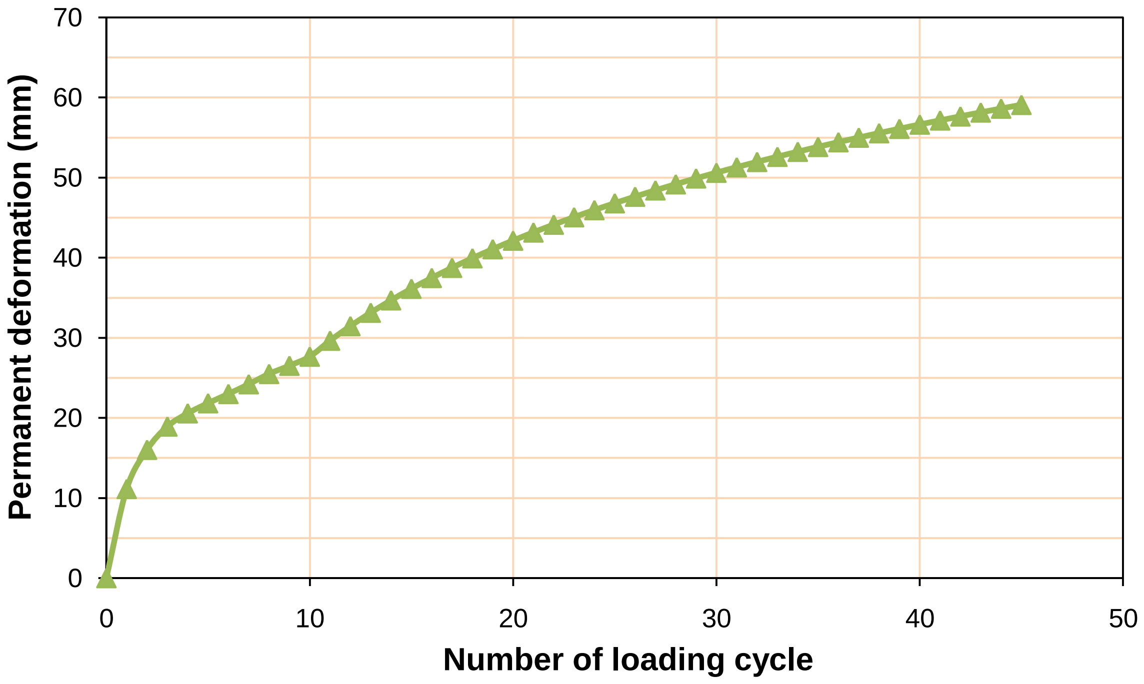

Figure 5.3.12 Permanent deformation at the center versus the number of loading cycles in the 30 cm thick geocell-reinforced base over soft subgrade

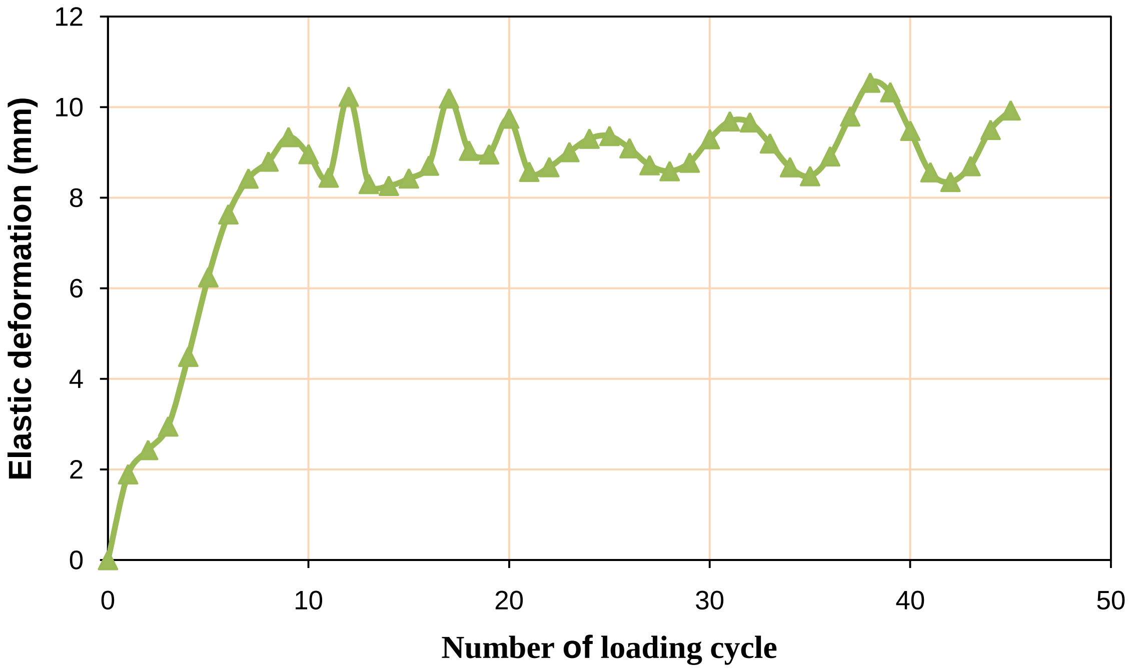

Figure 5.3.13 Elastic deformation at the center versus the number of loading cycles for the 30 cm thick geocell-reinforced base over soft subgrade

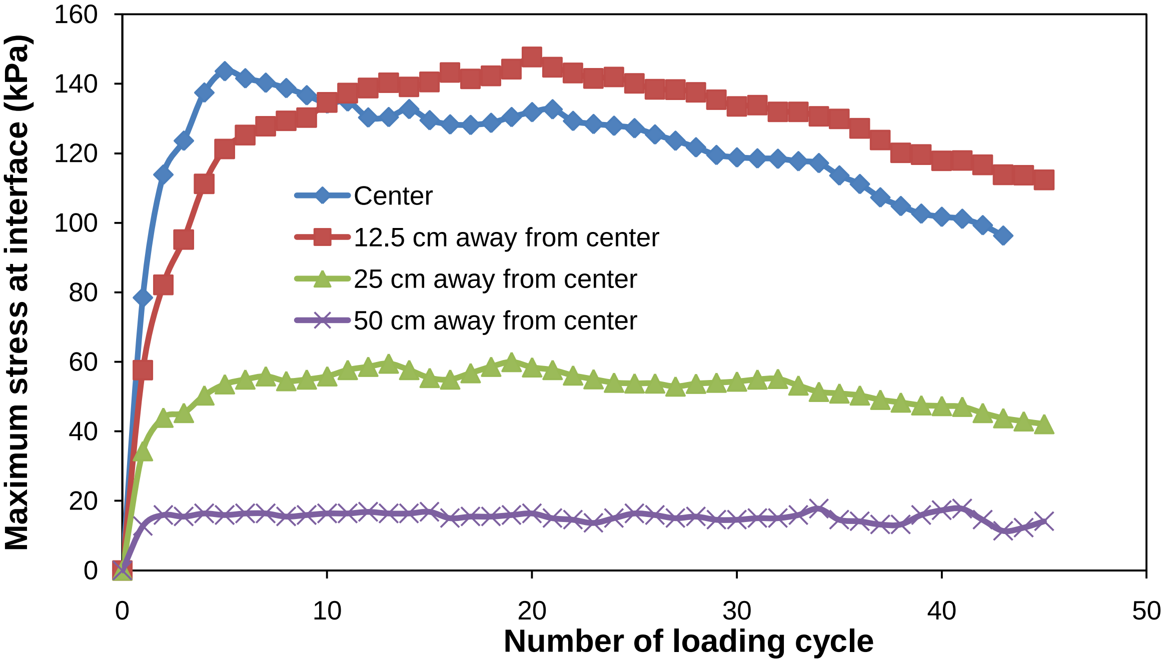

Figure 5.3.14 Measured vertical stresses at the interface of subgrade and base versus the number of loading cycles for the 30 cm thick geocell-reinforced base over soft subgrade

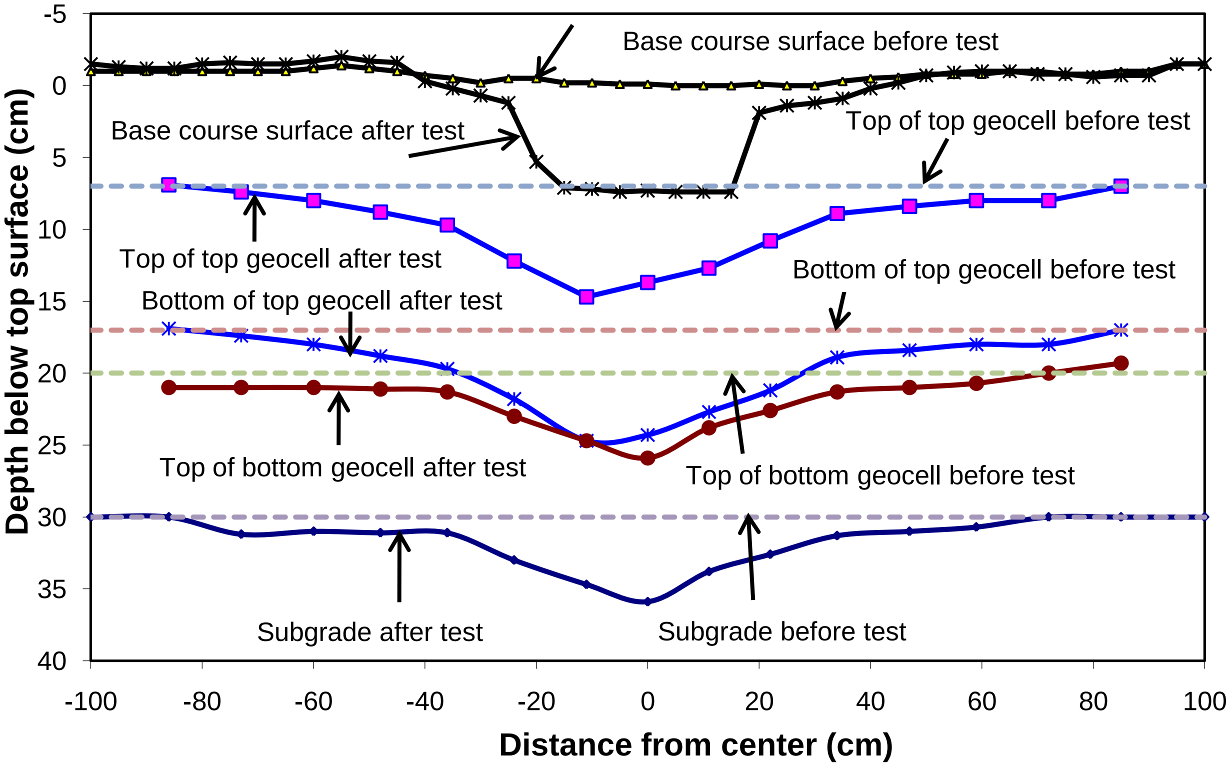

Figure 5.3.15 Profiles of 30 cm thick geocell-reinforced base over soft subgrade

5.3.4 30 cm thick unreinforced base over soft subgrade

Vane shear tests at three depths were conducted just after the preparation of subgrade at five randomly selected locations. The CBR values of subgrade were calculated using Equation (5.2.1) and are presented in Table 5.3.4. The average CBR of the subgrade was found 1.9% from the vane shear tests.

Table 5.3.4 Subgrade CBR values from vane shear tests

Depth (cm)	**CBR (%) at location**					**Average CBR (%)**
	1	**2**	**3**	**4**	**5**	
10	1.9	1.9	1.4	2.1	1.6	1.8
18	2.2	2.2	1.9	2.0	1.9	2.0
25	2.3	1.8	1.8	2.3	2.0	2.0
Average	2.1	1.9	1.7	2.1	1.8	1.9

The sand cone tests at two randomly selected locations in the RAP base were conducted after the cyclic plate load test and the average degree of compaction was found 91%.

The profiles of the calculated CBR values based on the DCP test data are shown in Figure 5.3.16. The average CBR values of the base course and subgrade were found 10.2% and 2.0% respectively by the DCP tests. Therefore, the subgrade CBR value determined by the DCP test is slightly higher than that by the vane shear test.

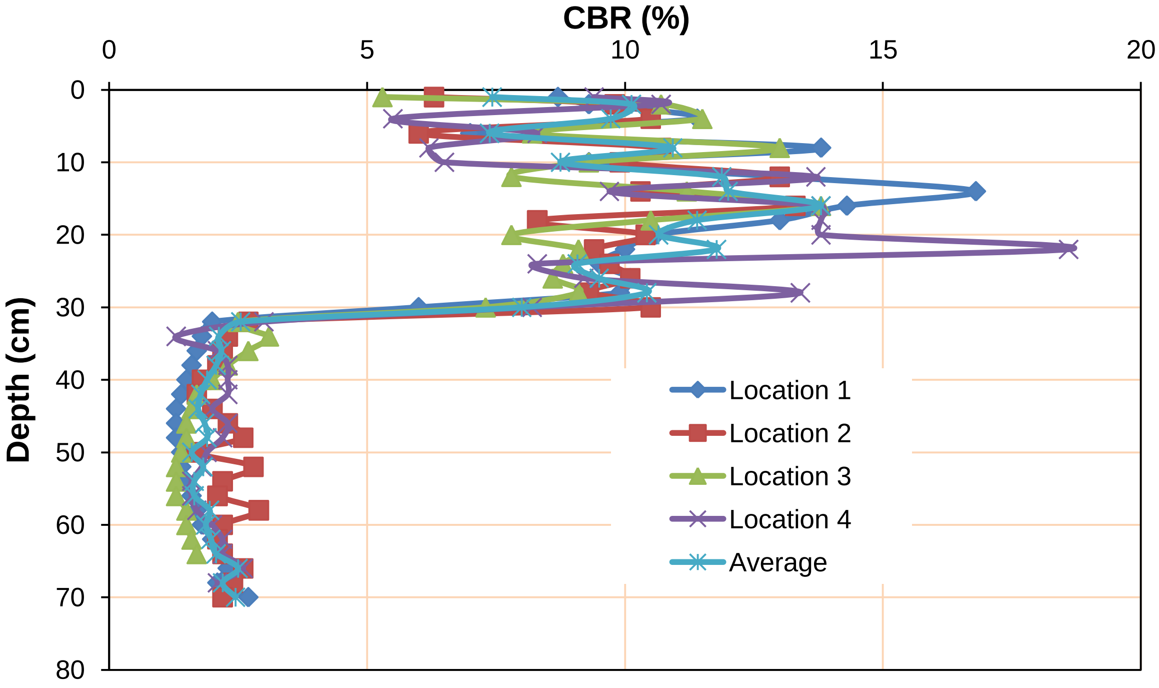

Figure 5.3.16 CBR profiles obtained from DCP tests in the 30 cm thick unreinforced base over soft subgrade

Figures 5.3.17, 5.3.18, 5.3.19, and 5.3.20 show the permanent deformations at center versus the number of loading cycles, the elastic deformations at center versus the number of loading cycles, the maximum stresses at the interface of subgrade and base course versus the number of loading cycles, and the test section profiles for 30 cm thick unreinforced base over soft subgrade respectively.

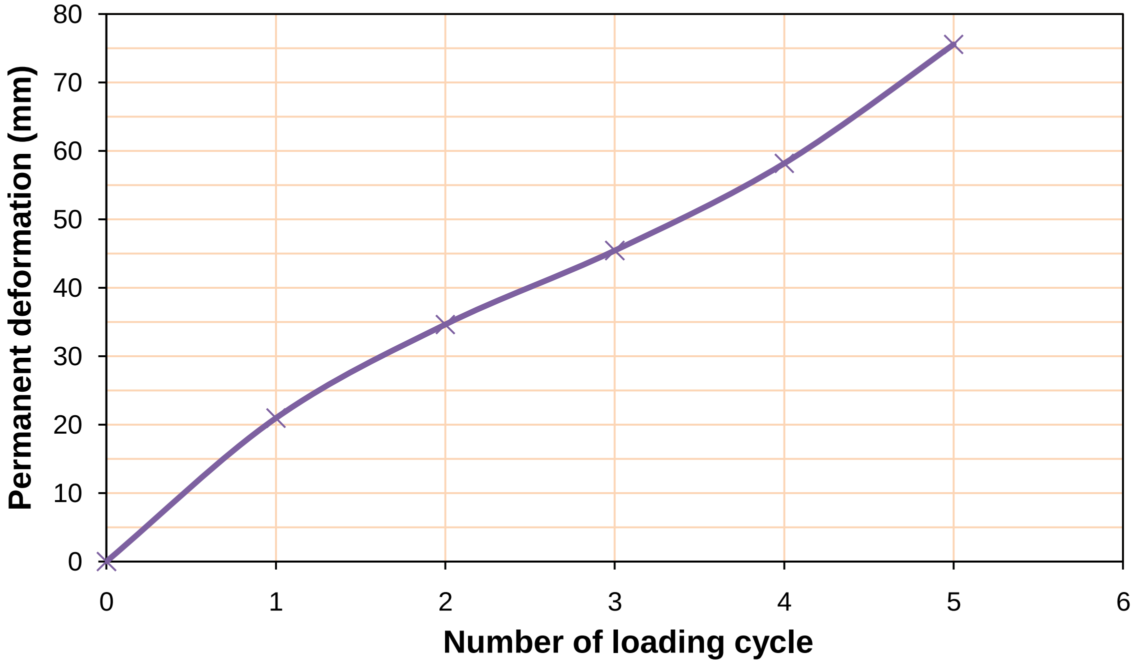

Figure 5.3.17 Permanent deformation at the center versus the number of loading cycles in the 30 cm thick unreinforced base over soft subgrade

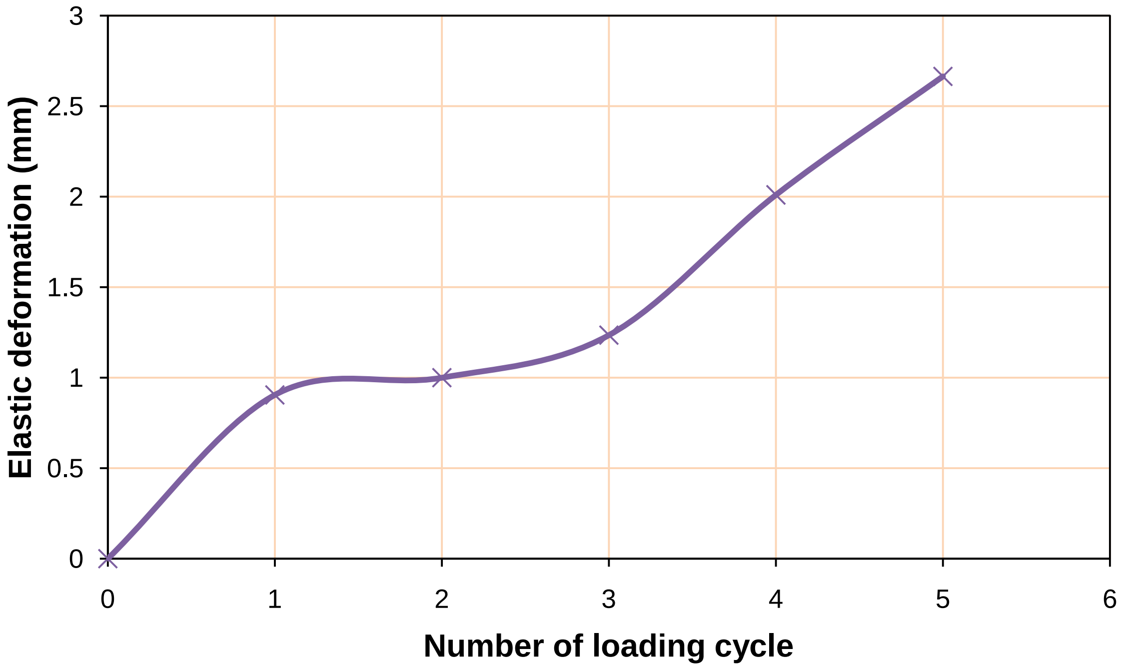

Figure 5.3.18 Elastic deformation at the center versus the number of loading cycles for the 30 cm thick unreinforced base over soft subgrade

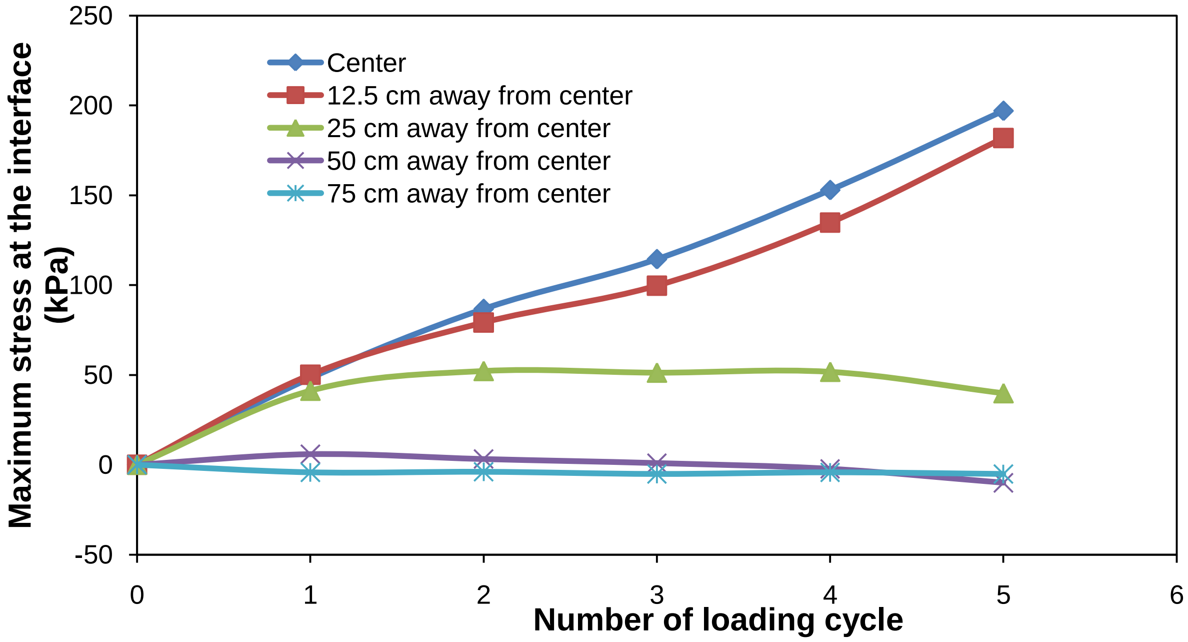

Figure 5.3.19 Measured vertical stresse at the interface of subgrade and base versus the number of loading cycles for 30 cm thick unreinforced base over soft subgrade

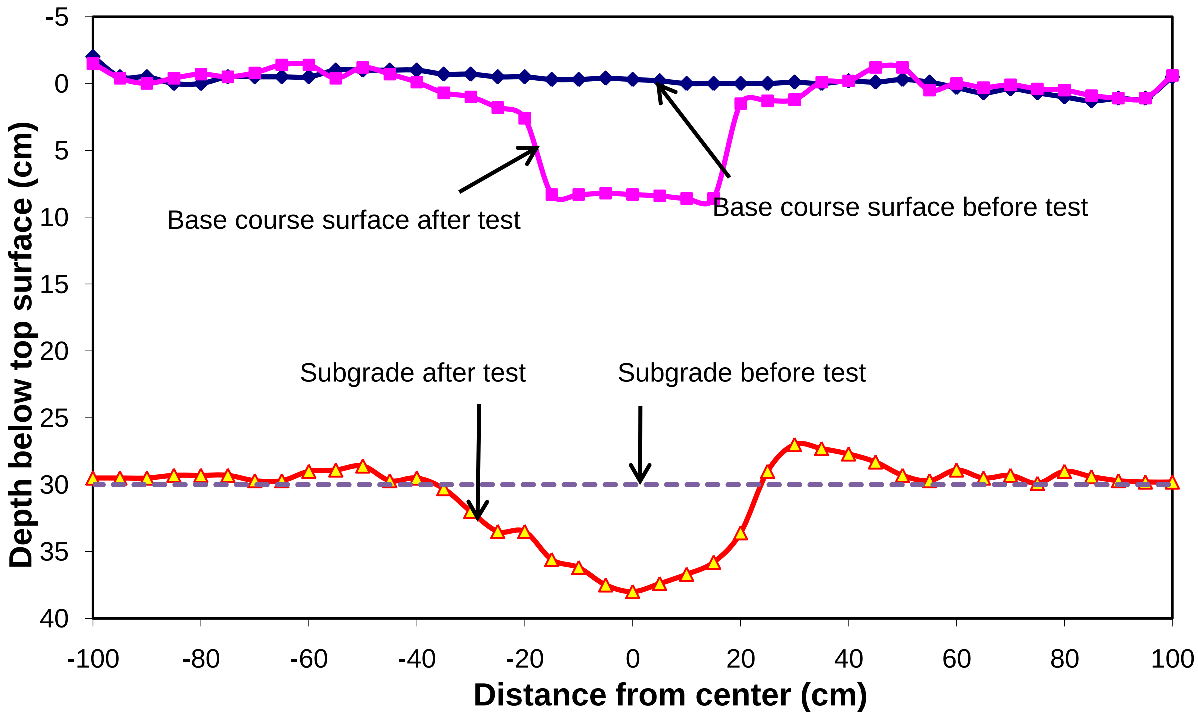

Figure 5.3.20 Profiles of 30 cm thick geocell-reinforced base over soft subgrade

5.3.5 15 cm thick unreinforced base over moderate subgrade

Vane shear tests at three depths were conducted just after the preparation of subgrade at five randomly selected locations. The CBR values of subgrade were calculated using Equation (5.2.1) and are presented in Table 5.3.5. The average CBR of the subgrade was found 4.8% from the vane shear tests.

Table 5.3.5 Subgrade CBR values from vane shear tests

Depth (cm)	CBR (%) at location					Average CBR (%)
	1	2	3	4	5	
10	5.1	4.2	5.1	4.9	4.0	4.7
18	4.1	4.1	5.3	5.3	4.6	4.7
25	5.1	5.4	4.7	5.4	5.4	5.2
Average	4.8	4.6	5.0	5.2	4.6	4.8

The sand cone tests at two randomly selected locations in the RAP base were conducted after the cyclic plate load test and the average degree of compaction was found 96%.

The profiles of the calculated CBR values based on the DCP test data are shown in Figure 5.3.21. The average CBR values of the base course and subgrade were found 10.5% and 5.0% respectively by the DCP tests. Therefore, the subgrade CBR value determined by the DCP test is slightly higher than that by the vane shear tests.

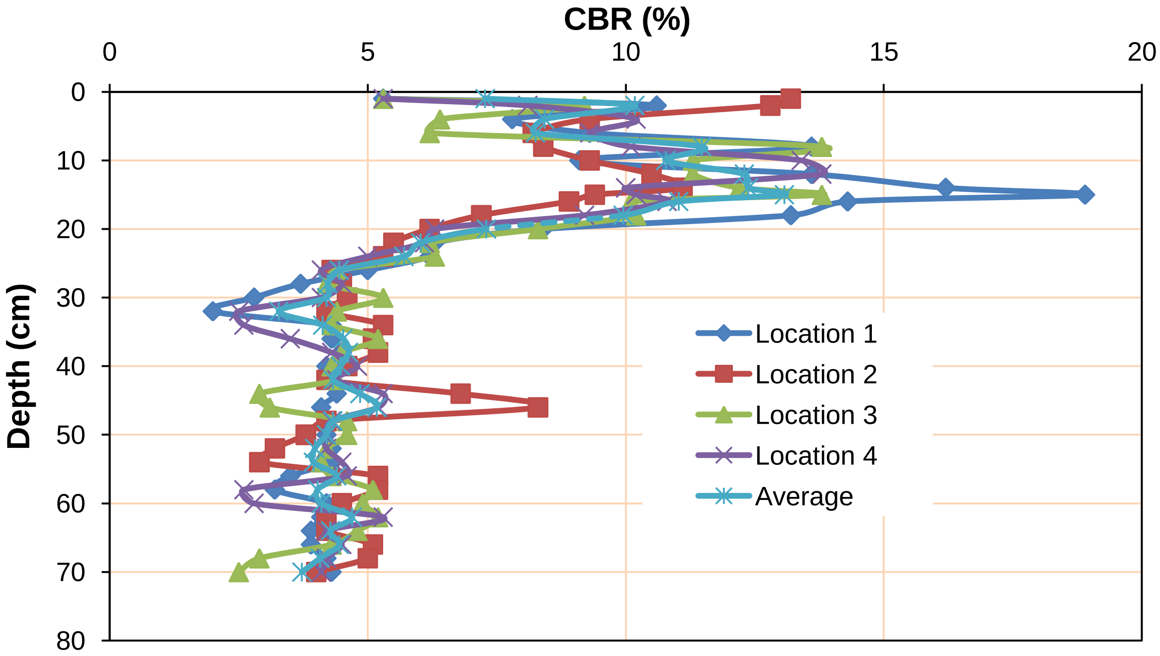

Figure 5.3.21 CBR profiles obtained from DCP tests in the 15 cm thick unreinforced base over moderate subgrade

Figures 5.3.22, 5.3.23, 5.3.24, and 5.3.25 show the permanent deformations at center versus the number of loading cycles, the elastic deformations at center versus the number of loading cycles, the maximum stresses at the interface of subgrade and base course versus the number of loading cycles, and the test section profiles for the 15 cm thick unreinforced base over moderate subgrade respectively.

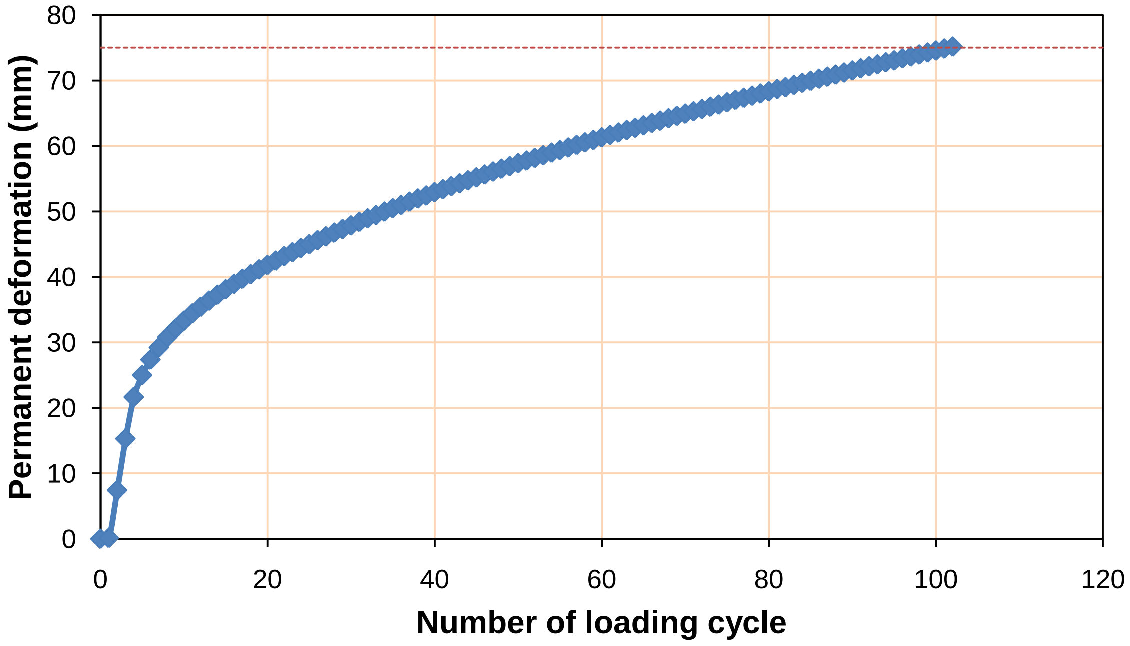

Figure 5.3.22 Permanent deformation at the center versus the number of loading cycles in the 15 cm thick unreinforced base over moderate subgrade

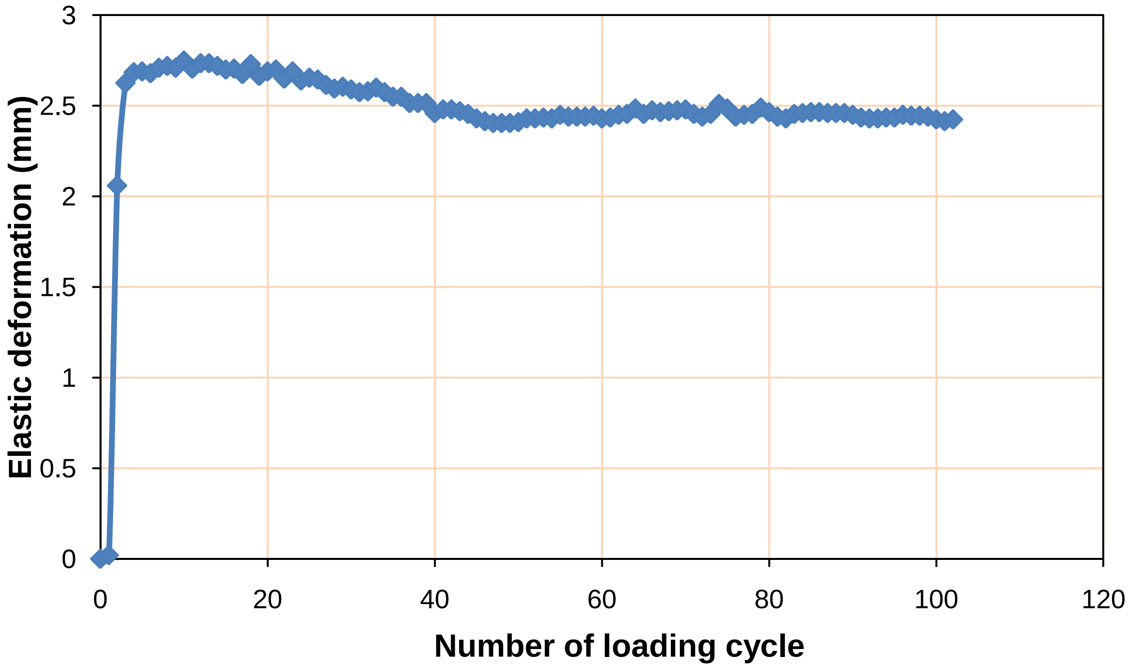

Figure 5.3.23 Elastic deformation at the center versus the number of loading cycles for the 15 cm thick unreinforced base over moderate subgrade

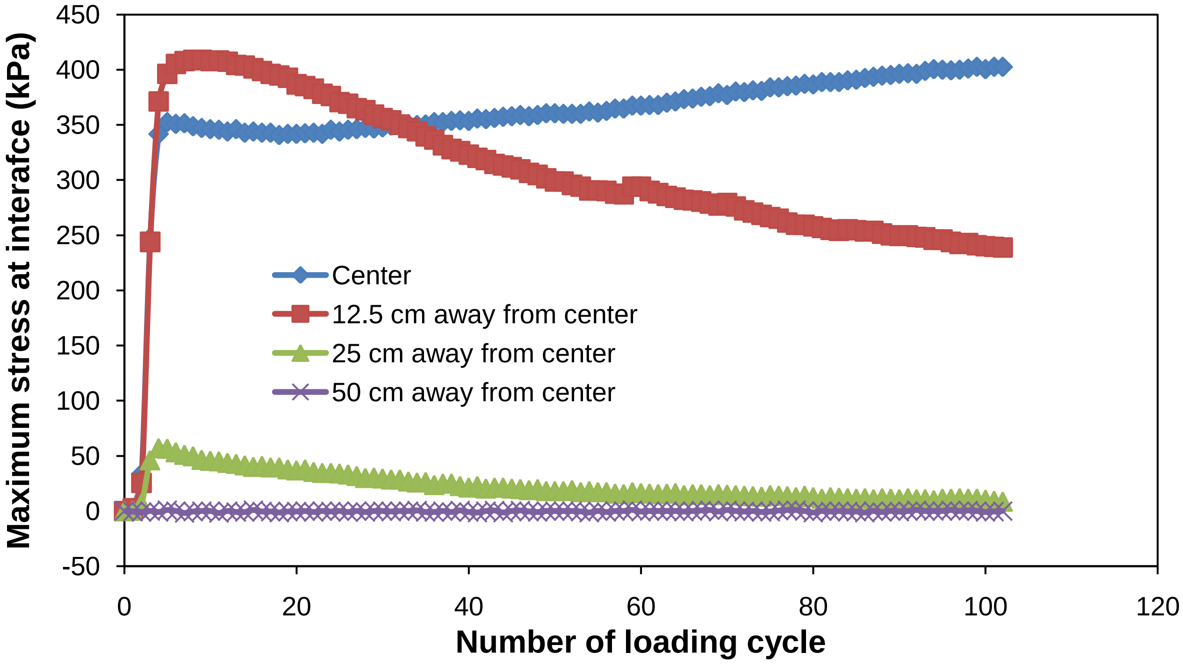

Figure 5.3.24 Measured vertical stresses at the interface of subgrade and base versus the number of loading cycle for the 15 cm thick unreinforced base over moderate subgrade

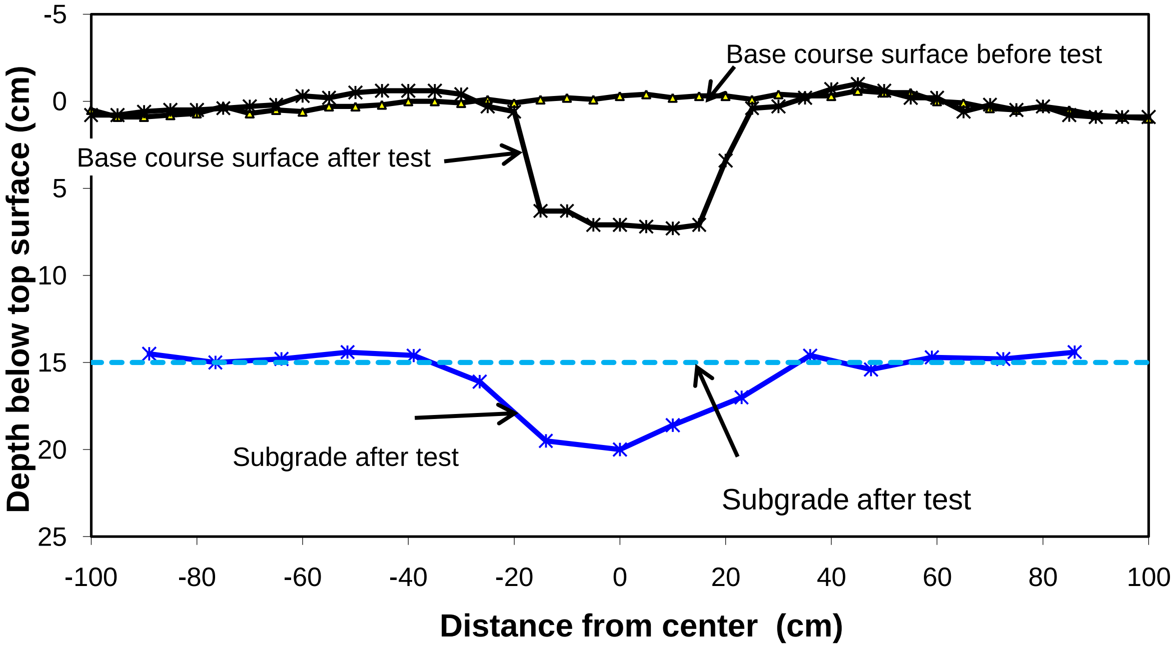

Figure 5.3.25 Profiles of 15 cm thick unreinforced base over moderate subgrade

5.3.6 15 cm thick geocell-reinforced base over moderate subgrade

Vane shear tests at three depths were conducted just after the preparation of subgrade at five randomly selected locations. The CBR values of subgrade were calculated using Equation (5.2.1) and are presented in Table 5.3.6. The average CBR of the subgrade was found 4.8% from the vane shear tests.

Table 5.3.6 Subgrade CBR values from vane shear tests

Depth (cm)	**CBR (%) at location**					**Average CBR (%)**
	1	**2**	**3**	**4**	**5**	
10	5.4	5.1	4.0	4.6	4.6	4.7
18	5.5	5.1	4.8	4.2	4.4	4.8
25	5.1	4.9	5.3	4.2	4.2	4.7
Average	5.3	5.1	4.7	4.3	4.4	4.8

The sand cone tests at two randomly selected locations on RAP base were conducted after cyclic plate load test and average degree of compaction was found 87%.

The profiles of the calculated CBR values based on the DCP test data are shown in Figure 5.3.26. The average CBR values of the base course and subgrade were found 10.4% and 4.8% respectively by the DCP tests. Therefore, the subgrade CBR value determined by the DCP test is equal to that by the vane shear tests.

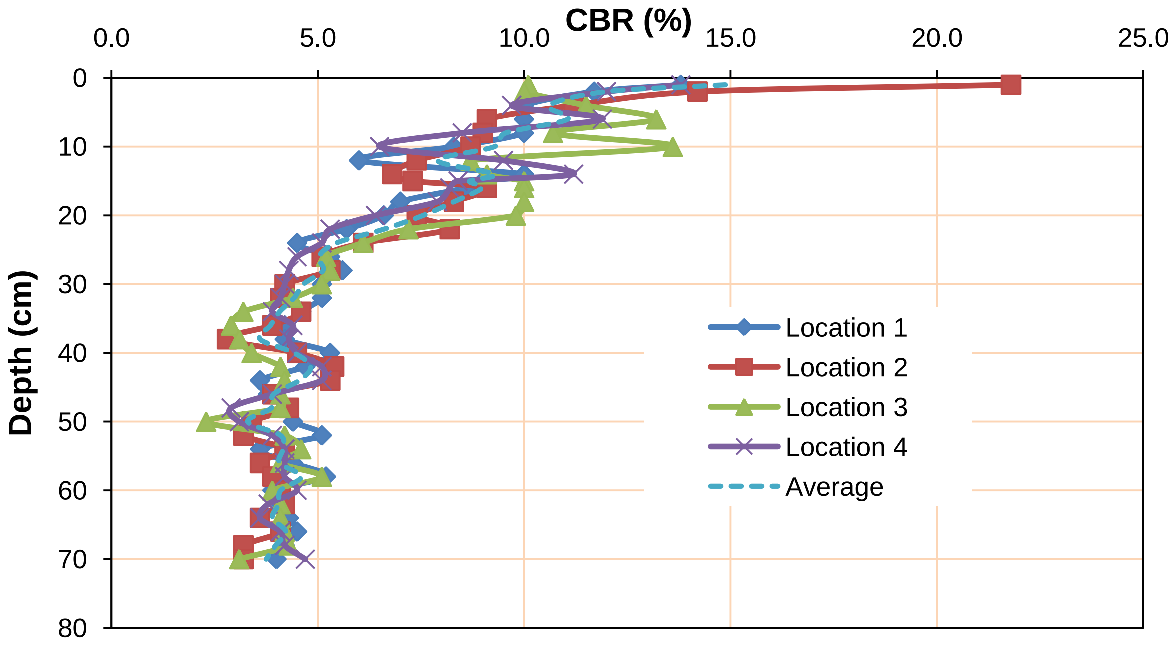

Figure 5.3.26 CBR profiles obtained from DCP tests in the 15 cm thick geocell-reinforced base over moderate subgrade

Figures 5.3.27, 5.3.28, 5.3.29, and 5.3.30 show the permanent deformations at center versus number of loading cycles, the elastic deformations at center versus the number of loading cycles, the maximum stresses at the interface of subgrade and base course versus the number of loading cycles, and the test section profiles for the 15 cm thick unreinforced base over moderate subgrade respectively.

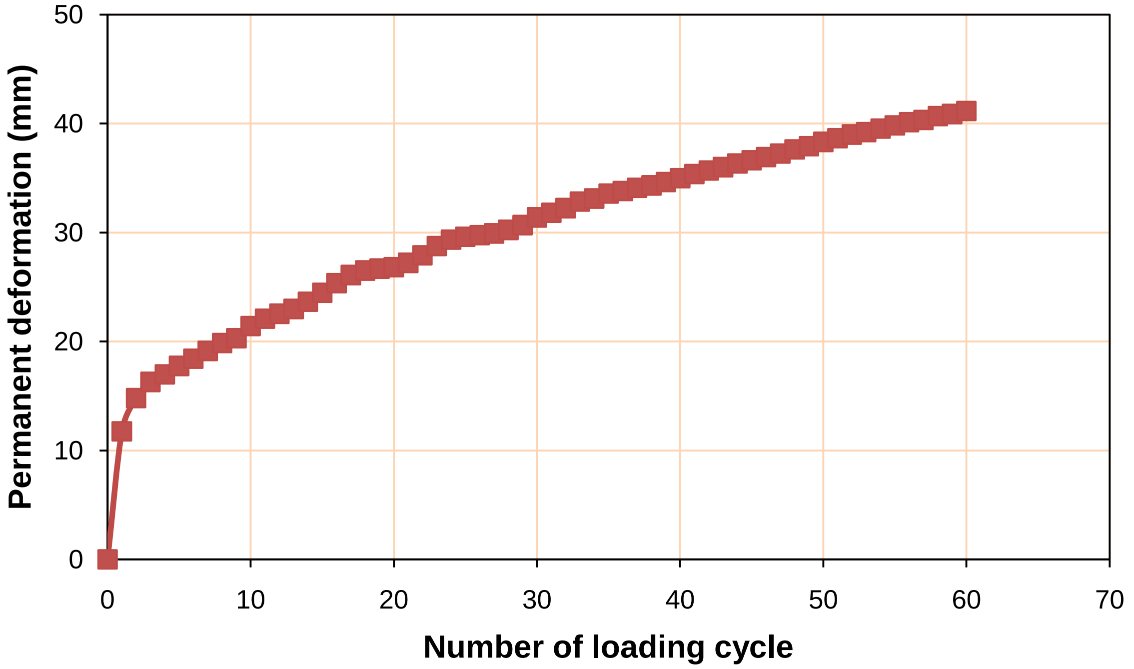

Figure 5.3.27 Permanent deformation at the center versus the number of loading cycles in the 15 cm thick geocell-reinforced base over moderate subgrade

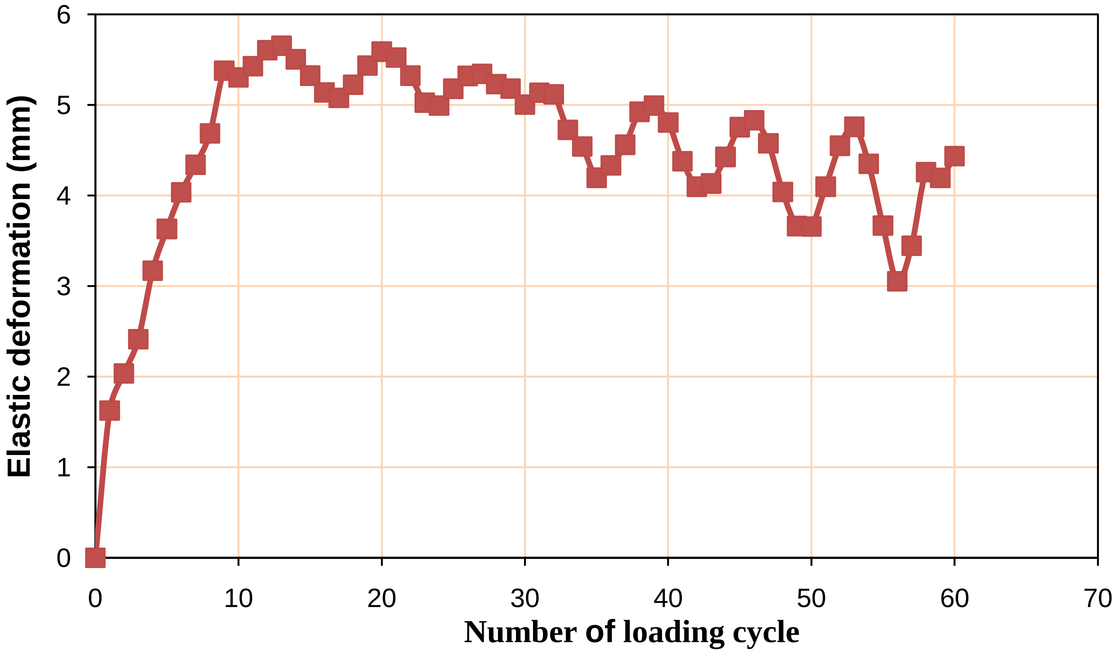

Figure 5.3.28 Elastic deformation at the center versus the number of loading cycles for the 15 cm thick geocell-reinforced base over moderate subgrade

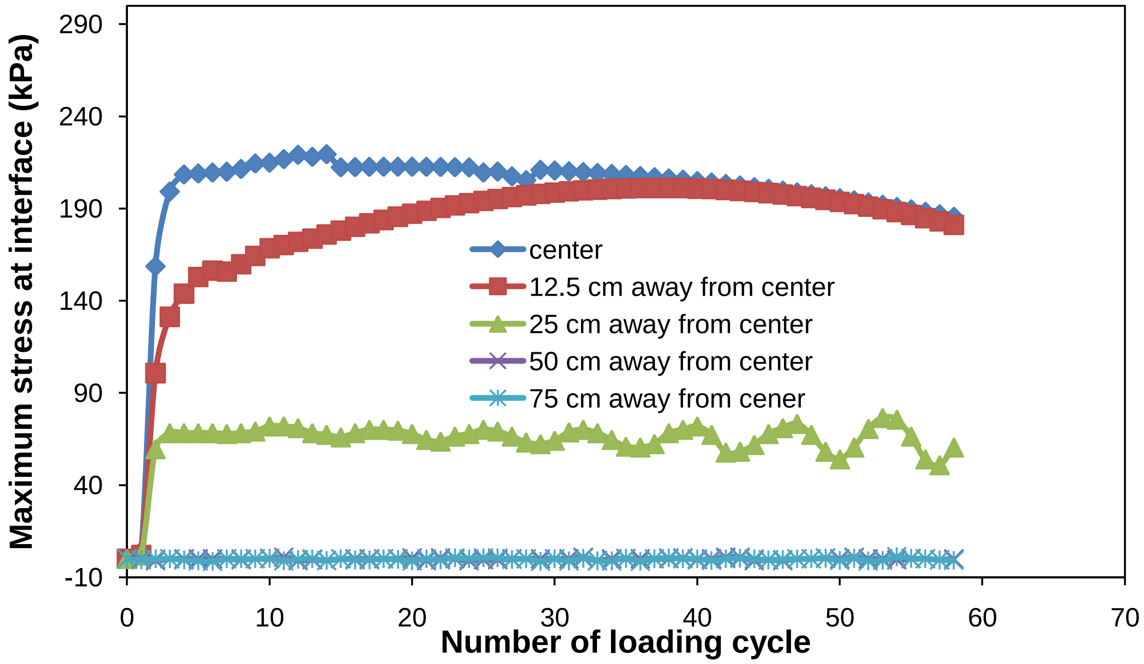

Figure 5.3.29 Measured vertical stresses at the interface of subgrade and base versus the number of loading cycles for the 15 cm thick geocell-reinforced base over moderate subgrade

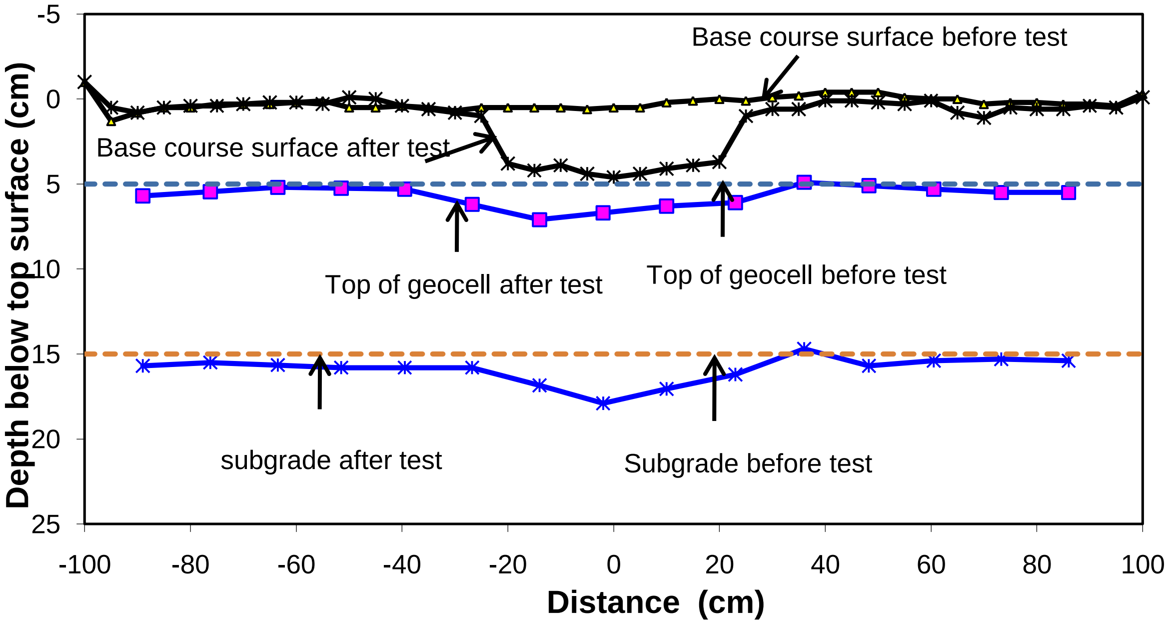

Figure 5.3.30 Profile of 15 cm thick geocell-reinforced base over moderate subgrade

5.3.7 23 cm thick geocell-reinforced base over moderate subgrade

Vane shear tests at three depths were conducted just after the preparation of subgrade at five randomly selected locations. The CBR values of subgrade were calculated using Equation (5.2.1) and are presented in Table 5.3.7. The average CBR of the subgrade was found 4.6% from the vane shear tests.

Table 5.3.7 Subgrade CBR values from vane shear tests

Depth (cm)	CBR (%) at location					Average CBR (%)
	1	2	3	4	5	
10	5	4.2	4.2	5.1	3.5	4.4
18	5.3	4	4.9	5.4	4	4.7
25	4.7	4.9	3.7	5.0	5.1	4.7
Average	5.0	4.4	4.3	5.2	4.2	4.6

The sand cone tests at two randomly selected locations in the RAP base were conducted after the cyclic plate load test and the average degree of compaction was found 91%.

The profiles of the calculated CBR values based on the DCP test data are shown in Figure 5.3.31. The average CBR values of the base course and subgrade were found 10.5% and 4.7% respectively by the DCP tests. Therefore, the subgrade CBR value determined by the DCP test is slightly higher than that by the vane shear tests.

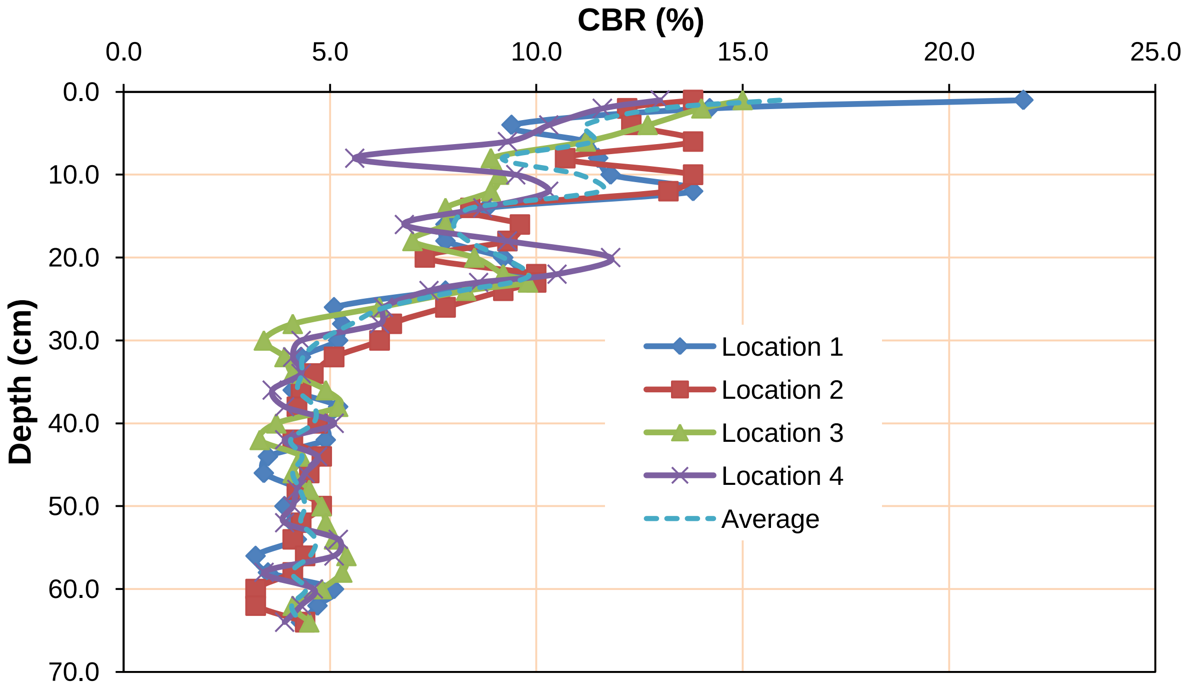

Figure 5.3.31 CBR profiles obtained from DCP tests in the 23 cm thick geocell-reinforced base over moderate subgrade

Figures 5.3.32, 5.3.33, 5.3.34, and 5.3.35 show the permanent deformations at center versus number of loading cycles, the elastic deformations at center versus the number of loading cycles, the maximum stresses at the interface of subgrade and base course versus the number of loading cycles, and the test section profiles for the 23 cm thick geocell-reinforced base over moderate subgrade respectively.

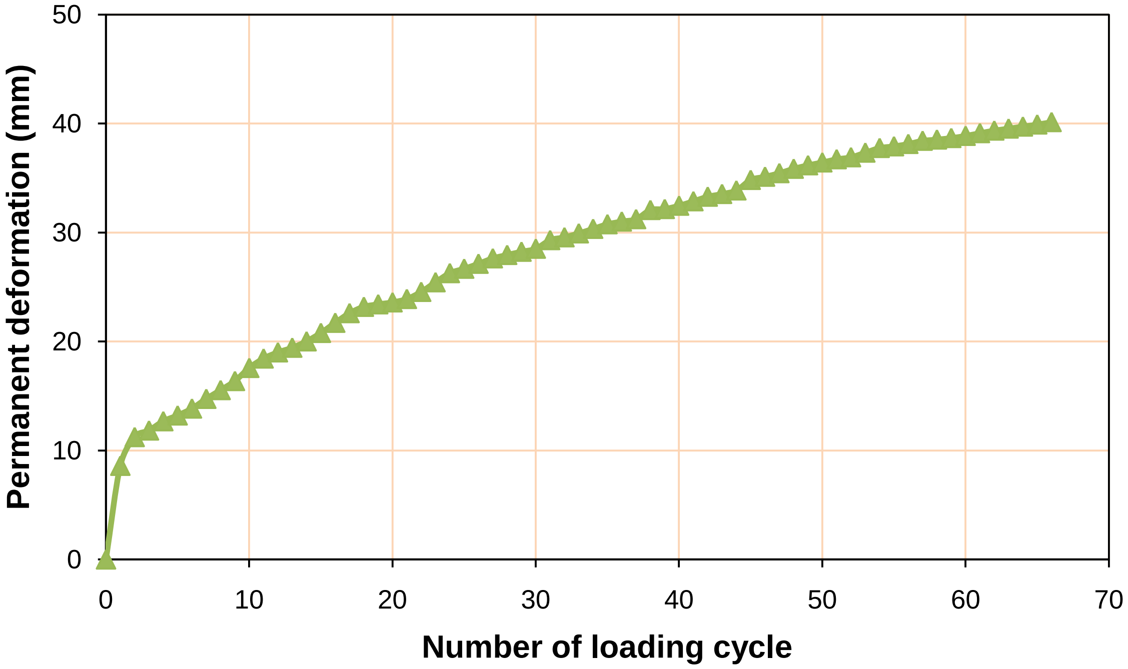

Figure 5.3.32 Permanent deformation at the center versus the number of loading cycles in the 23 cm thick geocell-reinforced base over moderate subgrade

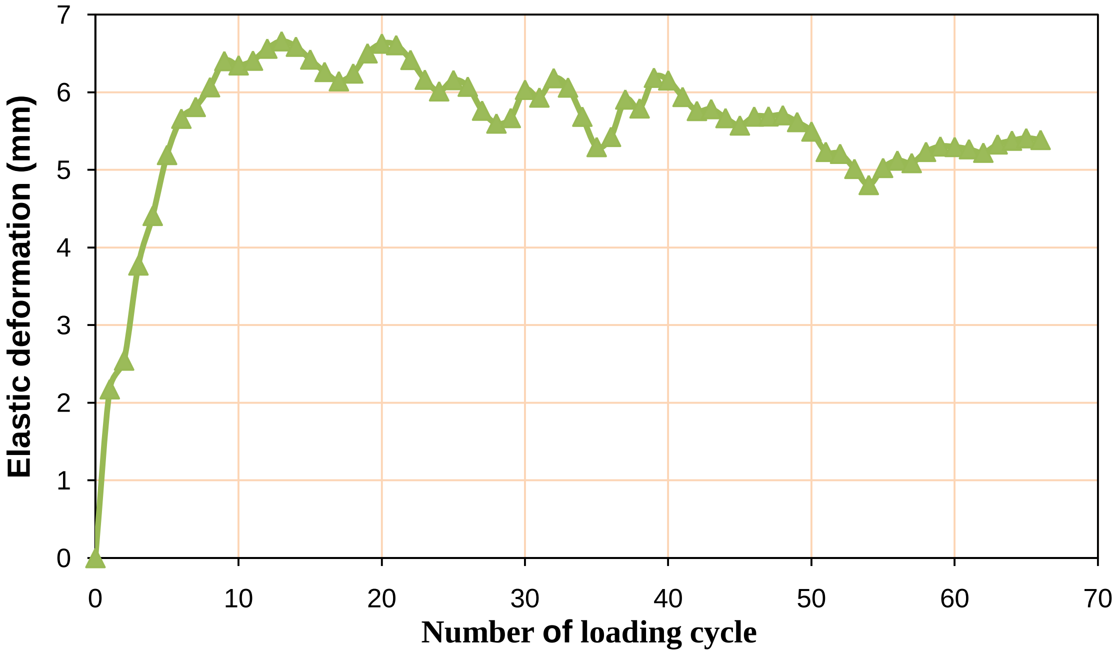

Figure 5.3.33 Elastic deformation at the center versus the number of loading cycles for the 23 cm thick geocell-reinforced base over moderate subgrade

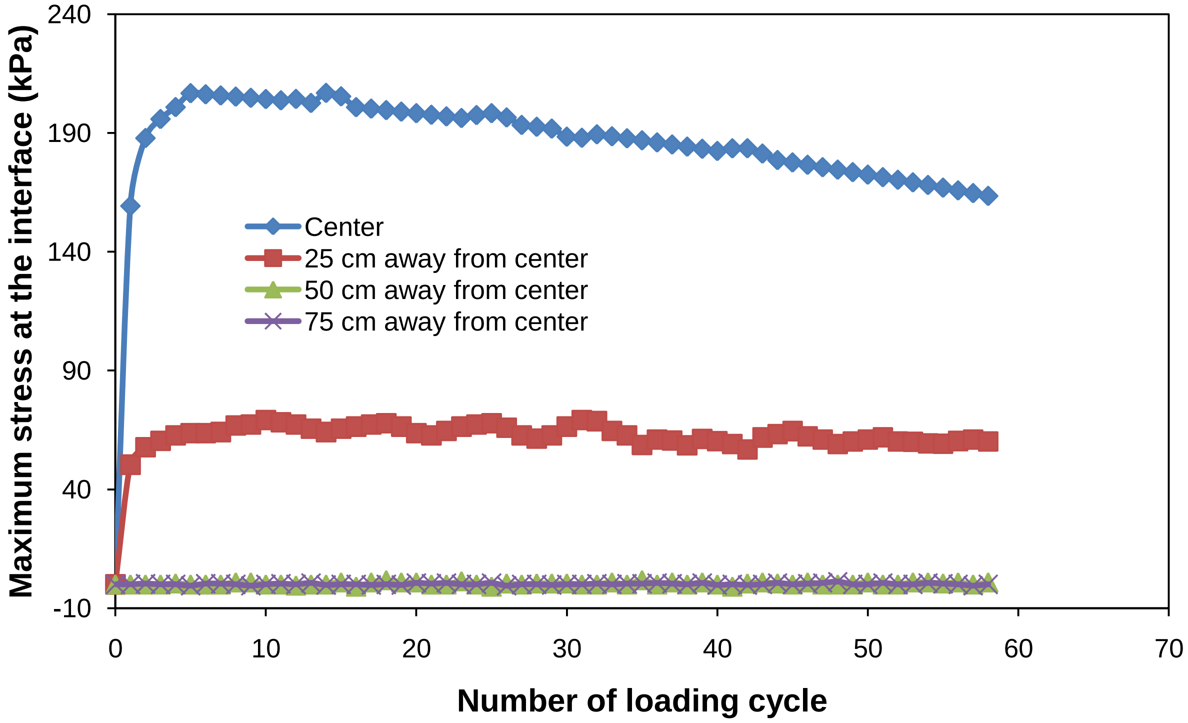

Figure 5.3.34 Measured vertical stresses at the interface of subgrade and base versus the number of loading cycles for the 23 cm geocell-reinforced base over moderate subgrade

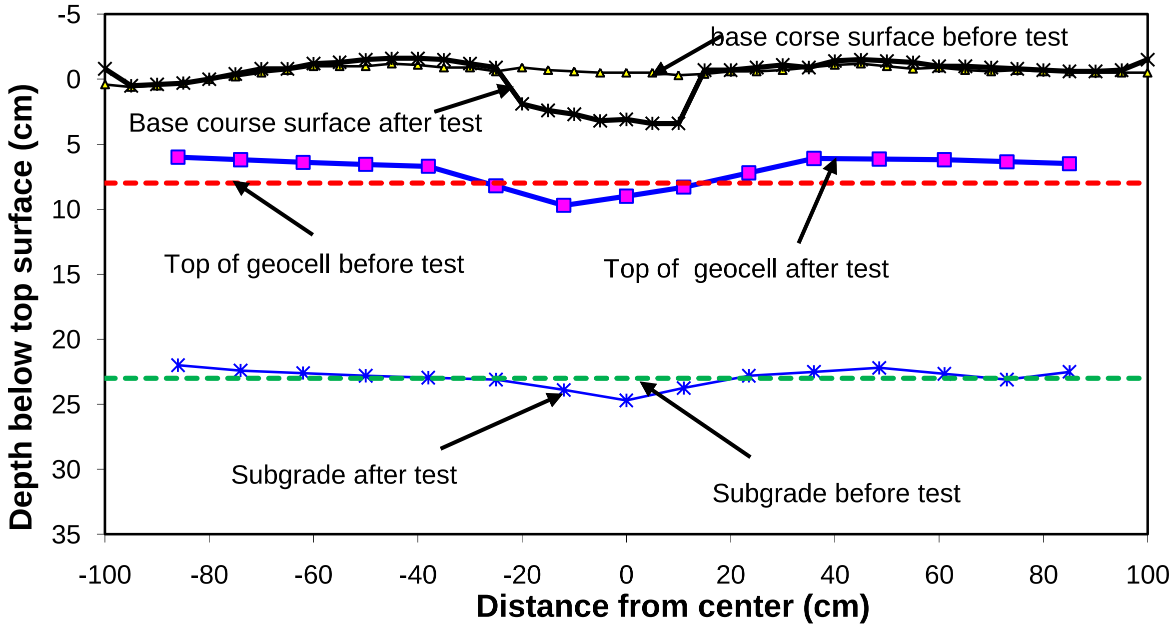

Figure 5.3.35 Profiles of 23 cm thick geocell-reinforced base over noderate subgrade

5.3.8 30 cm thick unreinforced base over moderate subgrade

Vane shear tests at three depths were conducted just after the preparation of subgrade at five randomly selected locations. The CBR values of subgrade were calculated using Equation (5.2.1) and are presented in Table 5.3.8. The average CBR of the subgrade was found 4.5% from the vane shear tests.

Table 5.3.8 Subgrade CBR values from vane shear tests

Depth (cm)	**CBR (%) at location**					**Average CBR (%)**
	1	**2**	**3**	**4**	**5**	
10	4.4	4.2	4.7	4.7	4.2	4.4
18	4.0	5.1	4.7	4.2	4.2	4.4
25	4.3	5.1	4.9	4.2	4.9	4.7
Average	4.2	4.8	4.8	4.4	4.4	4.5

The sand cone tests at two randomly selected locations in the RAP base were conducted after the cyclic plate load test and the average degree of compaction was found 88%.

The profiles of the calculated CBR values based on the DCP test data are shown in Figure 5.3.36. The average CBR values of the base course and subgrade were found 11.4% and 4.6% respectively by the DCP tests. Therefore, the subgrade CBR value determined by the DCP test is slightly higher than that by the vane shear tests.

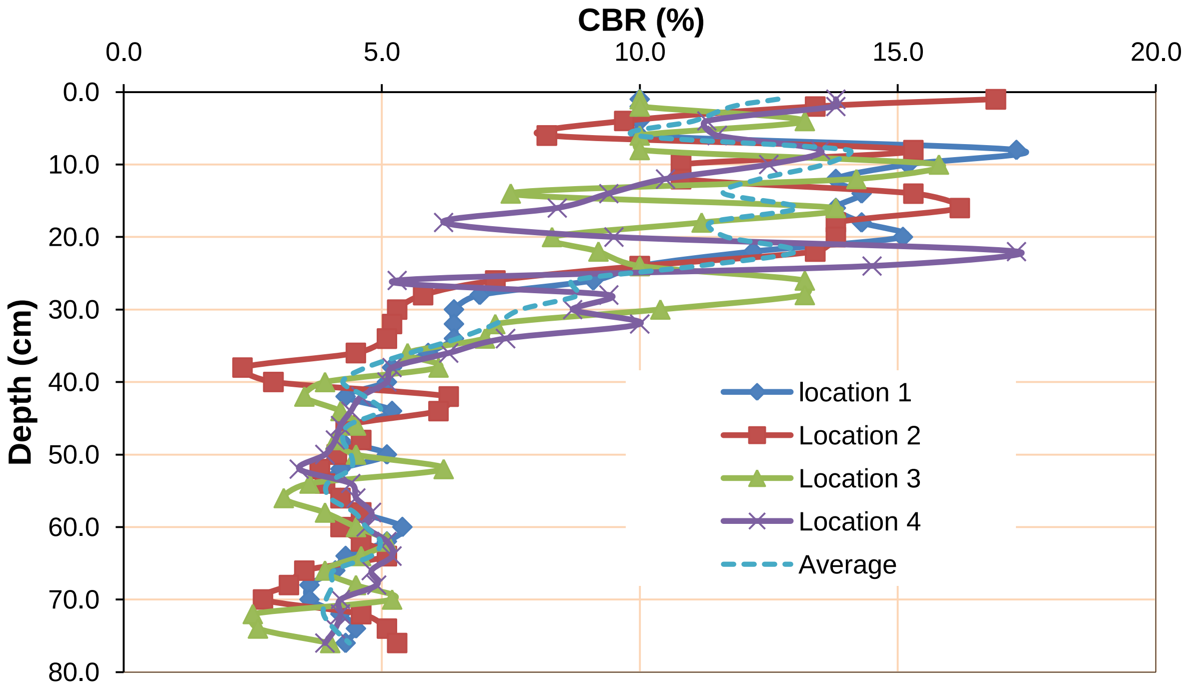

Figure 5.3.36 CBR profiles obtained from DCP tests in the 30 cm thick unreinforced base over moderate subgrade

Figures 5.3.37, 5.3.38, 5.3.39, and 5.3.40 show the permanent deformations at center versus number of loading cycles, the elastic deformations versus number of loading cycles, the maximum stresses at the interface of subgrade and base course at center versus the number of loading cycles, and the test section profiles for 30 cm thick unreinforced base over moderate subgrade respectively.

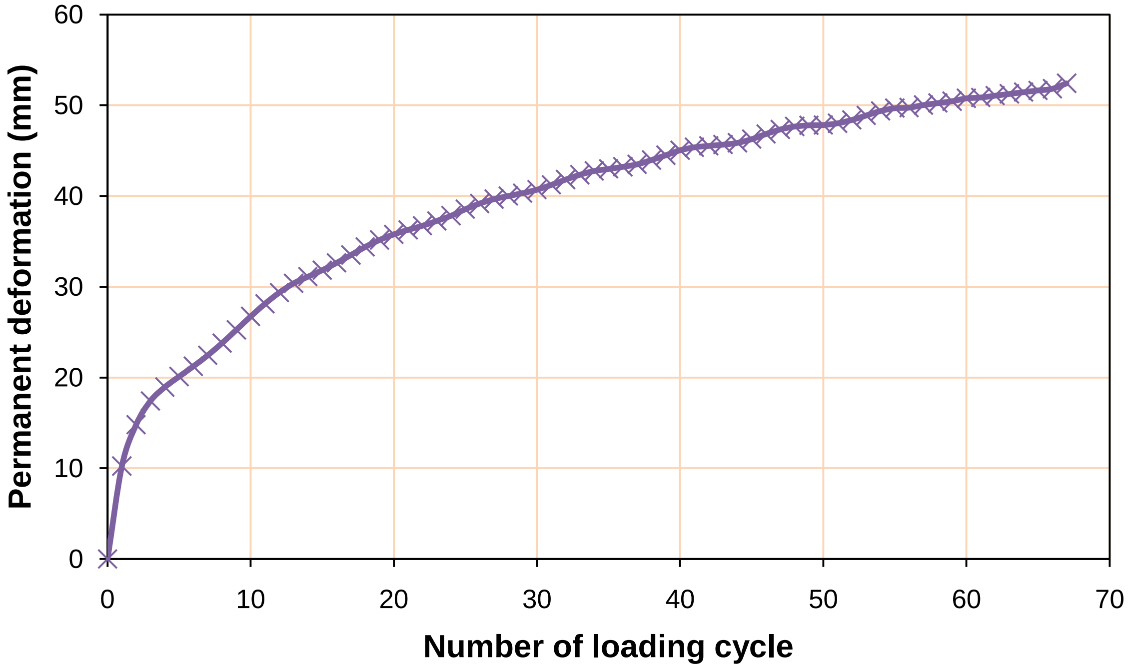

Figure 5.3.37 Permanent deformation at the center versus the number of loading cycle in the 30 cm thick unreinforced base over moderate subgrade

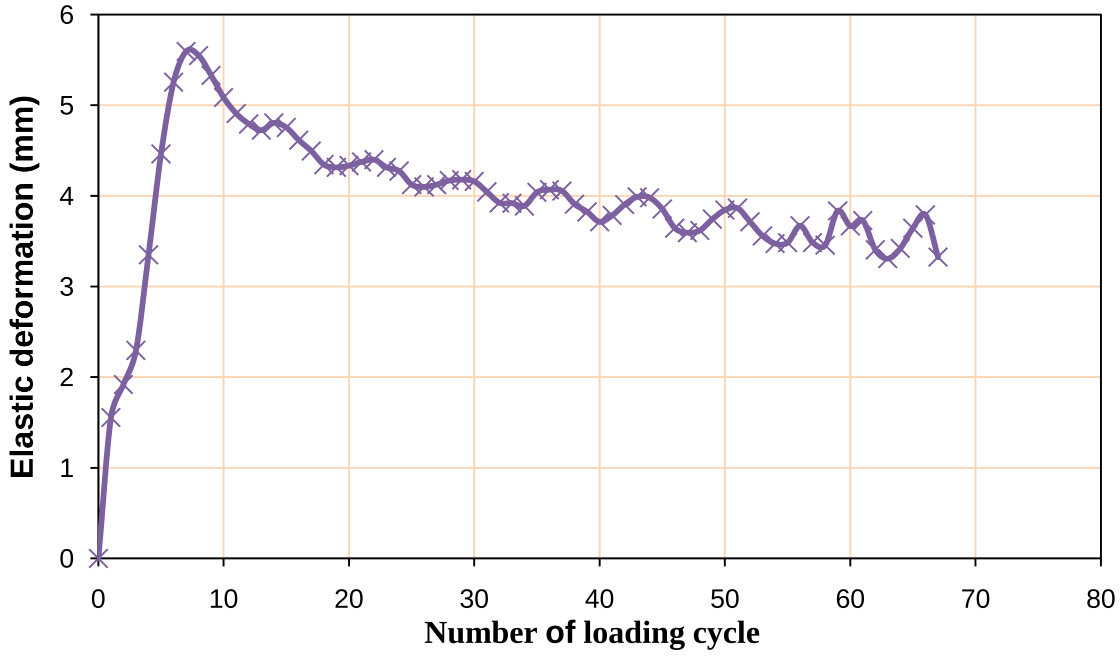

Figure 5.3.38 Elastic deformation at the center versus the number of loading cycles in the 30 cm thick unreinforced base over moderate subgrade

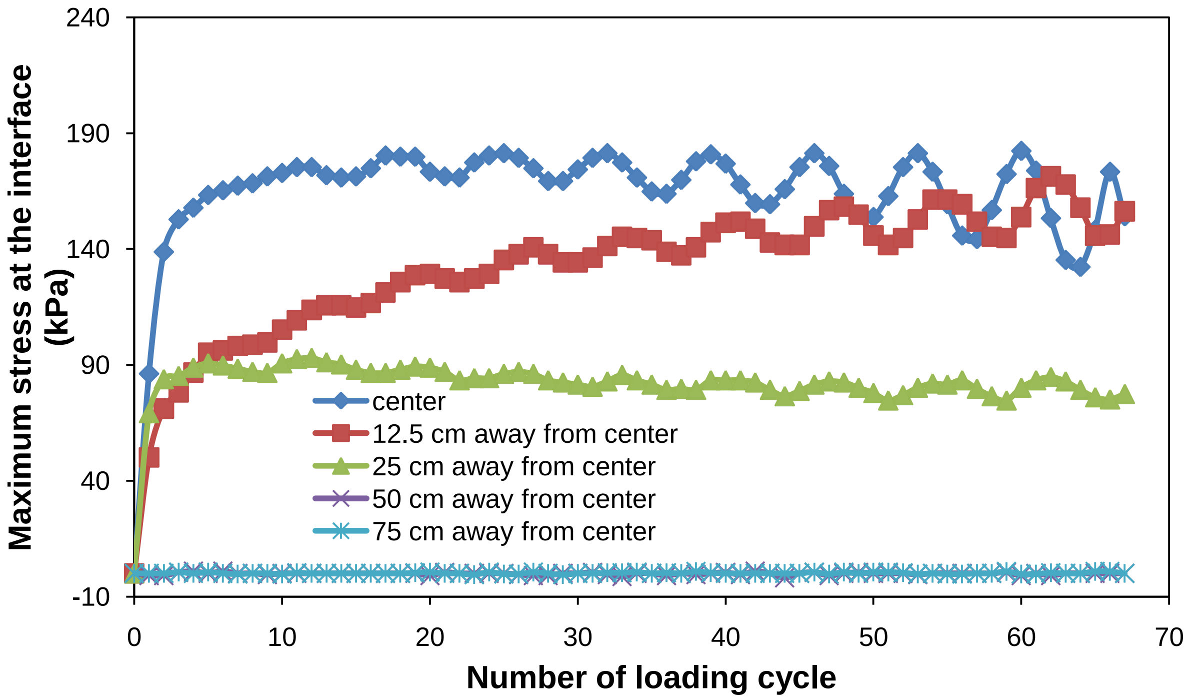

Figure 5.3.38 Measured vertical stresses at the interface of subgrade and base versus the number of loading cycles for the 30 cm thick unreinforced base over moderate subgrade

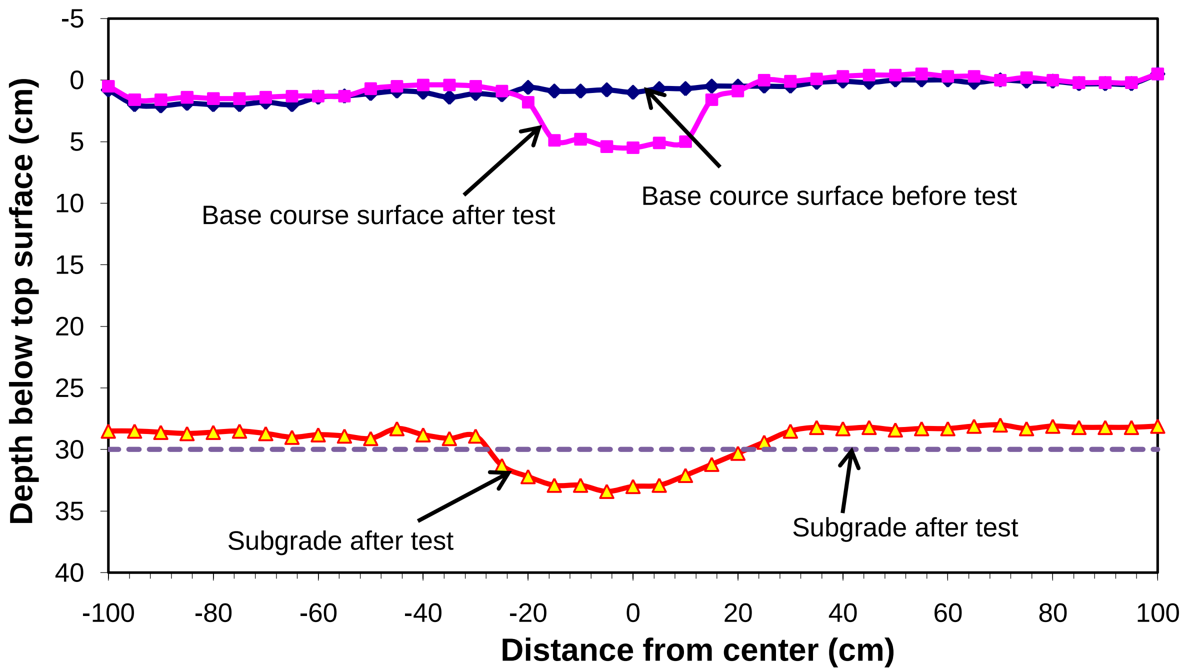

Figure 5.3.39 Profiles of 30 cm thick unreinforced base over moderate subgrade

5.3.9 30 cm thick geocell-reinforced base over moderate subgrade

Vane shear tests at three depths were conducted just after the preparation of subgrade at five randomly selected locations. The CBR values of subgrade were calculated using Equation (5.2.1) and are presented in Table 5.3.9. The average CBR of the subgrade was found 4.5% from the vane shear tests.

Table 5.3.9 Subgrade CBR values from vane shear tests

Depth (cm)	CBR (%) at location					Average CBR (%)
	1	2	3	4	5	
10	4.1	4.2	4.7	4.0	5.3	4.4
18	4.4	4.5	5.4	4.2	4.2	4.5
25	4.3	4.8	4.9	4.6	4.1	4.5
Average	4.3	4.5	5.0	4.3	4.5	4.5

The sand cone tests at two randomly selected locations in the RAP base were conducted after the cyclic plate load test and the average degree of compaction was found 89%.

The profiles of the calculated CBR values based on the DCP test data are shown in Figure 5.3.40. The average CBR values of the base course and subgrade were found 10.2% and 4.6% respectively by the DCP tests. Therefore, the subgrade CBR value determined by the DCP test is slightly higher than that by the vane shear test.

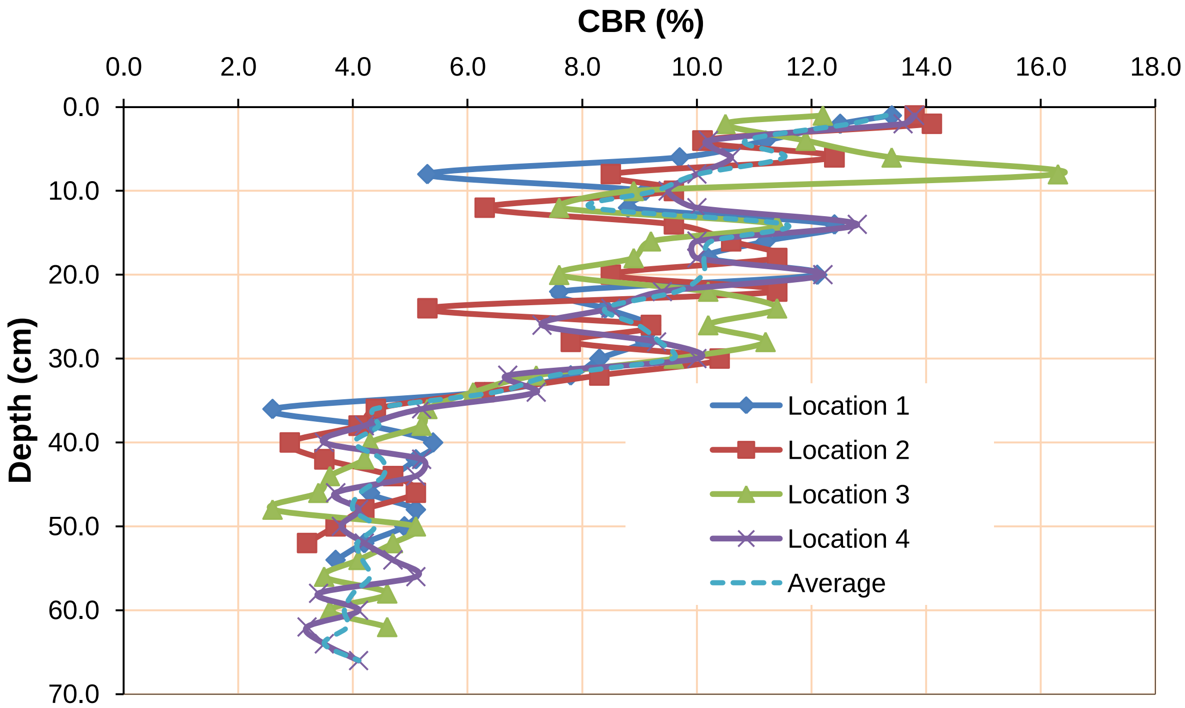

Figure 5.3.40 CBR profiles obtained from DCP tests in the 30 cm thick geocell-reinforced base over moderate subgrade

Figures 5.3.41, 5.3.42, 5.3.43, and 5.3.44 show the permanent deformations at center versus the number of loading cycles, the elastic deformations at center versus the number of loading cycles, the maximum stresses at the interface of subgrade and base course versus the number of loading cycles, and the test section profiles for 30 cm thick geocell-reinforced base over moderate subgrade respectively.

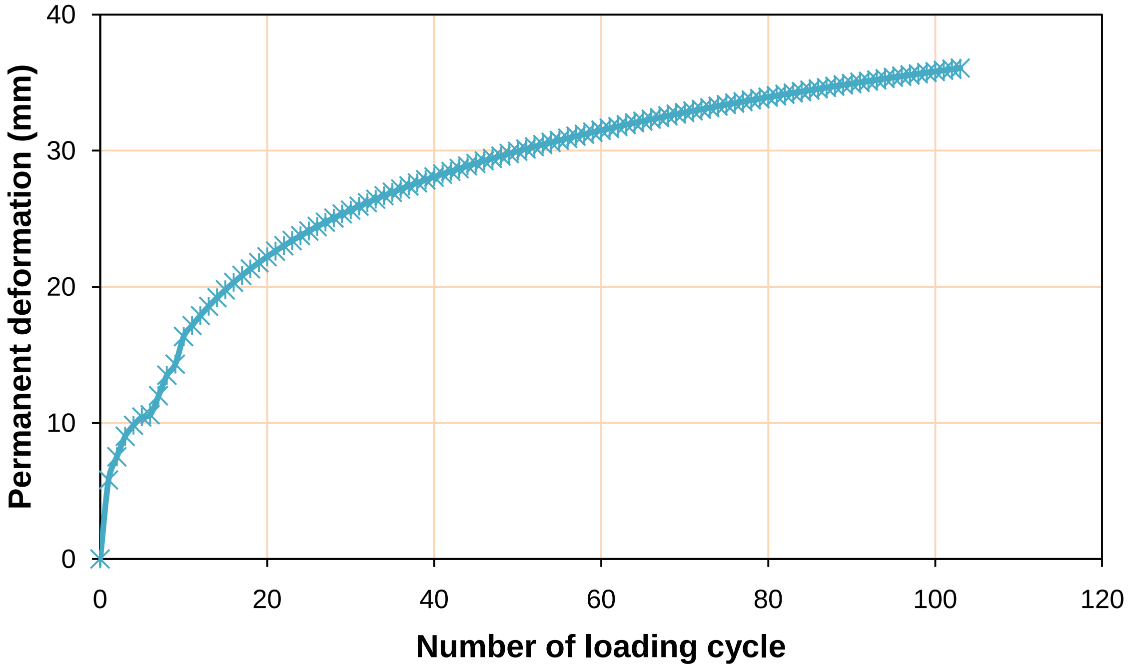

Figure 5.3.41 Permanent deformation at the center versus the number of loading cycles in the 30 cm thick geocell-reinforced base over moderate subgrade

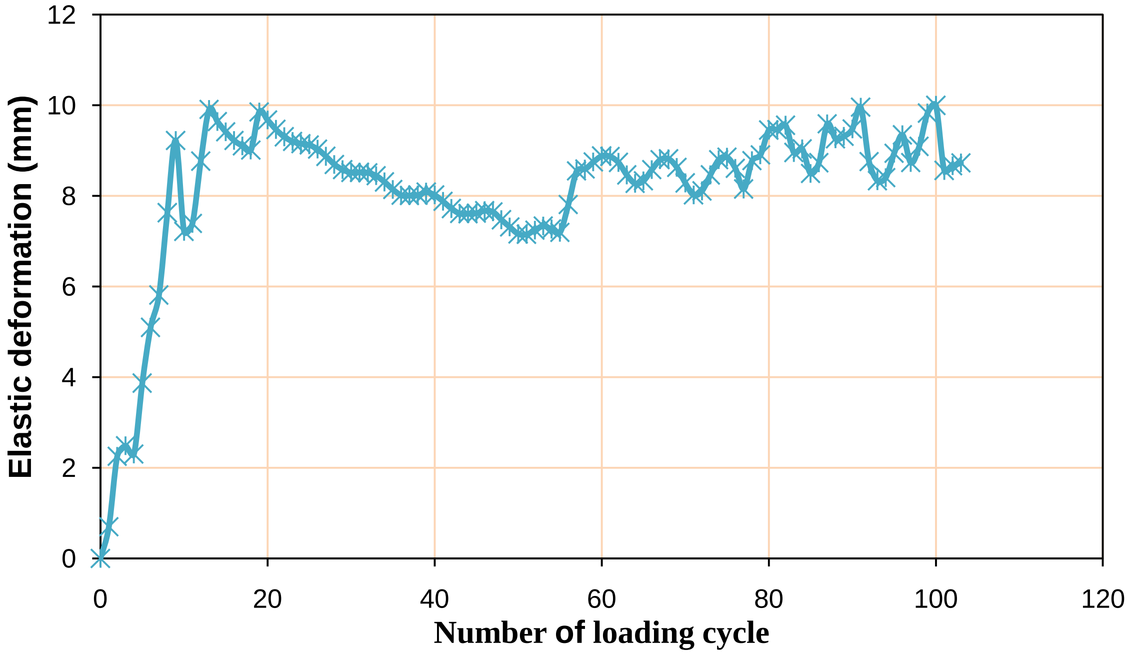

Figure 5.3.42 Elastic deformation at the center versus the number of loading cycles for the 30 cm thick geocell-reinforced base over moderate subgrade

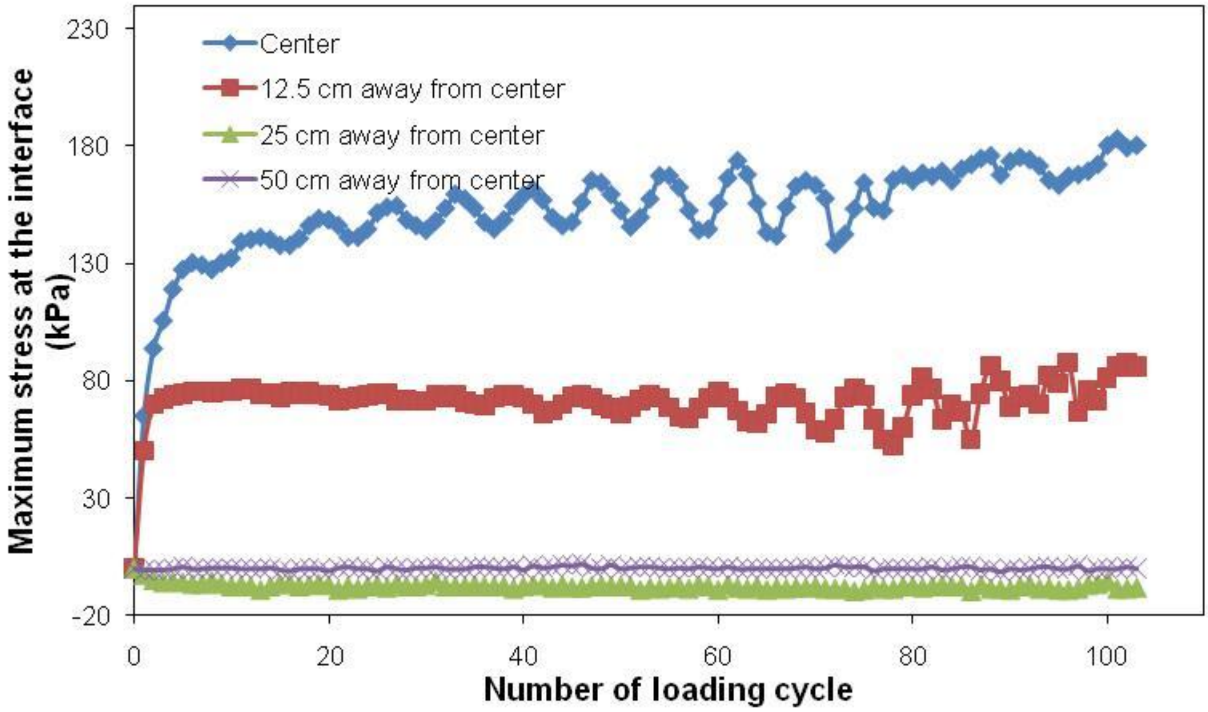

Figure 5.3.14 Measured vertical stresses at the interface of subgrade and base and subgrade versus the number of loading cycle for the 30 cm thick geocell-reinforced base over moderate subgrade

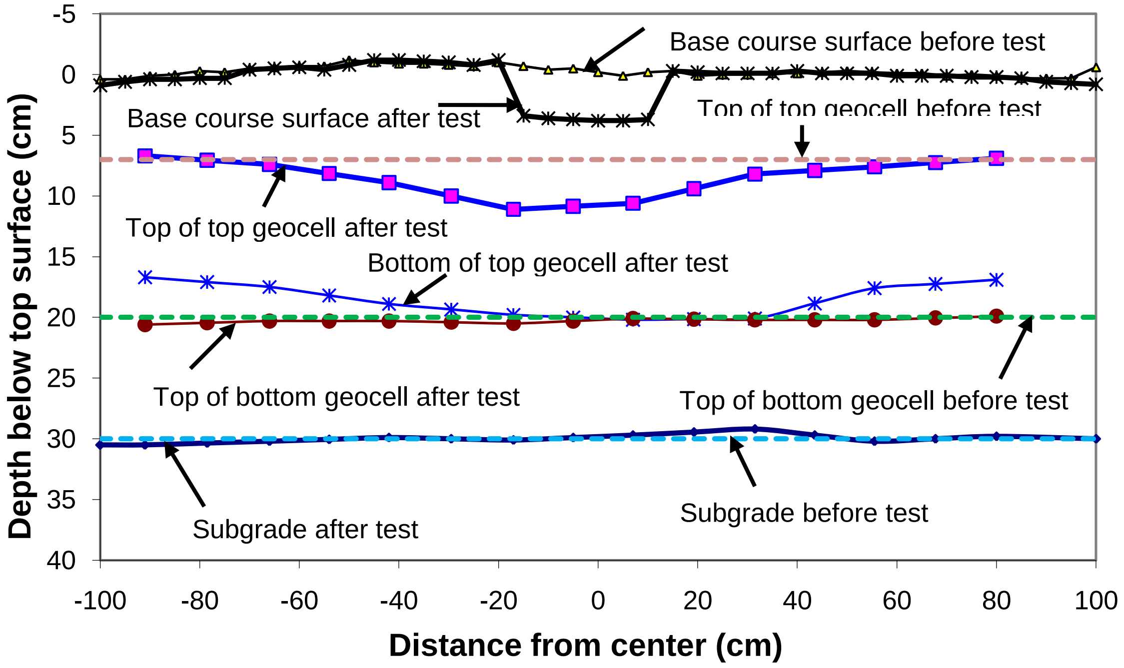

Figure 5.3.15 Profiles of 30 cm thick geocell-reinforced base over moderate subgrade

5.4 Analysis of test data for geocell-reinforced RAP bases on soft subgrade

5.4.1 Vane shear, DCP, and sand cone test results

Vane shear tests were performed just after the preparation of subgrade for each test to confirm that the target CBR was approximately achieved. The average CBR values of the subgrade obtained from the vane shear tests were 2.1 %, 1.9%, 2.0%, and 1.9% in the geocell-reinforced (15, 23, and 30 cm thick) and unreinforced (30 cm thick) bases respectively. The DCP tests were conducted one day after the base course was placed on top of the subgrade. The average CBR values of the base courses and subgrade were 11.4% and 2.8%, 6.3% and 2.0%, 10.2% and 2.1%, and 10.2% and 2.0% in the geocell-reinforced (15, 23, and 30 cm thick) and unreinforced (30 cm thick) sections respectively. The higher subgrade CBR values were obtained from DCP tests because the DCP tests were conducted one day after the preparation of the test sections and also because some compaction energy went into the subgrade during base material compaction. The average CBR profiles obtained from the DCP tests carried out on the test ready sections are also shown in Figure 5.4.1 to check the consistency of the test sections.

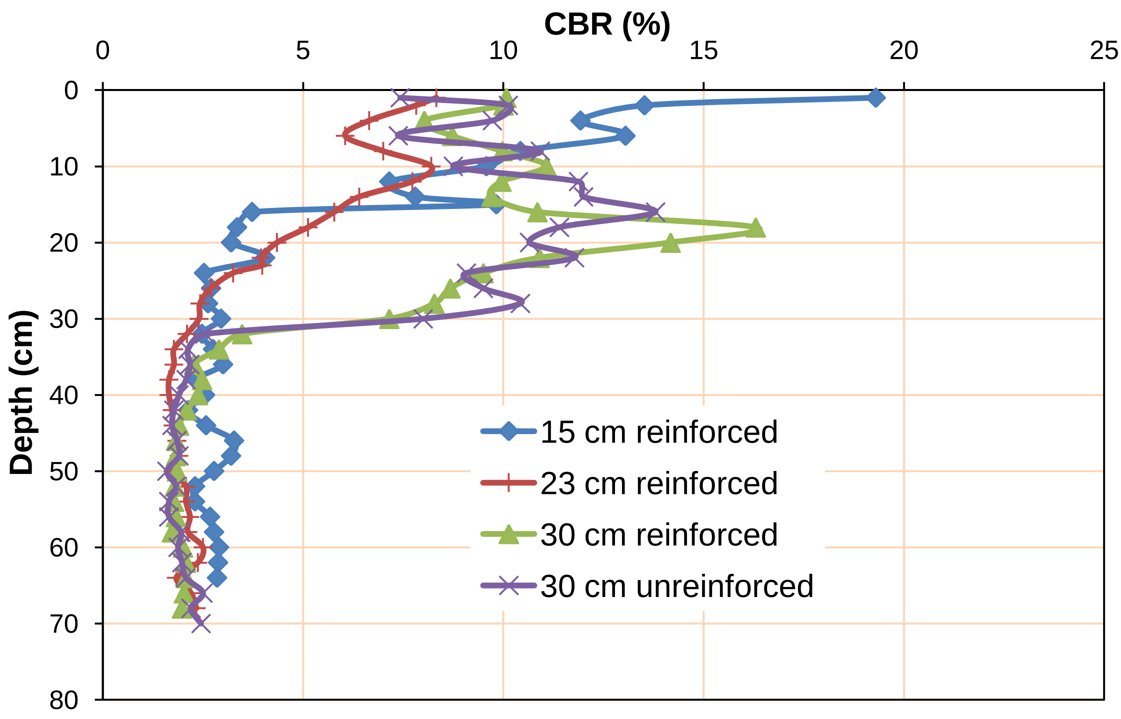

Figure 5.4.1 Average CBR profiles obtained from DCP tests in different sections with soft subgrade

Sand cone tests were carried out after each cyclic plate load test. The relative compaction was calculated as 94%, 84%, 86%, and 91% for the reinforced (15, 23, and 30 cm) and unreinforced (30 cm) bases, respectively. The CBR values increased with the degree of compaction.

5.4.2 Permanent deformation

The permanent deformation of 75 mm was used as the criteria to stop the cyclic loading test. This criterion was used by US Army Corps of Engineers (Hammitt, 1970 and Giroud and Han 2004 a, b) to define the failure of the unpaved roads. However, the test was stopped after 45 cycles and 59.1 mm permanent deformation in the 30 cm thick reinforced section due to the malfunction in the testing machine. The permanent deformations of the unreinforced and reinforced bases at the center versus the number of loading cycles are shown in Figure 5.4.2. The test data of the 30 cm thick reinforced section were extrapolated up to 75 mm permanent deformation for comparison purposes (the extrapolated results are presented by the dotted line). The permanent deformation increased with the number of loading cycles. The rate of increase in the permanent deformation decreased with an increase in the number of loading cycles. For the permanent deformation of 75 mm, the unreinforced (30 cm thick) and reinforced (15, 23, and 30 cm thick) bases lasted for 5, 32, 18, and 97 loading cycles, respectively. The 23 cm thick geocell-reinforced base lasted for less number of loading cycles than the 15 cm geocell-reinforced base. This result was due to less compaction resulting in lower CBR values of the base and subgrade in the 23 cm thick base as compared with the 15 cm thick base. The unreinforced RAP base section had the largest permanent deformation among all the test sections while the 30 cm thick reinforced base section had the smallest permanent deformation. The 23 and 15 cm thick reinforced base sections had smaller permanent deformations than the 30 cm thick unreinforced section, although they had thinner bases This comparison demonstrates the benefits of NPA geocell reinforcement including the improved performance of the reinforced section over the unreinforced section. The reinforced (15 cm, 23 cm, and 30 cm) bases improved the performance by a factor of 6.4, 3.6, and 19.4 over the 30 cm thick unreinforced base, respectively. If a corresponding thinner unreinforced base had been considered, the improvement factor would be even significant.

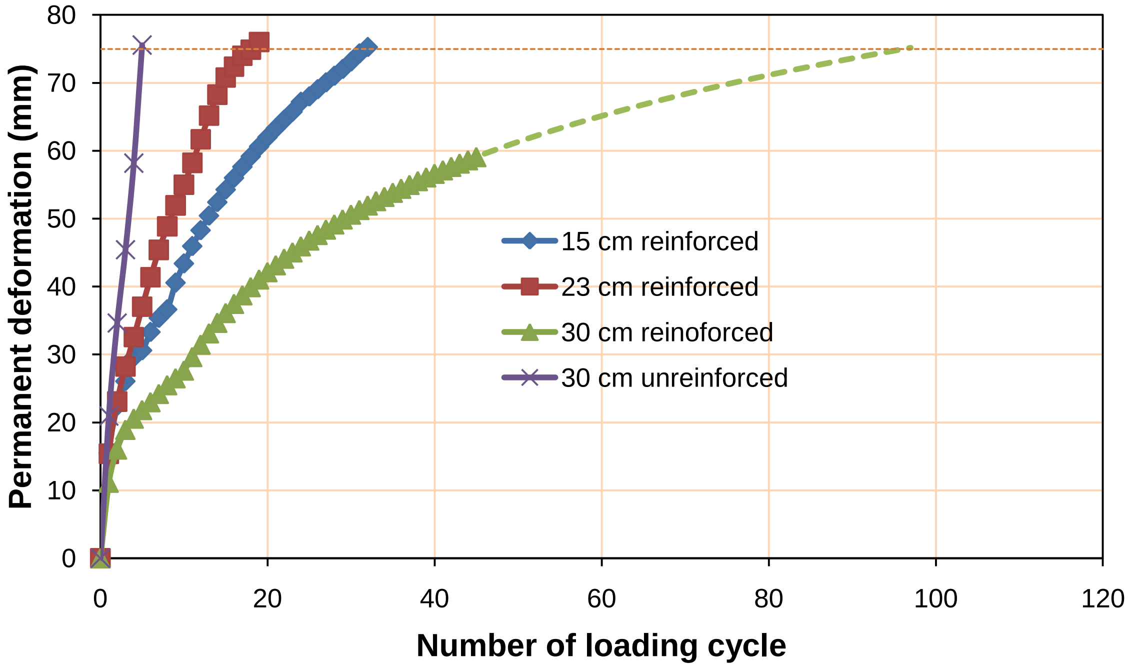

Figure 5.4.2 Permanent deformations at the center versus the number of loading cycles for RAP bases over soft subgrade

Figure 5.4.3 presents the permanent deformations at the 0, 25, 50, and 75 cm away from the center of the loading plate at the end of tests. For both unreinforced and reinforced sections, there was a small amount of heave (i.e., negative permanent deformation) at the locations of 50 cm and 75 cm away from the center. Only a small amount of compression was observed at 25 cm away from the center for all test sections.

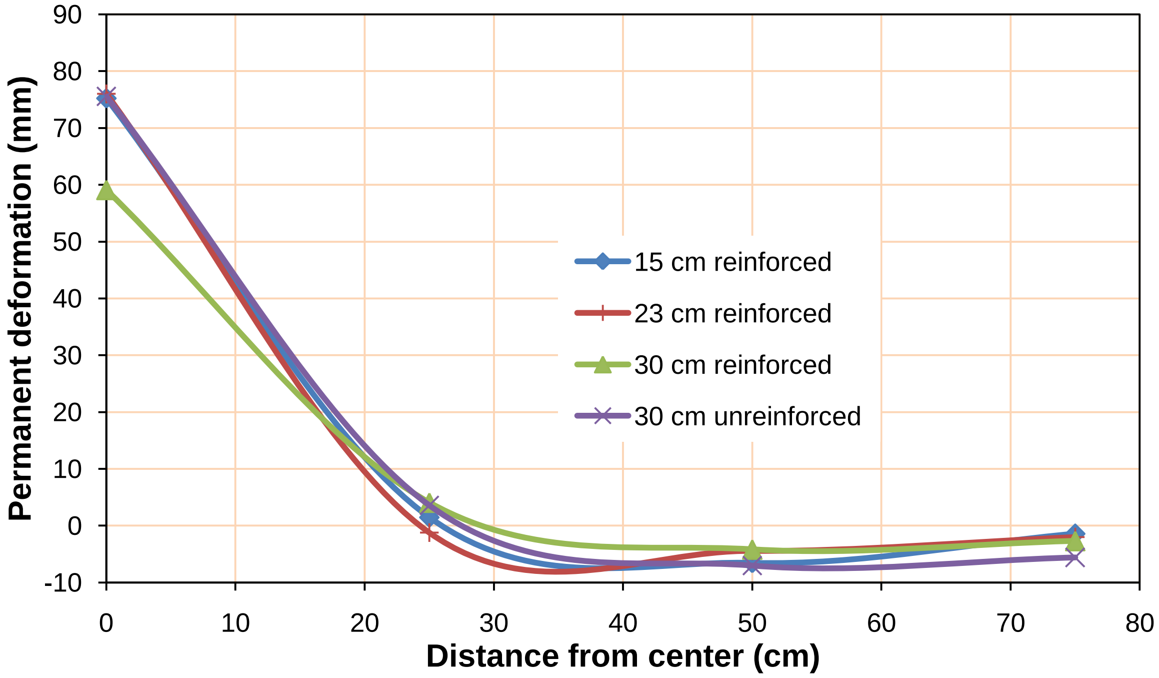

Figure 5.4.3 Permanent deformations at different locations at the end of tests for RAP bases over soft subgrade

5.4.3 Elastic deformation

The elastic deformation and percentage of elastic deformation at the center of the loading plate at different numbers of loading cycles are presented in Figures 5.4.4 and 5.4.5. The elastic deformation is defined as the rebound of the base when unloaded from the maximum load (40kN) to the minimum load (0.5kN). The percentage of elastic deformation was calculated by dividing the elastic deformation at each load cycle to the total deformation (i.e., the sum of elastic and plastic deformations) at that cycle. The amount of elastic deformation and percentage of elastic deformation increased rapidly at the initial few loading cycles but later stabilized to a constant value for the geocell-reinforced bases whereas they increased sharply until the failure for the unreinforced base. The maximum elastic deformations for the reinforced and unreinforced bases were approximately 10 mm and 2.7 mm, respectively. The percentages of elastic deformations were 90.6%, 89.2%, 94.5%, and 13.3% for the reinforced (15, 23, and 30 cm) bases and unreinforced (30 cm) bases, respectively. The unreinforced RAP base section had the least percentage of elastic deformation among all the test sections while the 30 cm thick reinforced base section had the most percentage of elastic deformation at the end of the test.

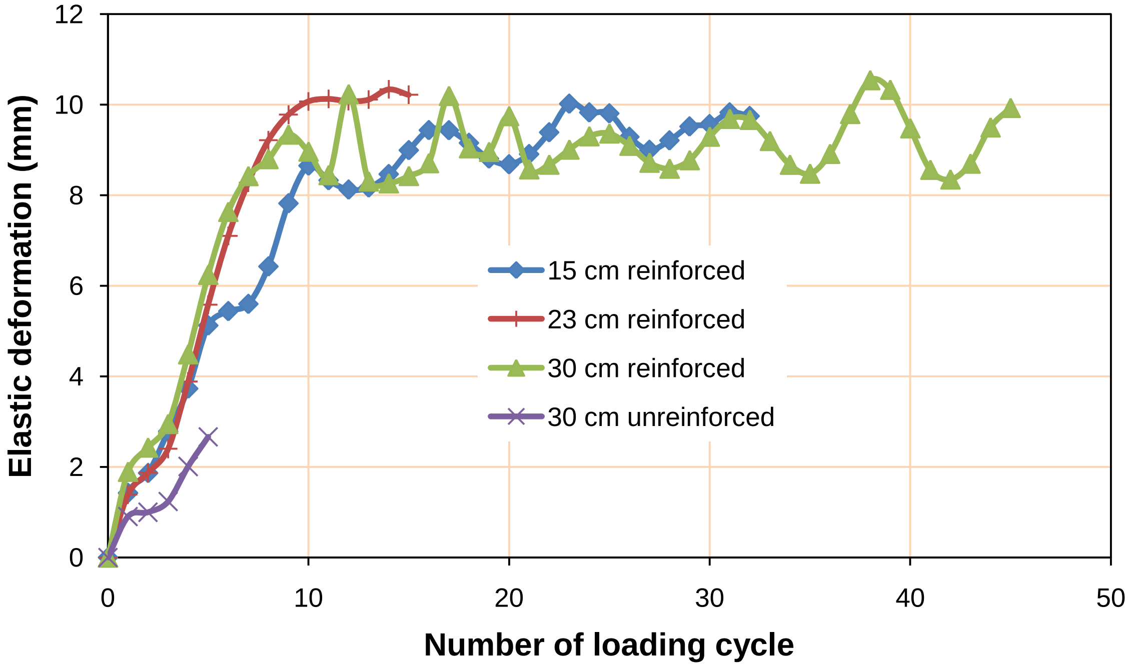

Figure 5.4.4 Elastic deformation at the center versus the number of loading cycles for RAP bases over soft subgrade

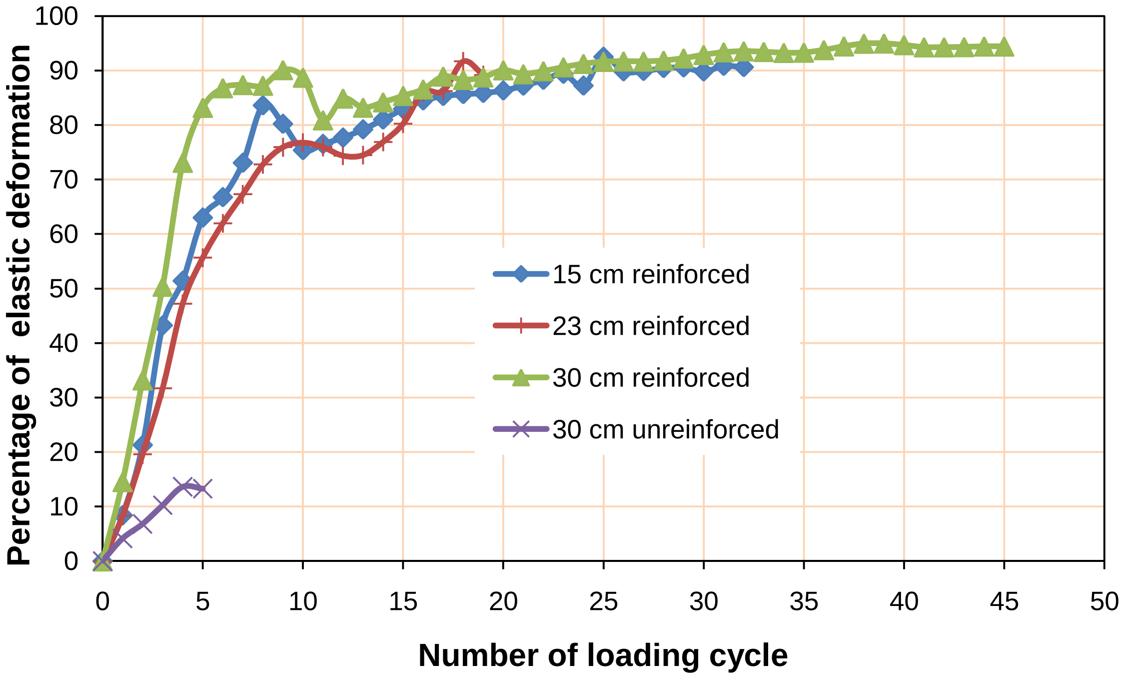

Figure 5.4.5 Percentage of elastic deformation at the center versus the number of loading cycles for RAP bases over soft subgrade

5.4.4 Vertical stress at interface

The vertical stresses at the interface of subgrade and base course were measured by the pressure cells located at 0, 12.5, 25, 50, and 75 cm from the center of the plate. In the reinforced bases, no pressure cell was installed at the 75 cm location due to the limited number of pressure cells available during those tests. Figures 5.4.6 and 5.4.7 show the maximum vertical stresses at the interface of subgrade and base course versus the number of loading cycles at the center and 12.5 cm away from the center respectively. The vertical stress increased rapidly at the initial few numbers of cycles and later it decreased slowly by a small magnitude or stabilized to a constant value in the reinforced cases whereas it kept increasing until failure in the unreinforced case. The vertical stresses at the interface of subgrade and base course at the center and 12.5 cm away from center were 291 and 329, 159 and 210, 144 and 144, and 197 and 182 kPa in the reinforced (15, 23, and 30 cm) and unreinforced (30 cm) bases, respectively. The vertical stress was highest in the 15 cm thick reinforced bases and lowest in the 30 cm thick reinforced bases. It demonstrates that the vertical stress decreased with an increase in the base thickness and geocell reinforcement.

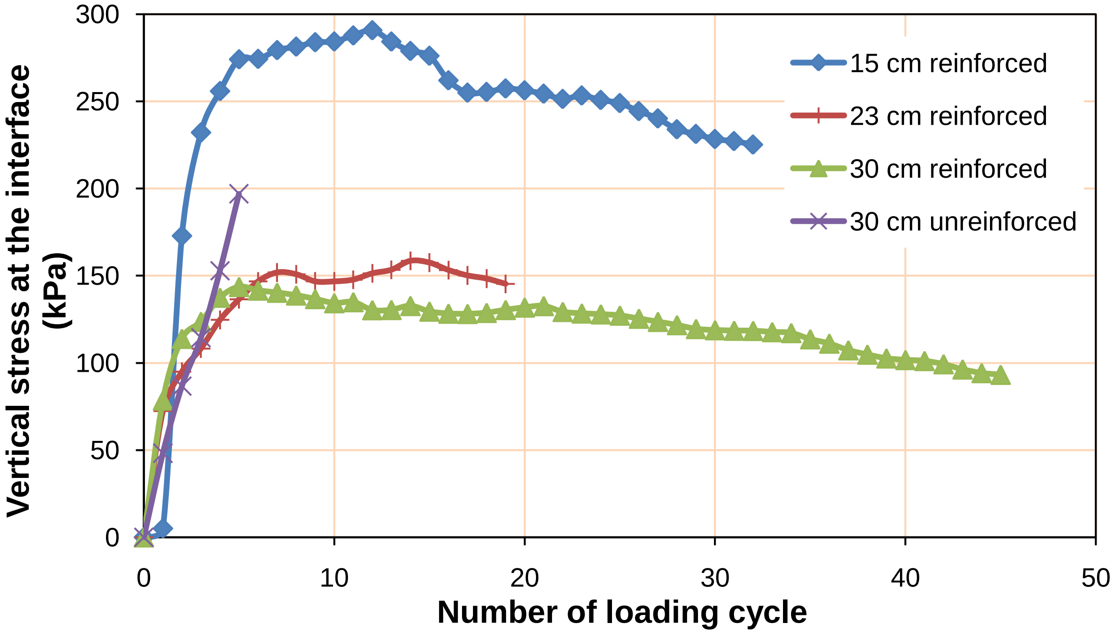

Figure 5.4.6 Vertical stresses at the interface of soft subgrade and RAP bases at the center

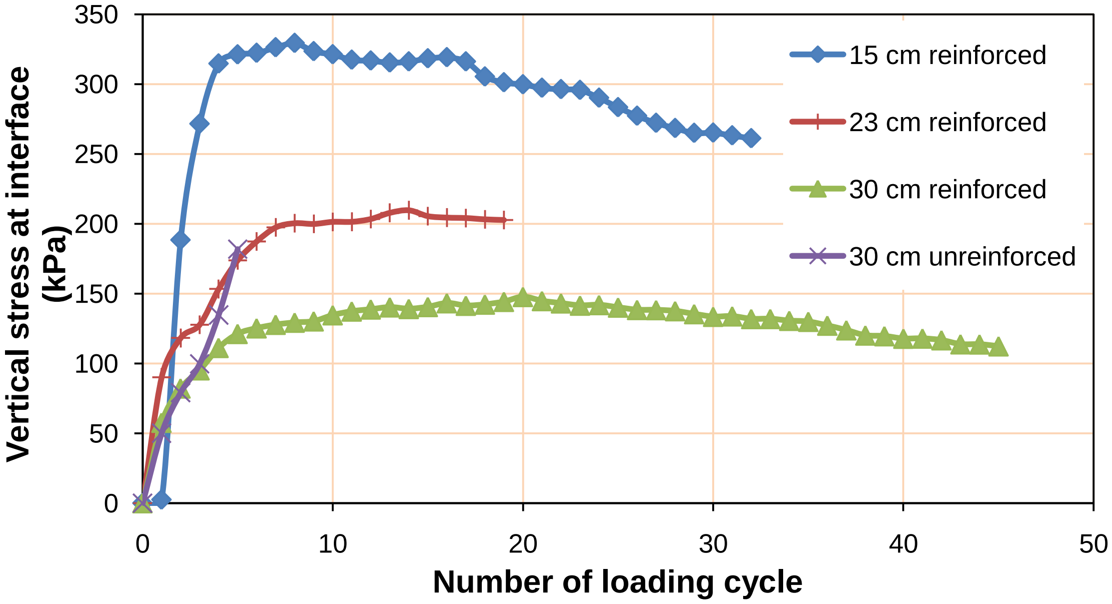

Figure 5.4.7 Vertical stresses at the interface of soft subgrade and RAP bases at 12.5 cm away from the center

5.4.5 Vertical stress distribution

Figures 5.4.8 and 5.4.9 present the vertical stress distribution at different locations at the interface of subgrade and base at 25 mm and 50 mm central permanent deformations. The verticle stress at 12.5 cm was slightly gretaer than or equal to that at the center for all those bases. The vertical stresses decreased rapidly after 12.5 cm away from the center and the least vertical stresses were observed at the farthest point from the the center. The sections having higher stresses at the center and 12.5 cm away from the center had lower stresses at other locations and vice versa.

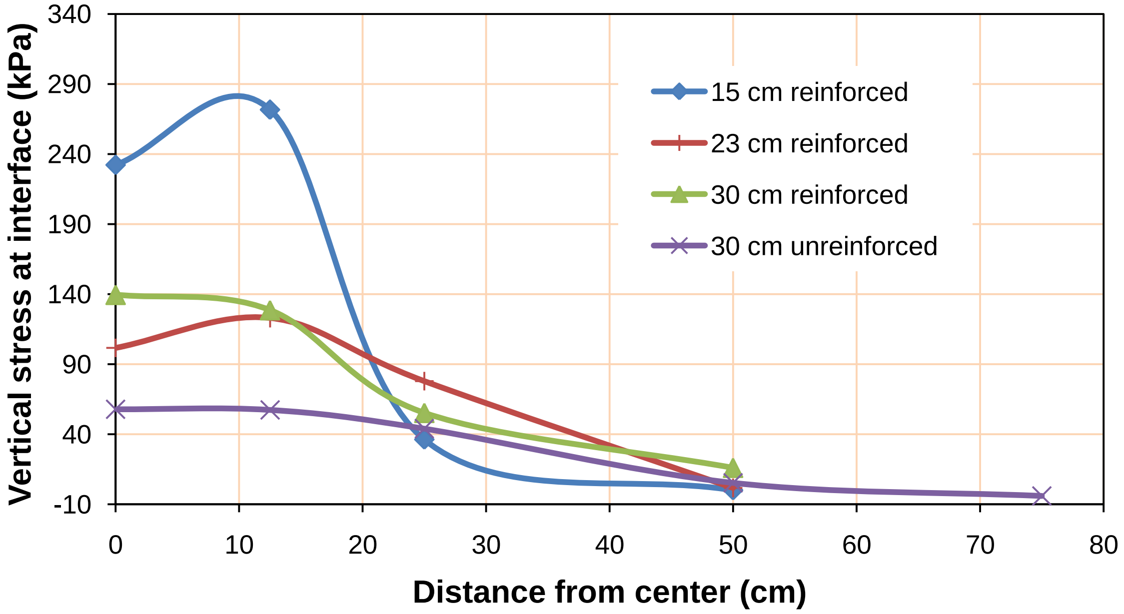

Figure 5.4.8 Vertical stress distribution at the interface of soft subgrade and RAP bases at 25 mm central permanent deformation

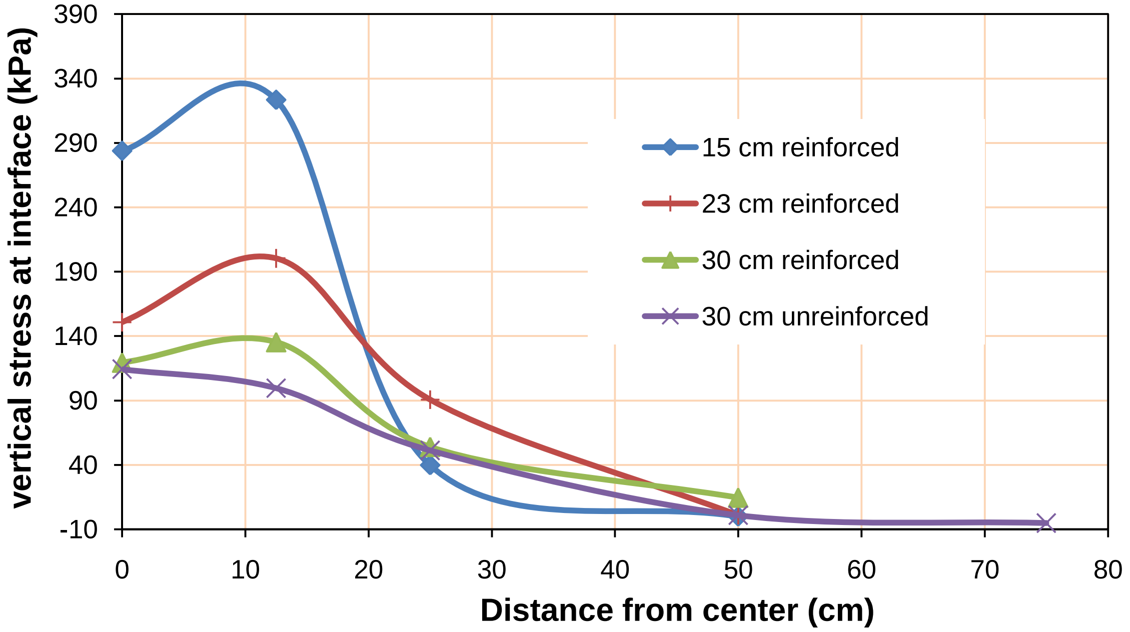

Figure 5.4.9 Vertical stress distribution at the interface of soft subgrade and RAP bases at 50 mm central permanent deformation

The stress distribution at the center of the base can be further expressed in terms of a stress distribution angle as follows:

$$p_i = \frac{P}{\pi(r + h\tan\alpha)^2} \qquad (5.4.1)$$

where p_i = the distributed vertical stress at the center of the interface of the base course and the subgrade (kPa); P = the applied load = 40 kN; r = the radius of the tire contact area = 0.304 m; h = the thickness of the base course (varied); and α = the stress distribution angle in degree. The calculated stress distribution angles at different loading cycles are shown in Figure 5.4.10. The stress distribution angle decreased rapidly during the initial few loading cycles and then stabilized to a constant value or increased slowly by a small magnitude for the reinforced bases, whereas it continued to decrease to a minimum value for the unreinforced base. The minimum stress distribution angles for the three reinforced (15, 23, and 30 cm) and the unreinforced (30 cm) bases were 29.4°, 22.9°, 35.5°, and 18.5° respectively. It can be concluded that the NPA geocell reinforcement reduced the vertical stress by distributing the load to a wider area.

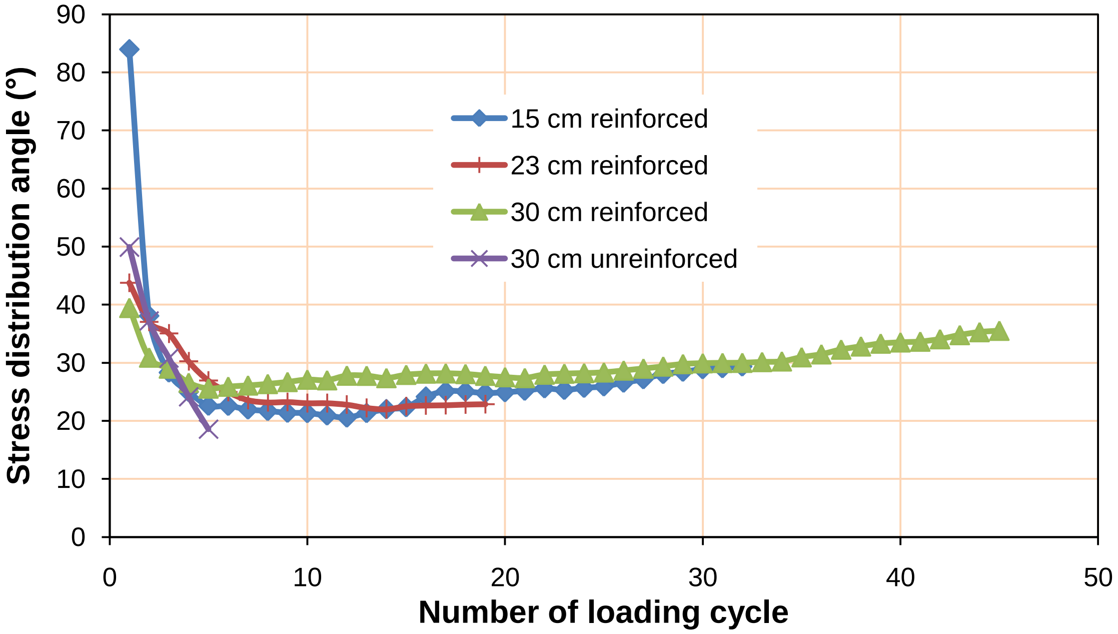

Figure 5.4.10 Stress distribution angle versus the number of loading cycles

5.4.6 Maximum strain in the geocell

The strain gages were installed at the geocell walls to measure the induced strains due to the deformation of geocell under cyclic loading. Three strain gages were installed at the central geocell , two were installed at the locations adjacent to the central geocell, and one was installed at the next neighbouring geocell as shown in Figure 5.2.2 . The total number of strain gages installed for 15, 23 and 30 cm thick reinforced sections were 6, 6, and 12 respectively. There were only six slots available in the data recorder for strain gage connection. Therefore, for the 30 cm thick reinforced section, only six strain gages were connected to the data recorder for recording during tests while other strain gages were connected to the data recorder for recording after the tests. All the strain gages affixed on the top and bottom of the geocell walls were used to measure the horizontal strains while the strain gages affixed at the middle of the wall were used to measure the vertical strains. The maximum strain induced at different locations of geocell wall versus number of the loading cycles for 15 cm, 23 cm, and 30 cm thick reinforced sections are shown in Figures 5.4.11, 5.4.12, and 5.4.13 respectively. There is no strain data for the middle strain gage at the central geocell of 23 cm thick reinforced base. For the top gages affixed on both top and bottom central geocells of 30 cm thick reinforced section since they were already broken during the base course preperation. The positive and negative strains refer to tensile and compressive strains respectively. All the strain gages affixed at the bottom of geocell walls showed tensile strains with the highest value for the central geocell. The top gages affixed at the central geocell showed compressive strains up to the certain cycle and then tesile strains for 15 cm and 23 cm thick reinforced bases. The top gages afixed at 25 and 50 cm away from the central geocell showed tensile strains with a least value for the geocell wall located 50 cm away from center. All the middle gages showed compressive strains irrespective of the location of geocell with the highest value for the central geocell. The final strains measured at the end of the test for 30 cm thick reinforced sections were -1.3%, -0.37%, -1.2%, and 0.09% for the middle gage at the central bottom geocell, the middle gage at the upper geocell located 25 cm away from the center, the middle gage at the lower geocell located 25 cm away from center, and the top gage at the lower geocell located 50 cm away from the center respectively.

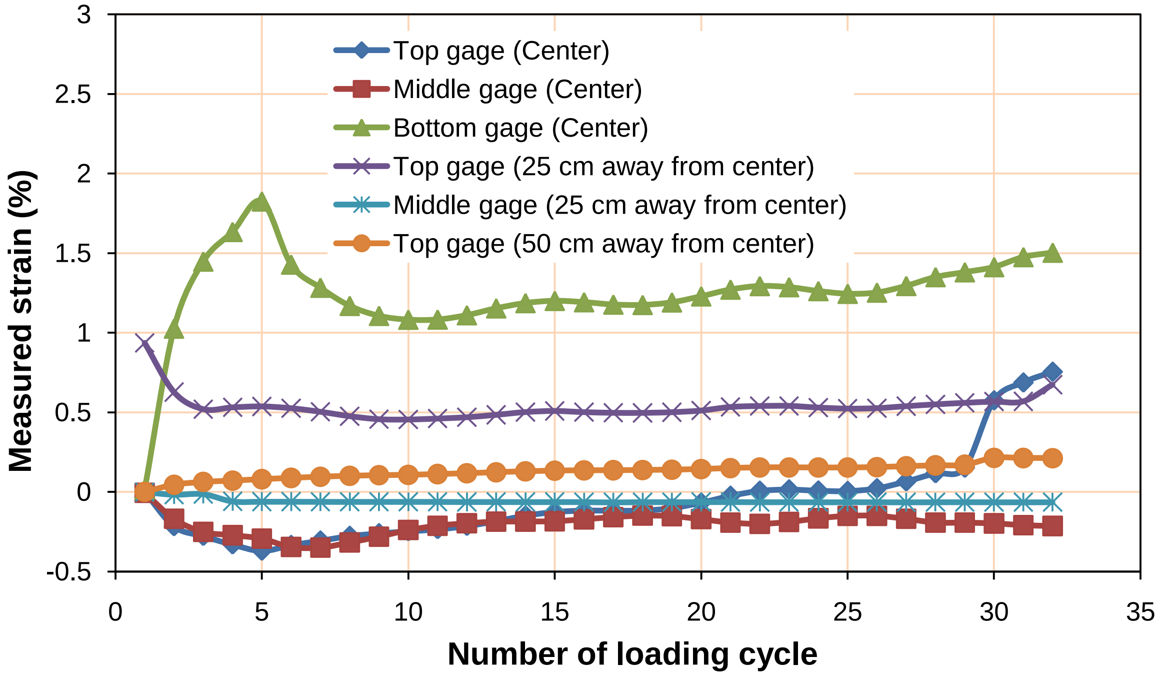

Figure 5.4.11 Measured strain at the geocell wall versus number of loading cycles for the 15 cm thick geocell-reinforced base over soft subgrade

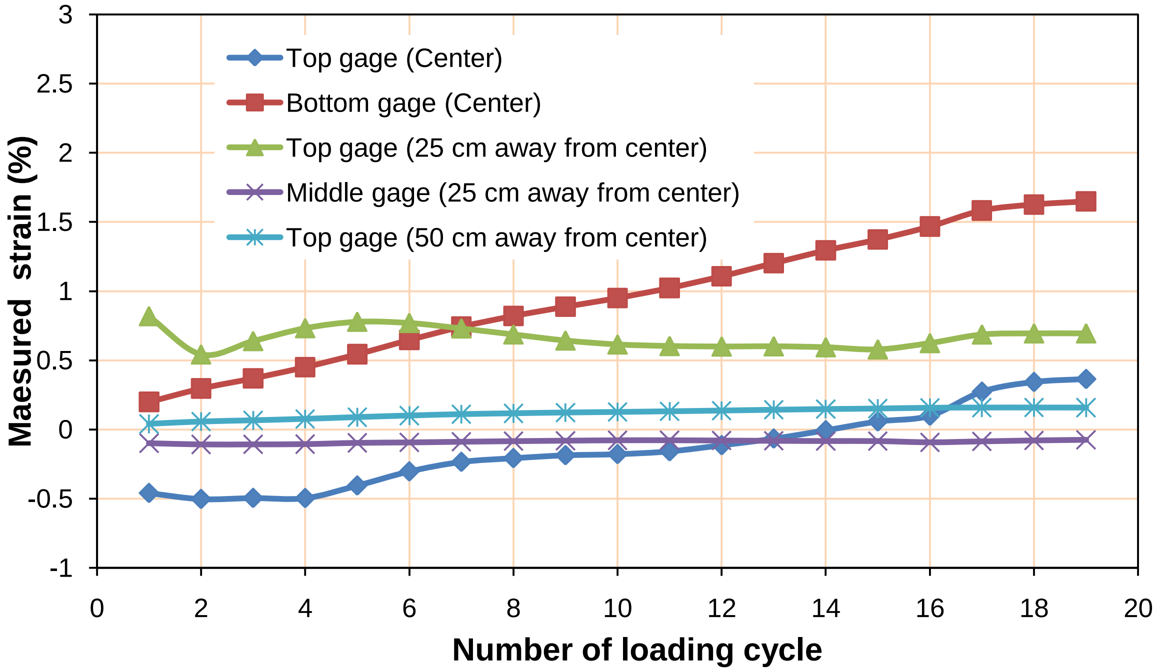

Figure 5.4.12 Measured strain at the geocell wall versus the number of loading cycles for 23 cm thick geocell-reinforced base over soft subgrade

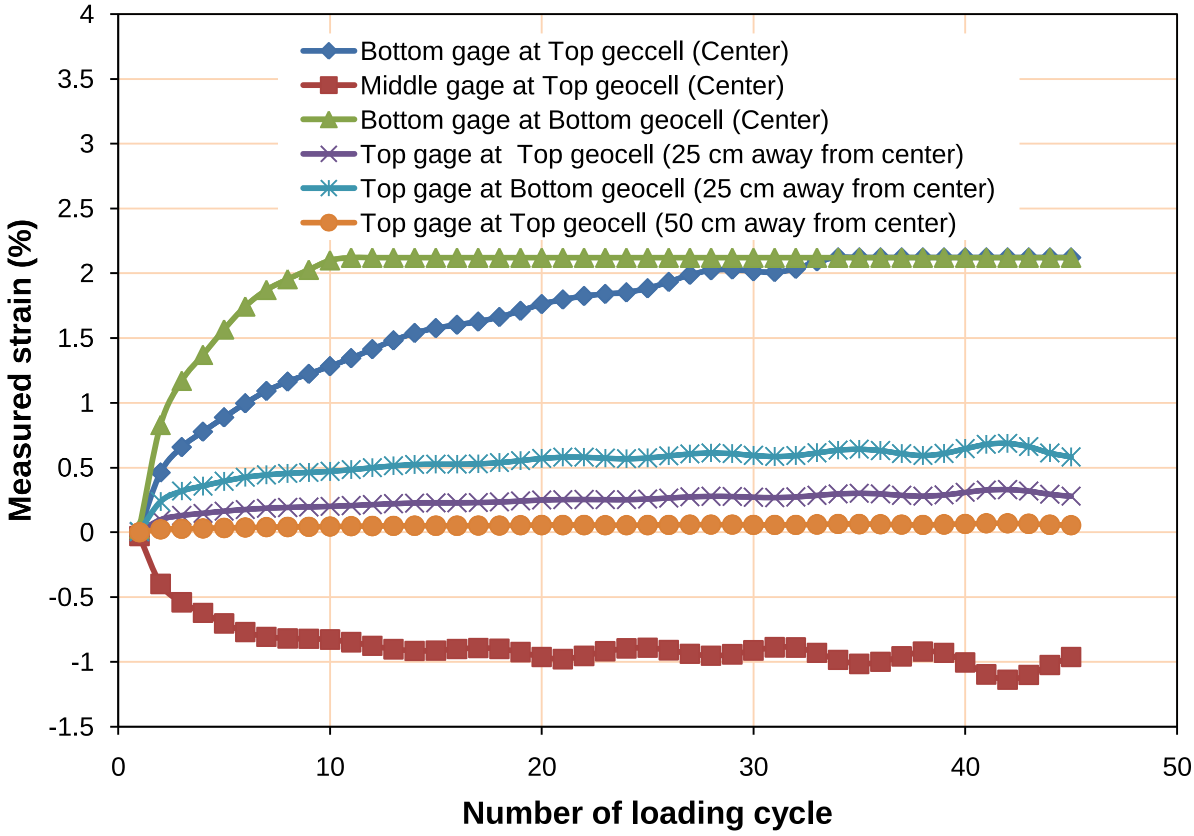

Figure 5.4.13 Measured strain at the geocell wall versus the number of loading cycles for 30 cm thick geocell-reinforced base over soft subgrade

5.5 Analysis of test data for geocell-reinforced RAP bases on moderate subgrade

5.5.1 Vane shear, DCP, and sand cone test results

Vane shear tests were performed just after the preparation of subgrade for each test to confirm that the target CBR was approximately achieved. The average CBR values of the subgrade obtained from the vane shear tests were 4.8 %, 4.6%, 4.5%, 4.8%, and 4.5% in the geocell-reinforced (15, 23, and 30 cm thick) and unreinforced (15 and 30 cm thick) bases respectively. The DCP tests were conducted one day after the base course was placed on top of the subgrade. The average CBR values of the base courses and subgrades were 10.4% and

4.8%, 10.5% and 4.7%, 10.2% and 4.6%, 10.5 and 5.0, and 10.2% and 2.0% in the geocell-reinforced (15, 23, and 30 cm) and unreinforced (15 cm and 30 cm) sections respectively. The higher subgrade CBR values were obtained from DCP tests because the DCP tests were conducted one day after the preparation of the test sections and also because some compaction energy went into the subgrade during base material compaction. The average CBR profiles obtained from the DCP tests carried out on the test ready sections are also shown in Figure 5.5.1 to check the consistency of the test sections.

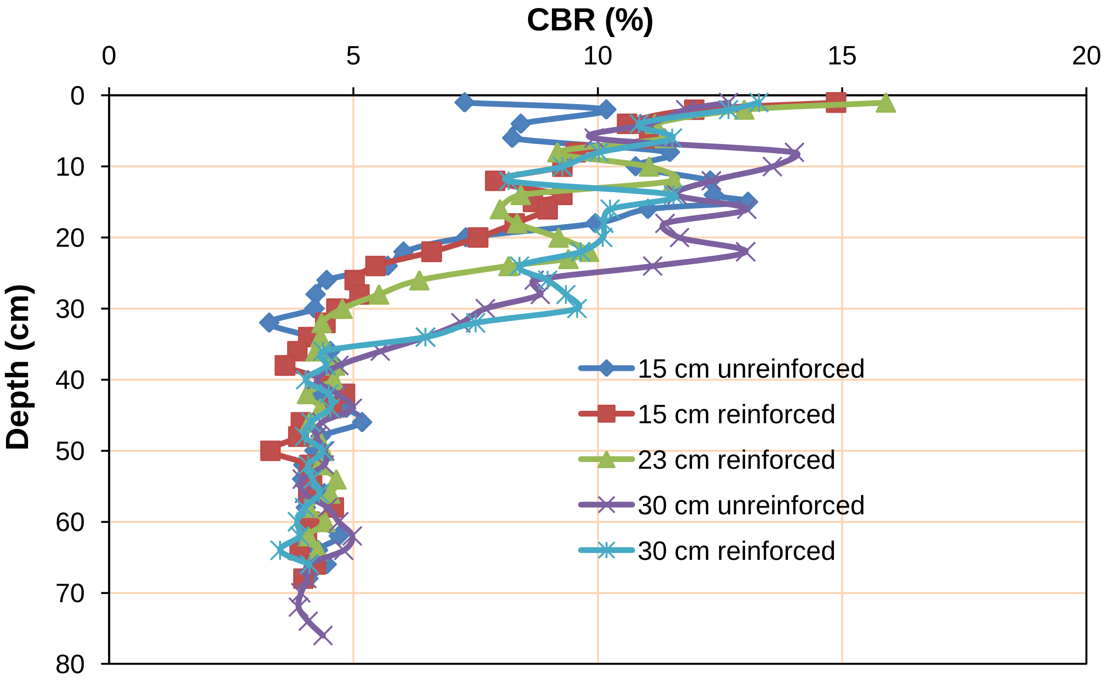

Figure 5.5.1 Average CBR profiles obtained from DCP tests in different sections with moderate subgrade.

Sand cone tests were carried out after each cyclic plate load test. The relative compaction was calculated as 87%, 91%, 84%, 96%, and 91.0% for the reinforced (15, 23, and 30 cm) and unreinforced (15 and 30 cm) bases, respectively. The CBR value increased with the degree of compaction

5.5.2 Permanent deformation

The permanent deformation of 75 mm was used as the criteria to stop the cyclic loading test. This criteria was used by US Army Corps of Engineers (Hammitt, 1970); and Giroud and Han (2004 a, b) to define the failure of the unpaved roads. However, all the tests except 15 cm unreinforced section were stopped earlier than the target deformation due to the malfunction in the testing machine. The permanent deformations of the unreinforced and reinforced bases at the center versus the number of loading cycles are shown in Figure 5.5.2. The permanent deformation increased with number of loading cycles. The rate of increase in the permanent deformation decreased with an increase in the number of loading cycles. For the permanent deformation of 35 mm (taken only for comparison purpose), the unreinforced (15 and 30 cm) and reinforced (15, 23, and 30 cm) bases lasted for 12, 19, 41, 46, and 91 loading cycles, respectively. The 15 cm thick unreinforced RAP base section had the largest permanent deformation among all the test sections while the 30 cm thick reinforced base section had the smallest permanent deformation. The 23 and 15 cm thick reinforced base sections had smaller permanent deformation than the 30 cm thick unreinforced base section, although they had thinner base thickness. This comparison demonstrates the benefits of NPA geocell. The reinforced (15, 23, and 30 cm) and unreinforced (30 cm) bases improved the performance by a factor of 1.6, 3.4, 3.8, and 7.6 over the 15 cm thick unreinforced base, respectively. The improvement factors obtained for moderate subgrade was smaller than those for soft subgrade. This is due to the fact that geocell was not fully mobilized at lesser permanent deformation. It can also be concluded that the geocell improved performance of the bases over soft subgrade more than that of the bases over moderate subgrade.

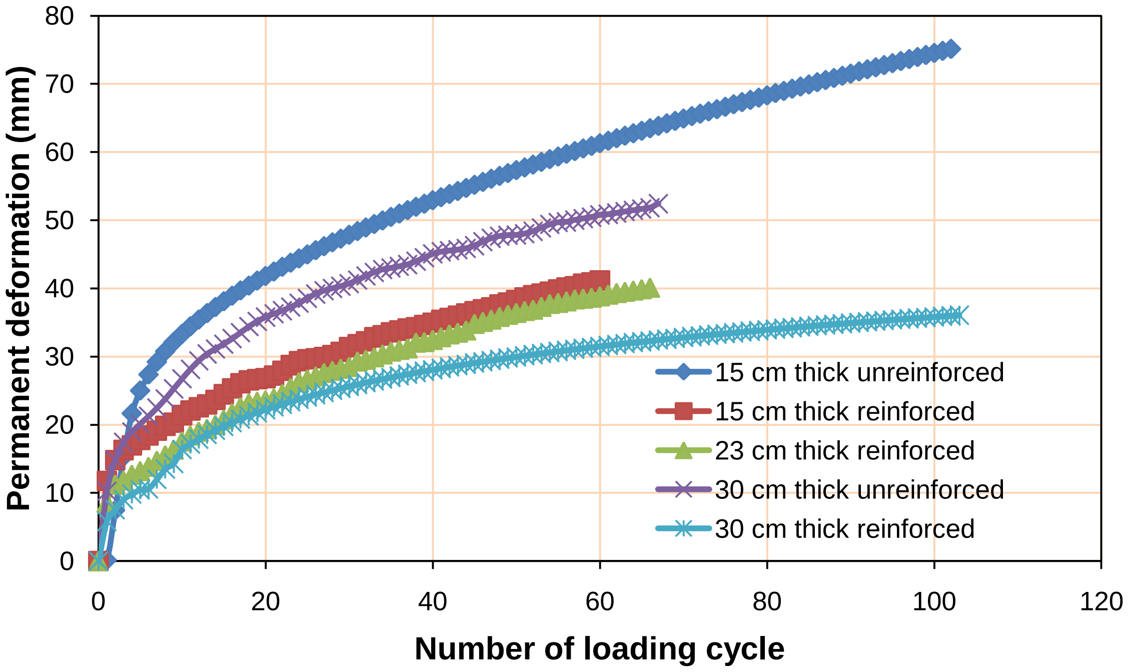

Figure 5.5.2 Permanent deformations at the center versus the number of loading cycles for RAP bases over moderate subgrade

Figure 5.5.3 presents the permanent deformations at 0, 25, 50, and 75 cm away from the center of the loading plate at the end of tests. For both unreinforced and reinforced sections, there was a small amount of heave at the locations of 25, 50, and 75 cm away from the center.

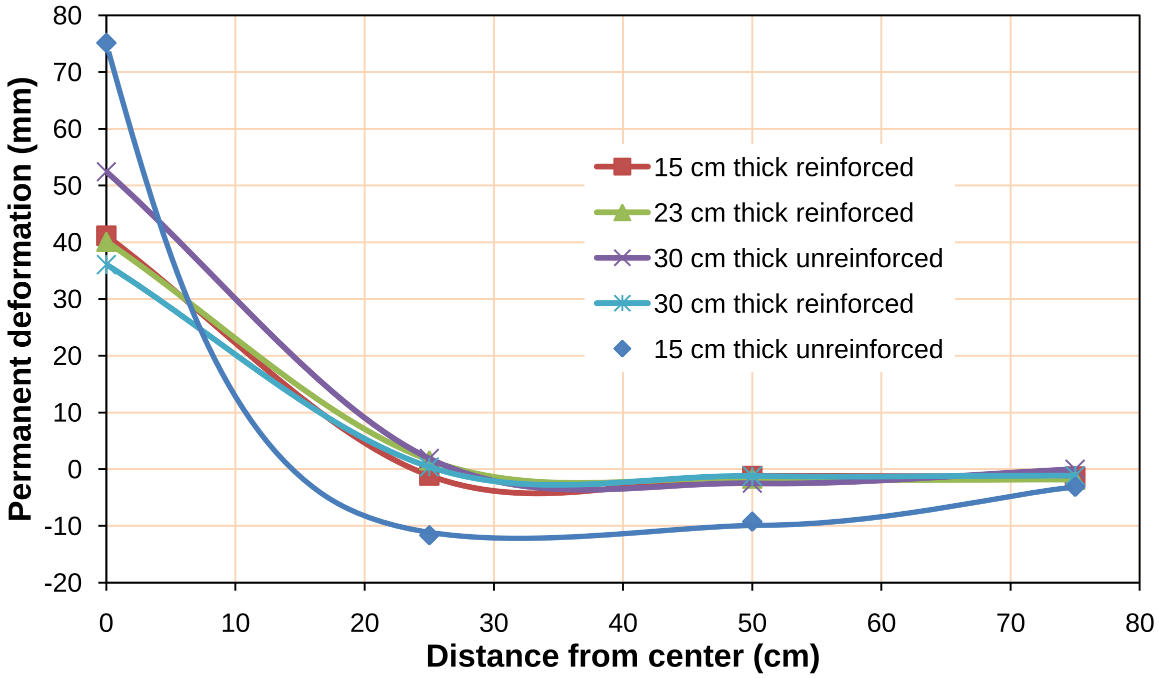

Figure 5.5.3 Permanent deformation at different locations at the end of test for RAP bases over moderate subgrade

5.5.3 Elastic deformation

The elastic deformation and percentage of elastic deformation at the center of the loading plate at different numbers of loading cycles are presented in Figures 5.5.4 and 5.5.5. The elastic deformation is defined as the rebound of the base when unloaded from the maximum load (40kN) to the minimum load (0.5kN). The percentage of elastic deformation was calculated by dividing the elastic deformation at each load cycle to the total deformation (i.e., the sum of elastic and plastic deformations) at that cycle. The amount of elastic deformation and percentage of elastic deformation increased rapidly at the initial few loading cycles but later stabilized to a constant value for the geocell-reinforced bases whereas they increased sharply until the failure for the unreinforced base. The maximum elastic deformations for the reinforced (30, 23, and 15 cm) and unreinforced (30 and 15 cm) bases were about 10, 7, 6, 6, 2.7 mm, respectively. The percentages of elastic deformations were 99%, 97%, and 95% for the reinforced (30, 23, and 15 cm) bases and 97% and 89% for unreinforced (30 and 15 cm) bases, respectively. The 15 cm thick unreinforced RAP base section had the least percentage of elastic deformation among all the test sections while the 30 cm thick reinforced base section had the most percentage of elastic deformation at the end of the test.

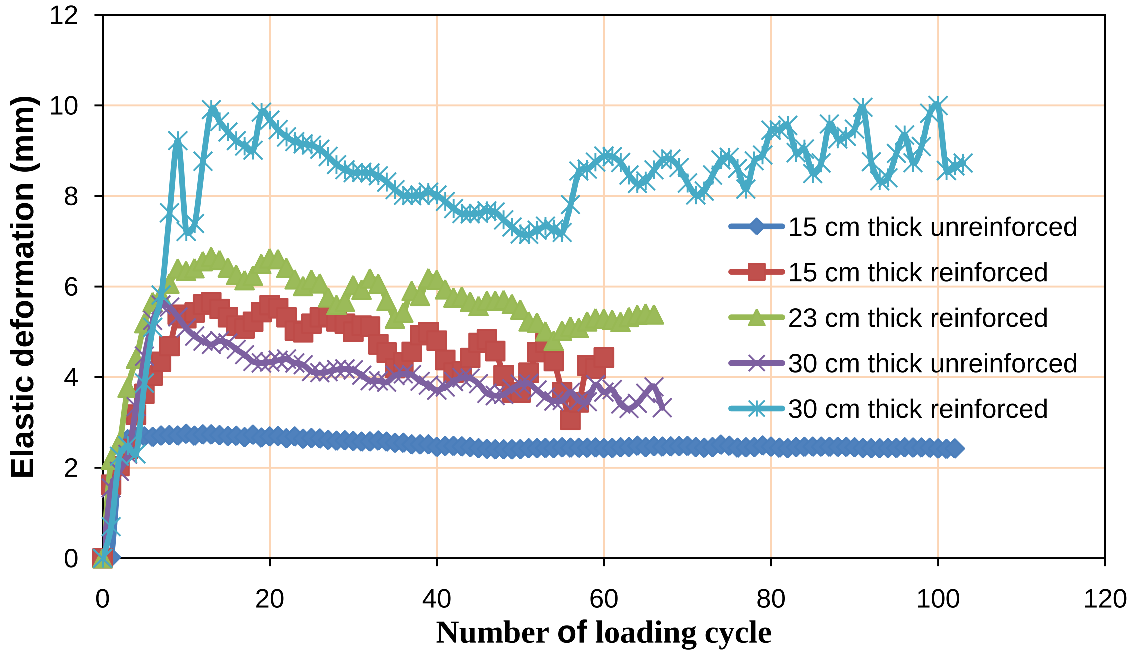

Figure 5.5.4 Elastic deformation at the center versus the number of loading cycles for RAP bases over moderate subgrade

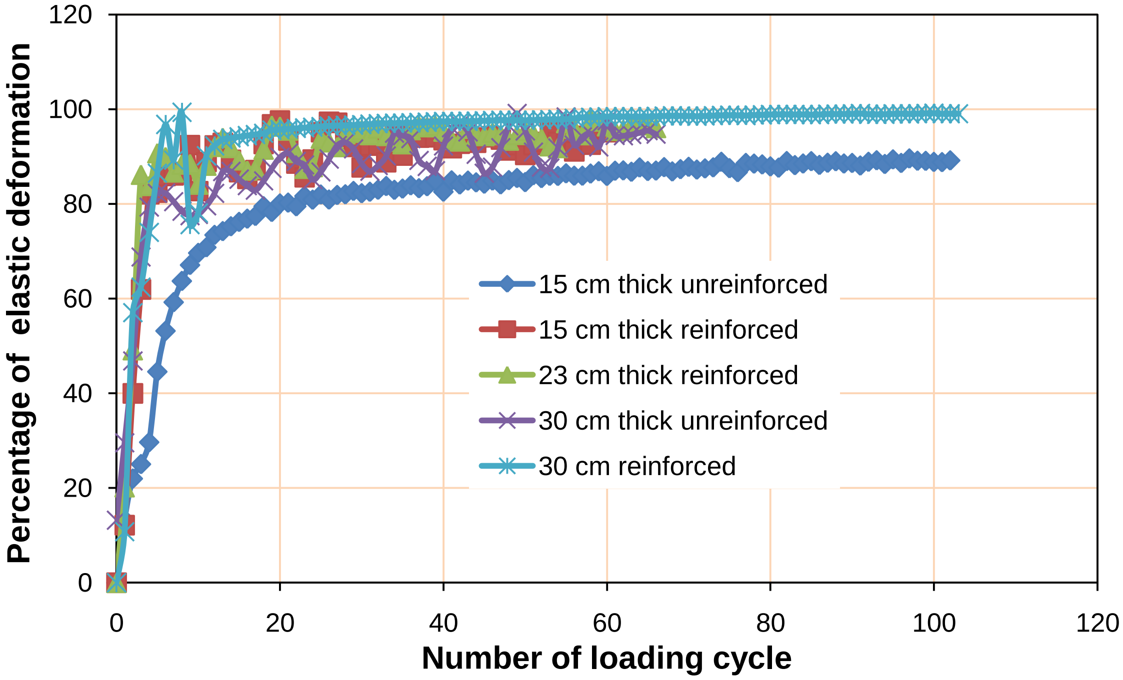

Figure 5.5.5 Percentage of elastic deformation at the center versus the number of loading cycles for RAP bases over moderate subgrade

5.5.4 Vertical stress at interface

The vertical stresses at the interface of subgrade and base course were measured by the pressure cells located at 0, 12.5, 25, 50 and 75 cm from the center of the plate. Figures 5.5.6 and 5.5.7 show the maximum vertical stresses at the interface of subgrade and base course versus the number of loading cycles at the center and 12.5 cm away from the center respectively. The vertical stress increased rapidly at the initial few numbers of cycles and later it decreased slowly by a small magnitude or stabilized to a constant value in the reinforced cases whereas it kept increasing until failure for unreinforced case. The vertical stresses at the interface of subgrade and base course at the center and 12.5 cm away from the center were 185 and 180, 161 and N/A, 180 and 86, 402 and 238, and 183 and 156 kPa in the reinforced (15 cm, 23 cm, and 30 cm) and unreinforced (15 cm and 30 cm) bases, respectively. N/A stands for the pressure value not available at 12.5 cm away from center for the 23 cm thick reinforced base. The vertical stress was highest in the 15 cm thick reinforced base and lowest in the 30 cm thick reinforced base. It demonstrates that the vertical stress decreased with an increase in the base thickness and the geocell reinforcement.

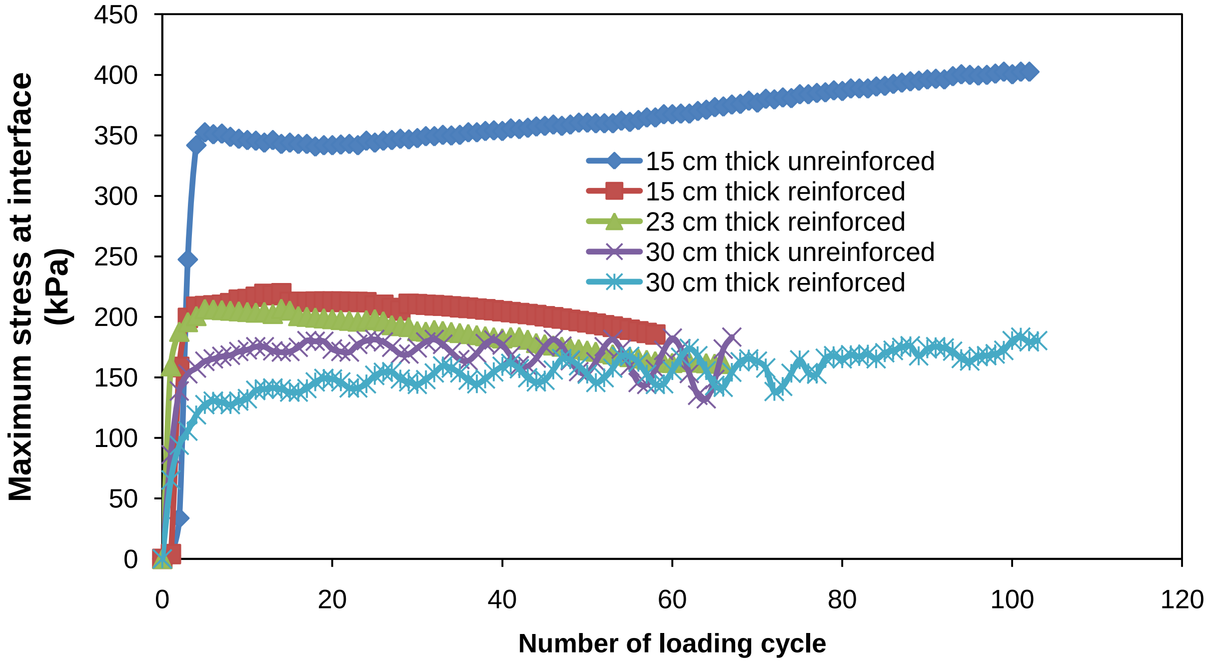

Figure 5.5.6 Vertical stresses at the inerface of moderate subgrade and RAP bases at the center

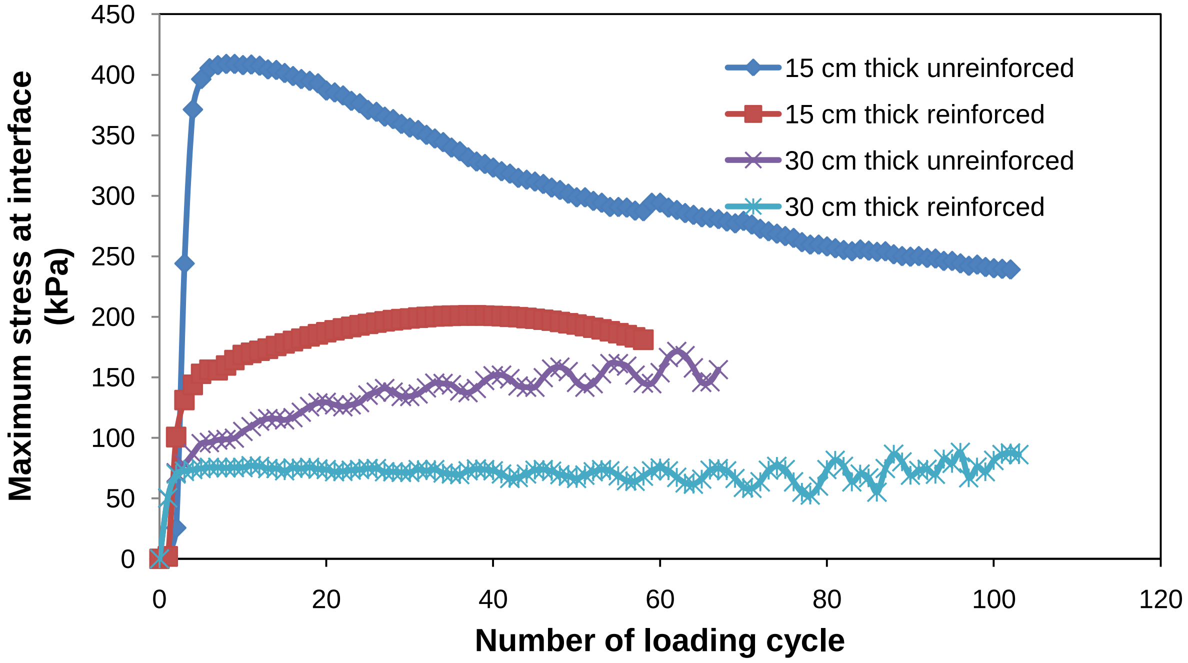

Figure 5.5.7 Vertical stresses at the inerface of moderate subgrade and RAP bases at 12.5 cm away from the center

5.5.5 Vertical stress distribution

Figures 5.5.8 presents the vertical stress distribution at different locations at the interface of subgrade and base at 35 mm central permanent deformation. The verticle stress at 12.5 cm from the center of the pate was gretaer than that at the center for the 15 cm thick unreinforced base. Except the 15 cm thick unreinforced section, the verticall stresses had the greatest value at the center and it decresed when it moved away from the center. The vertical stresses decreased rapidly after 12.5 cm away from the center and the least vertical stresses were observed at the farthest point from the the center. The sections having higher stresses at the center and 12.5 cm away from the center had lower stresses at other locations and vice versa.

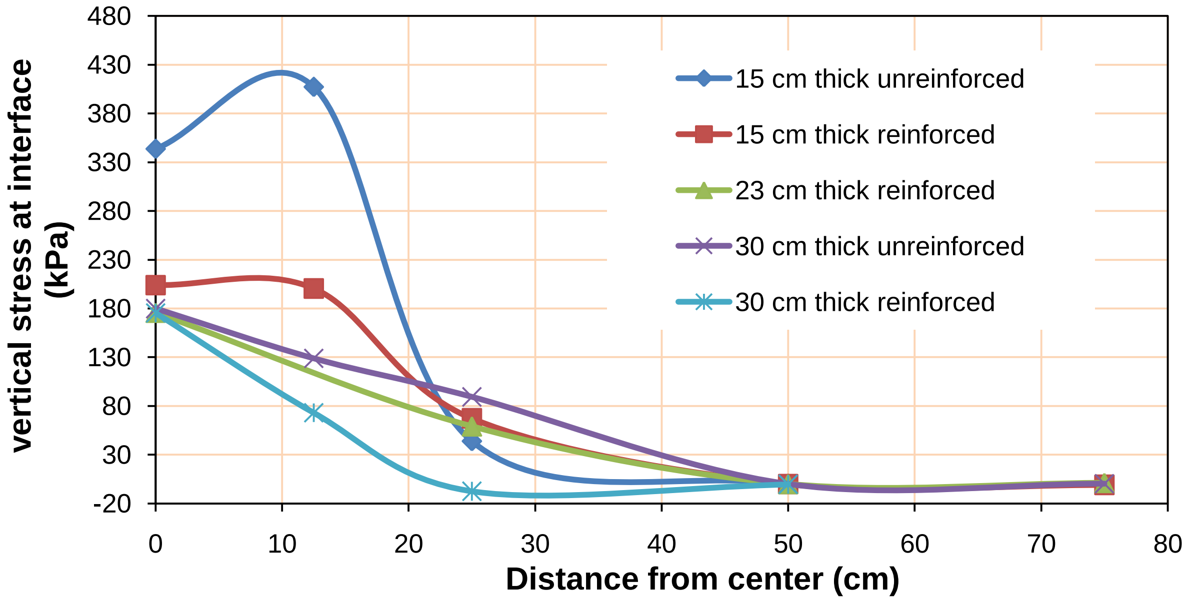

Figure 5.5.8 Vertical stres distribution at the inerface of moderate subgrade and RAP bases at 35 mm central permanent deformation

The stress distribution at the center of the base is further expressed in terms of a stress distribution angle which was calculated using Equation 5.4.1 presented in the Section 5.4. The calculated stress distribution angles at different loading cycles are shown in Figure 5.5.9. The stress distribution angle decreased rapidly during the initial few loading cycles and then stabilized to a constant value or increased slowly by a small magnitude. The minimum stress distribution angles for the three reinforced (30, 23, and 15 cm) and the two unreinforced (30 and 15 cm) bases were 56°, 55°, 52°, 55°, and 38° corresponding to 35 mm permanent deformation respectively. It can be concluded that the NPA geocell reinforcement and an increase of the base thickness reduced the vertical stress by distributing the load to a wider area.

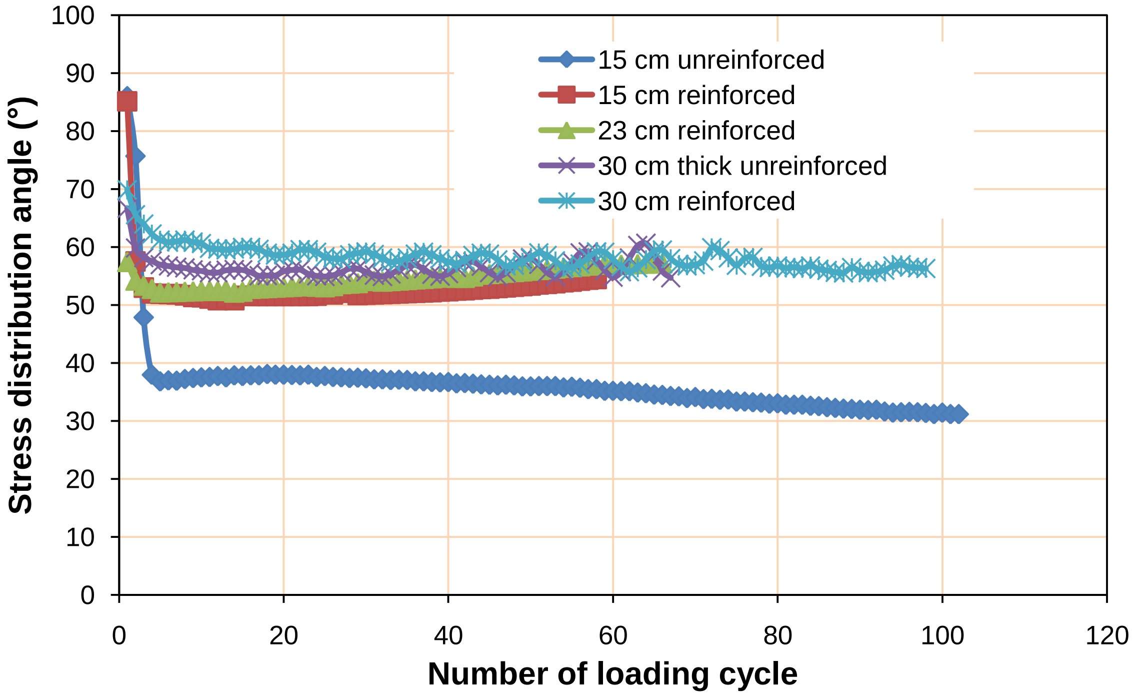

Figure 5.5.9 Stress distribution angle versus the number of loading cycles

5.5.6 Maximum strain in the geocell

The strain gages were installed at the geocell walls to measure the induced strains due to the deformation of geocell under cyclic loading. Three strain gages were installed at the central geocell , two were installed at the locations adjacent to the central geocell, and one was installed at the next neighbouring geocell as shown in Figure 5.2.2. The total number of strain gages installed for 15, 23, and 30 cm reinforced sections were 6, 6, and 12 respectively. There were only six slots available in the data recorder for strain gage connection. Therefore, for the 30 cm reinforced section, only six strain gages were connected to the data recorder for recording during tests while other strain gages were recorded to the data recorder for recording after the tests. All the strain gages affixed on the top and bottom of the geocell walls were used to measure horizontal strains while the strain gages affixed at the middle of the wall were used to measure the vertical strains. The maximum strain induced at different locations of geocell wall versus the number of loading cycles for 15 cm, 23 cm, and 30 cm reinforced sections are shown in Figures 5.5.10, 5.5.11, and 5.5.112 respectively. There is no strain data for the middle strain gage afixed at 50 cm away from the center for 15 cm thick reinforced base, the bottom gage affixed at the center for the 23 cm thick reinforced base, and the top gage affixed at 25 cm away from the center for the 23 cm thick reinforced base since they were already broken during the base course compaction. Also there is no strain data for the top gages affixed on both upper and lower central geocells of the 30 cm thick reinforced section, the top gage afixed at the lower geocell located at 50 cm away from the center, and the bottom gage affixed at the lower geocell located at 25 cm away from the center. The positive and negative strains refer to tensile and compressive strains respectively. All the strain gages affixed at the bottom of geocell walls showed tensile strains with the highest value for the central geocell. The top gages showed tensile strains with the greatest value for the central geocell and the least value for the geocell wall located at 50 cm away from the center. All the middle gages showed compressive strains irrespective of the location of geocell with the highest value for the central geocell. The final strain measured at the end of the test for 30 cm thick reinforced sections were 0.4% for the bottom gage at the central upper geocell.

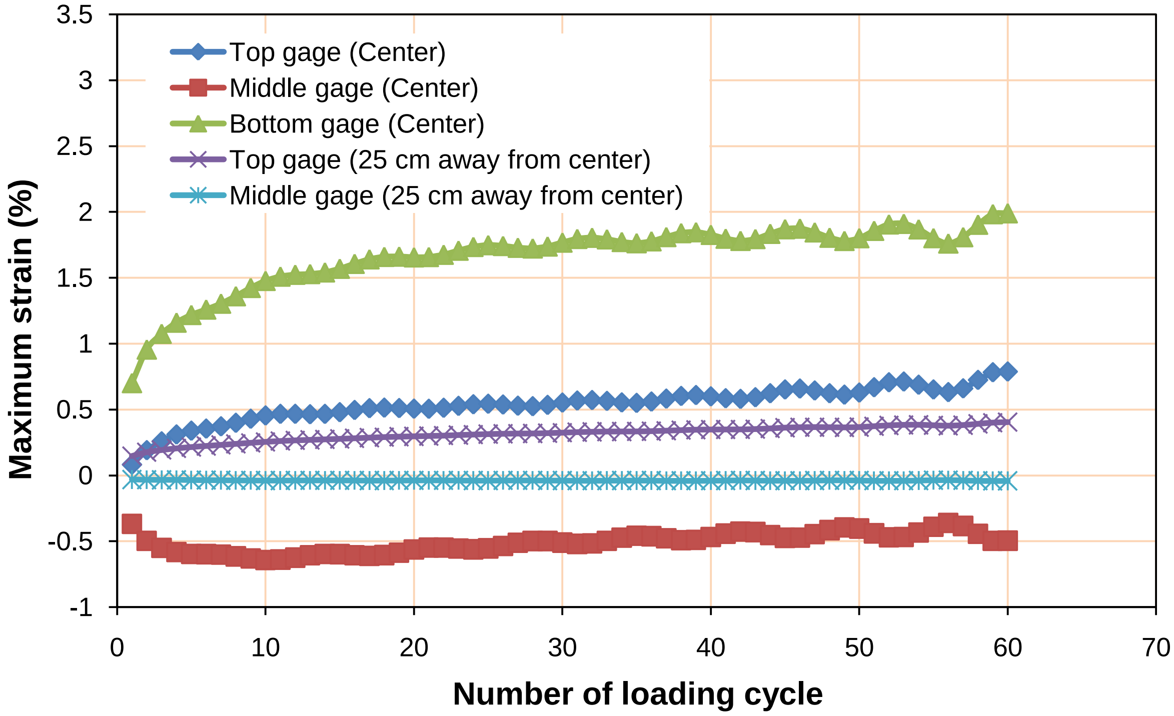

Figure 5.5.11 Maximum strain at the geocell wall versus number of loading cycles for 15 cm thick geocell-reinforced base over moderate subgrade

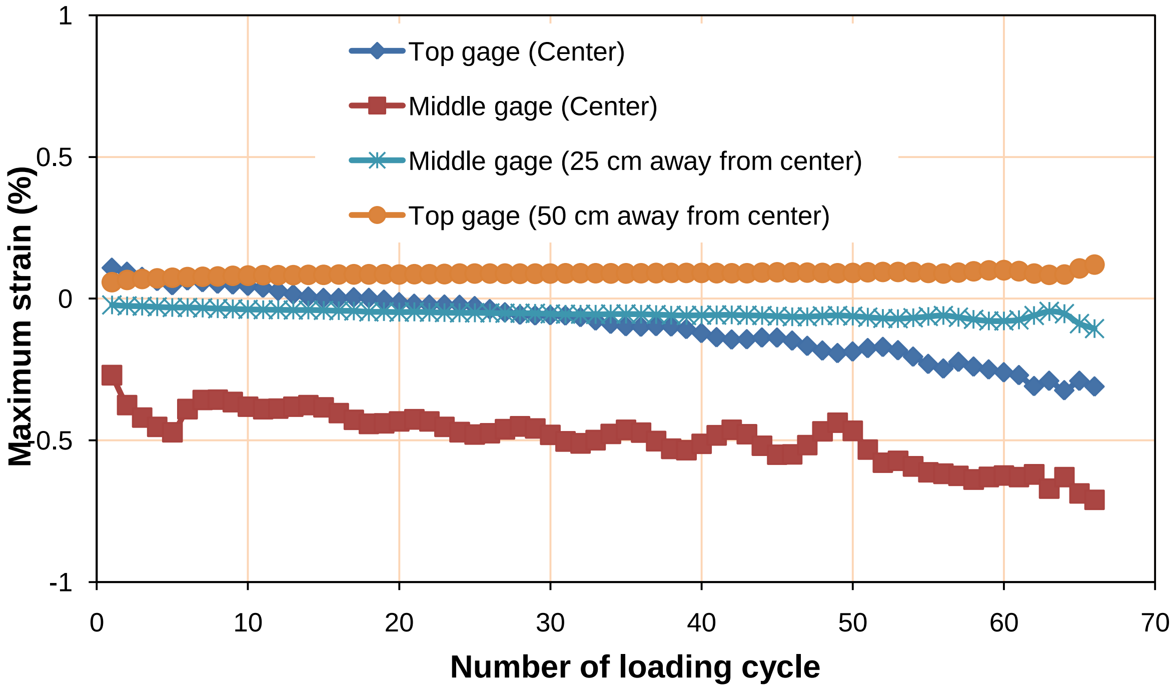

Figure 5.5.12 Maximum strain at the geocell wall versus number of loading cycles for 23 cm thick geocell-reinforced base over moderate subgrade

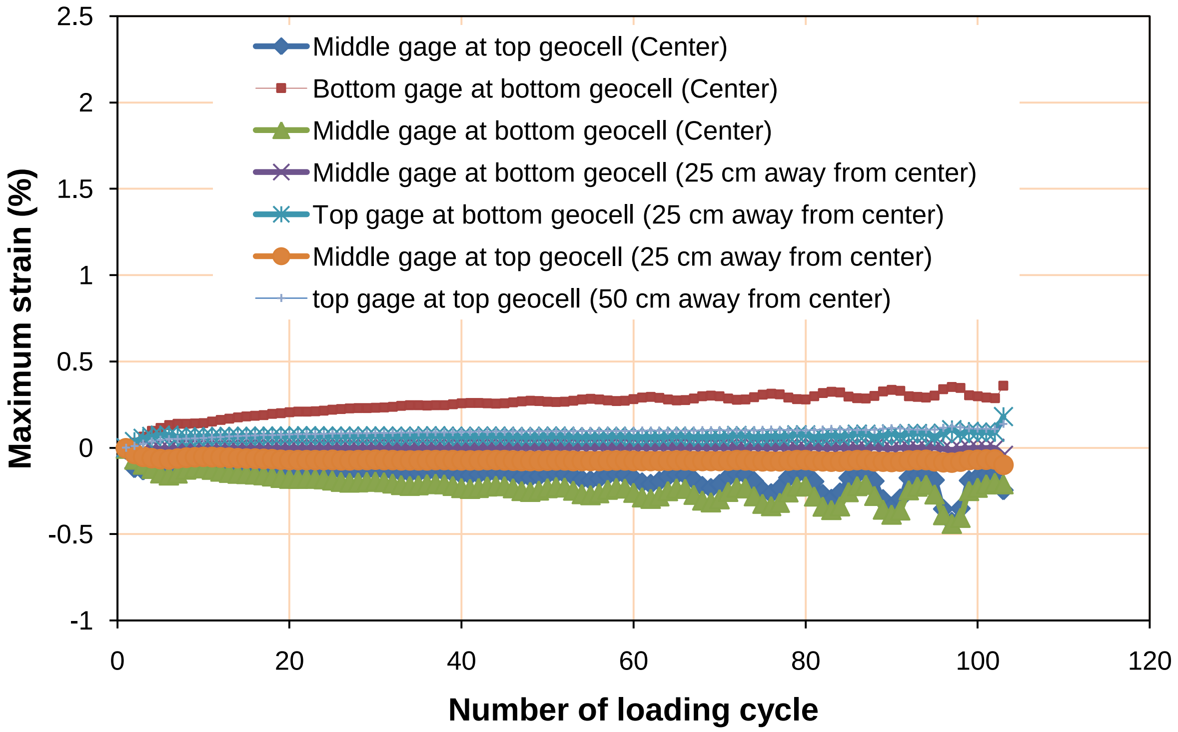

Figure 5.5.13 Maximum strain at the geocell wall versus number of loading cycles for 30 cm thick geocell-reinforced base over moderate subgrade

5.6 Conclusions

This chapter presents an experimental study of cyclic plate load testing of NPA geocell-reinforced recycled asphalt pavement (RAP) bases over soft (CBR about 2%) and moderate (CBR about 5%) subgrades to evaluate the performance of NPA geocell-reinforced RAP bases and the benefit of geocell reinforcement. The following conclusions can be made from this study:

1) The California bearing ratio (CBR) values of the base and subgrade controlled the performance of RAP bases.

2) The geocell improved the performance of reinforced recycled asphalt pavement bases over soft subgrade compared to unreinforced bases. The improvement factors for 15 cm, 23 cm, and 30 cm thick reinforced RAP bases over 30 cm thick unreinforced RAP base on soft subgrade were 6.4, 3.6, and 19.4 respectively corresponding to 75 mm permanent deformation. The reinforced (15 cm, 23 cm, and 30 cm) and unreinforced (30 cm) bases over moderate subgrade improved performance by a factor of 1.6, 3.4, 3.8, and 7.6 over 15 cm thick unreinforced base respectively corresponding to 35 mm permanent deformation. Therefore, NPA geocell improved the performance of bases over soft subgrade more significantly compared to bases over moderate subgrade.
3) The NPA geocell significantly increased the percentage of elastic deformation of the RAP bases and increased service life of the pavement.
4) The NPA geocell reinforcement reduced vertical stresses transferred to the subgrade and increased the stress distribution angle.
5) The vertical stresses for the unreinforced section increased with the number of cycles throughout the tests, whereas those for the reinforced sections increased for initial few cycled and then decreased or became constant when the geocell was mobilized. This phenomenon can be clearly seen from the soft subgrade cases. In case of moderate subgrade, the geocell was not fully mobilized because the tests were stopped at lower permanent deformations.
6) The vertical stresses were the greatest at 12.5 cm away from the center and then at the center for bases over soft subgrade whereas, the vertical stresses were the maximum

at the center and then at 12.5 cm away from the center for bases over moderate subgrade. The vertical stresses decreased rapidly when moved away from center.

7) The middle strain gages showed compression whereas the bottom and top gages showed tensile strains. The strain measurements demonstrated that the NPA geocell-reinforced RAP bases behaved as a slab.

CHAPTER 6

CONCLUSIONS AND RECOMMENDATIONS

6.1 Conclusions

The following conclusions can be made from this study through three types of experimental studies:

6.1.1 Laboratory evaluation of characteristics of recycled asphalt pavement (RAP)

(i) The binder content of the RAP by the ignition method (6.87%) was slightly higher than that by the centrifuge method (6.71%).

(ii) Compaction following the modified Proctor test standard did not change the gradation of the RAP aggregate.

(iii) The fine aggregate had a higher specific gravity than the coarse aggregate.

(iv) The uncompacted void content of the fine aggregate extracted from RAP was 39.15%.

(v) The kinematic viscosity of the asphalt binder at 135°**C** was 1.408 Pa-s.

(vi) The maximum dry density of RAP based on the modified Proctor tests was 1.96 g/cm^3, which corresponds to the optimum moisture content (OMC) of 6.6%.

(vii) The CBR of RAP at the moisture content corresponding to 98% compaction was 24.8%.

(viii) The minimum and maximum index densities were 1.415 g/cm^3 and 1.740 g/cm^3 respectively.

(ix) The geocell-RAP interface cohesion and friction angle were 8.95 kPa and 11.06° respectively. In addition, the cohesion and friction angle of RAP were 30.68 kPa and 12.90° respectively.

(x) The average interaction coefficient between geocell and RAP and interface efficiencies of cohesion and friction angle were 0.477, 0.292, and 0.853 respectively.

6.1.2 Creep tests of geocell-reinforced RAP

(i) The confinement of a RAP sample significantly increased the strength and stiffness of the sample.

(ii) The NPA-geocell significantly reduced the initial deformation and the rate of creep of the RAP and further reduction could be achieved if the RAP was fully confined.

(iii) The creep deformations decreased with an increase in the degree of confinement and a decrease in the applied vertical stress and vice versa.

(iv) The well-graded aggregate AB-3 cover significantly reduced the creep of geocell-confined RAP bases.

6.1.3 Large-scale plate load tests

(i) The novel polymeric alloy (NPA) geocell improved the performance of RAP bases. The improvement was significantly higher for RAP bases over soft subgrade compared to that over moderate subgrade.

(ii) The NPA geocell reinforcement reduced permanent deformations and increased percentage of elastic deformations of RAP bases.

(iii) The NPA geocell reinforcement reduced vertical stresses transferred to the subgrade and increased the stress distribution angle.

(iv) Thick and stiff bases distributed applied vertical stresses to a wider area resulting in less vertical stresses at the interface of subgrade and base course.

(v) The strain measurements on the geocell demonstrated that the NPA geocell-reinforced RAP bases behaved as a slab.

6.2 RECOMMENDATIONS

This study was focused on the experimental study on evaluation of characteristics of RAP, creep behavior of RAP, and cyclic behavior of RAP. The test results provide the basis for predicting rutting and deformation potential of RAP bases. In addition, the test results can be used as a base for numerical modeling in the future.

Since the literature review showed that RAP is a time and temperature dependent material, more research is needed in future to quantify the creep behavior of RAP at different temperatures. A future study is also needed to focus on geocell-reinforced RAP pavements, resilient modulus of RAP, and field performance.

REFERENCES

Al-Qadi, I.L., Carpenter, S.H., Roberts, G., Ozer, H., Aurangzeb, Q., Elsie, M., and Trepanier, J. (2009). *Determination of usable residual asphalt binder in RAP*. Research Report FHWA-ICT-09-031, 101.

Asphalt Pavement Recycling with Reclaimed Asphalt Pavement (RAP). Retrieved December 10, 2010 from: http://www.fhwa.dot.gov/pavement/recycling/rap/index.cfm.

Barenberg, E.J. (1980). *Design procedures for soil-fabric-aggregate systems with Mirafi 500X fabric.* University of Illinois Transportation Engineering Series No. 30, UILU-ENG-80-2019, October 1980, 2.

Barenberg, E.J., Dowlad, J.H., and Hales, J. (1975). *Evaluation of soil-aggregate systems with Mirafi fabric.* Department of Civil Engineering, University of Illinois.

Bartnev, G.M. and Zuyeb, S. (1969). *Strength and Failure of Viscoelastic Materials*. Pergaman Press.

Bathurst, R.J. and Karpurapu, R. (1993). "Large-scale triaxial compression testing of geocell-reinforced granular soils." *Geotechnical Testing Journal*, *GTJODJ*, 16 (32), 296-303.

Bennert, T. and Maher, A. (2005). *The development of a performance specification for granular base and subbase material.* Report no. FHWA-NJ-2005-003, February, 2005, New Jersey Department of Transportation, CN 600 Trenton, NJ 08625, 55p.

Bennert, T., Papp Jr., W.J., Maher, A., and Gucunski, N. (2000). "Utilization of construction and demolition debris under traffic-type loading in base and subbase applications." *Transportation Research Record, 1714,* National Research Council, Washington, D.C., 33-39.

Burd, H.J. (1995). "Analysis of membranes action in reinforced unpaved roads." *Canadian Geotechnical Journal,* National Research Council of Canada, Ottawa, 32 (6), 946-956.

Canadian Strategic Highway Research Program (C-SHRP) (2000). *Asphalt: Current issues and research needs*. Millennium Research Brief # 1, 1-5, retrieved December 20, 2010 from: http://www.cshrp.org/products/milbr-1.pdf.

Cold In-place Recycling (CIR). U.S. department of Transportation, Federal Highway Administration, retrieved December 10, 2010 from: http://www.fhwa.dot.gov/pavement/recycling/cir/.

Copeland, A., Jones, C., and Bukowski, J. (2010). *Reclaiming Roads*. Publication Number FHWA-HRT-10-001, 73 (5), retrieved November 2, 2010 from: http://www.fhwa.dot.gov/publications/publicroads/10fmar/06.cfm.

Cosentino, P.J., Kalajian, E.H., Shieh, C.S, Mathurin, W.J.K., Gomez, F.A., Cleary, E.D., and Treeratrakoon, A. (2003). *Developing specifications for using recycled asphalt pavement as base, subbase or general fill materials,* Phase II. Final report, Report no. FL/DOT/RMC/06650-7754, Florida Institute of Technology, Civil Engineering Department, 272p.

Doig, B (2000). *Influence of Storage Time and Temperature on the Triaxial Characterization of RAP.* M.S. thesis in Civil Engineering, Florida Institute of Technology, Melbourne, Florida.

Federal Highway Administration and Environmental Protection Agency (1993). *A study of the use of recycled paving material – report to Congress.* Report no. FHWA-RD-93-147, EPA/600/R-93/095. 78p.

Garg, N. and Thompson, M.R. (1996). "Lincoln Avenue Reclaimed Asphalt Pavement Base Project." *Transportation Research Record. 1547,* 89-95.

Giroud, J.P., Ah-line, C., and Bonaparte, R. (1985). "Design of unpaved roads and trafficked areas with geogrids." *Proceedings of Symposium on Polymer Grid Reinforcement,* Thomas Telford Limited, London, 116-127.

Giroud, J.P. and Han, J. (2004a). “Design method for geogrid-reinforced unpaved roads. I. Development of design method.” *Journal of Geotechnical and Geoenvironmental Engineering*, 130 (8), 775-786.

Giroud, J.P. and Han, J. (2004b). “Design method for geogrid-reinforced unpaved roads. II. Calibration of applications.” *Journal of Geotechnical and Geoenvironmental Engineering,* 130 (8), 787-797.

Giroud, J.P. and Noiray, L. (1981). “Geotextile- reinforced unpaved road design.” *Journal of the Geotechnical Engineering Division*, 107 (GT9), 1233-1254.

Haliburton, T.A. and Barron, J.V. (1983). “Optimum depth method for design of fabric reinforced unsurfaced roads.” *Transportation Research Record 916*, Transportation Research Board, Washington, D.C., 26-32.

Hammitt, G. M. (1970). “Thickness requirement for unsurfaced roads and airfields, bare base support, Project 3782-65.” *Technical Report S-70-5*, U.S. Army Engineer Waterways Experiment Station, CE, Vicksburg, Miss.

Hanks, A. J. and E. R. Magni (1989). *The use of bituminous and concrete material in granular base and earth*. Materials Information Report MI-137, Engineering Materials Office, Ontario Ministry of Transportation, Downsview, Ontario.

Han, J., Yang, X.M., Leshchinsky, D., and Parsons, R.L. (2008). "Behavior of geocell-reinforced Sand under a vertical load," *Journal of Transportation Research Board,* No. 2045, 95-101.

HAPI Asphalt Pavement Guide (2006). Retrieved June 18, 2010 from http:www.hawaiiasphalt.com/HAPI/modules/04_pavement_types/04_recycled_hma.htm.

Henkel, D.J. and Gilbert, G.D. (1952). "The effect of the rubber membrane on the measured triaxial compression strength of clay samples." *Geotechnique,* 3 (1), 20-29.

Holtz, R.D. and Sivakugan, N. (1987). "Design charts for roads with geotextiles." *Geotextiles and Geomembranes,* 5 (3), 191-199.

Kandhal, P.S. and Cooley, L.A. (2002). *Evaluation of permanent deformation of asphalt mixtures using loaded wheel tester.* NCAT Report 02-08, 16p.

Kelly, T., 1998, *Crushed cement concrete substitution for construction aggregates- A material flow analysis.* U.S. Department of the Interior, U.S. Geological Survey Circular 1177, retrieved November 05, 2010 from: http://purl.access.gpo.gov/GPO/LPS22459.

Kinney, T.C. (1979). *Fabric induced changes in high deformation soil-fabric-aggregate systems. Ph.D thesis,* Graduate College, University of Illions, Urbana.

Lane, M. (2009). *Rehabbing Maine's I-295 Southbound.* U.S. Department of Transportation, Federal Highway Administration, Publication Number FHWA-HRT-10-001, Nov-Dec 2009, 73 (3), retrieved December 5, 2010 from: http://www.fhwa.dot.gov/publications/publicroads/09novdec/02.cfm.

Little, D.N, Button, J.W., and Youssef, H. (1993). "Development of criteria to evaluate uniaxial creep data and asphalt concrete pavement deformation potential." *Transportation Research Record,* 1417, 49-57.

Mamlouk, M.S. and Ayoub, N.F. (1983). "Evaluation of long term behavior of cold recycled asphalt mixture." *Transportation Research Record,* 64-66.

Mandal, N.J. and Gupta, P. (1994). "Stability of geocell-reinforced soil." *Construction and Building Materials,* 8 (1), 55-62.

Mcdaniel, R. and Anderson, R.M. (2001). *Recommended use of reclaimed asphalt pavement in the superpave mix design method: Technician's manual.* National Cooperative Highway Research Program (NCHRP) report 452, 58p.

McGarrah, E.J. (2007). *Evaluation of current practices of reclaimed asphalt pavement/virgin aggregate as base course material.* WSDOT Research report, Report No. WA-RD 713.1, 41p.

Mhaiskar, S.Y. and Mandal, J.N. (1992a). “Comparison of geocell and horizontal inclusion for paved road structure.” *Earth Reinforcement Practice*, Ochiai, Hayashi and Otani, Balkema, Rotterdam.

Mhaiskar, S.Y. and Mandal, J.N. (1992b). “Subgrade stabilization using geocells.” *ASCE Geotechnical Special Publication*, 2 (30), 1092-1103.

Mhaiskar, S.Y. and Mandal, J.N. (1996). “Investigation on soft clay subgrade strengthening using geocells.” *Construction and Building Materials*, 10 (4), 281-286.

Milligan, G.W.E., Jewell, R.A., Houlsby, G.T., and Burd, H.J. (1989). “A new approach to the design of unpaved roads- parts I.” *Ground Engineering,* 22 (3), 25-29.

Missouri Asphalt Pavement Association (2010). *Recycling of asphalt pavement*. Retrieved December 10, 2010 from: http://www.moasphalt.org/facts/environmental/recycling.htm.

Mokwa, R.L. and Peebles, C.S. (2005). "*Evaluation of the engineering characteristics of RAP/ Aggregate blends.*" Report no. FHWA/MT-05-008/8117-24, 103p.

New Jersey Department of Environmental Protection (NJDEP*)* (2001). *Asphalt millings guidance document,* retrieved November 17, 2010 from: www.state.nj.us/dep/dshw/rrtp/amgd.htm.

Peploe, R. J. (2006). *Applications for asphalt millings on New Zealand roads.* Land Transport New Zealand Research Report 298, retrieved Novemeber 10, 2010 from: www.landtransport.govt.nz.

Pokharel, S.K., Han, J., Leshchinsky, D., Parsons, R.L., and Halahmi, I. (2009a). "Experimental evaluation of influence factors for single geocell-reinforced sand". *Transportation Research Board 88th annual meeting*, January 11-15, 2009, Washington, DC.

Pokharel, S.K., Han, J., Leshchinsky, D., Parsons, R.L., and Halahmi, I. (2009b). "Behavior of geocell-reinforced granular bases under static and repeated loads." *International Foundation Congress & Equipment Expo 2009,* March 15-19, 2009 , Orlando, Florida.

Pokharel, S.K., Han, J., Parsons, R.L., Qian, Y., Leshchinsky, D., and Halahmi, I. (2009c).

"Experimental study on bearing capacity of geocell-reinforced bases." 8th *International Conference on Bearing Capacity of Roads, Railways and Airfields*, June 29 - July 2, 2009, Champaign, Illinois.

Pokharel, S.K. (2010). *Experimental Study on Geocell-Reinforced Bases under Static and Dynamic Loadings.* Ph.D. dissertation, CEAE Department, the University of Kansas.

Pokharel, S.K., Han, J., Leshchinsky, D., Parsons, R.L, and Halahmi, I. (2010). "Investigation of factors influencing behavior of single geocell-reinforced bases under static loading." *Geotextiles and Geomembranes*, in press.

Putman, B.J., Aune, J., and Amirkhanian, S.N. (2002). "*Recycled asphalt pavement used in superpave mixes made with rubberized asphalt.*" Retrieved December 12, 2010 from: http://www.clemson.edu/ces/arts/Mairepav4%20-0RAP%20in%20Rubberized%20Asphalt2.pdf.

Rajagopal, K., Krishnaswamy, N.R., and Madhavi Latha, G. (1999). "Behaviour of sand confined with single and multiple geocells." *Geotextiles and Geomembranes*, 17 (3), 171 - 184.

Schimmoller, V.E., Holtz, k., Eighmy, T.T., Wiles, C., Smith, M., Malasheskie, G., Rohrbach, G.J., Schaftlein, S., Helms, G., Campbell, R.D., Van Deusan, C.H., Ford, B., and Almborg, J.A. (2000). *Recycled materials in European highway environements: uses, technologies, and policies*. Report No. FHWA-PL-00-025.

Senior, S. A., S. I. Szoke, and C. A. Rogers (1994). "Ontario's Experience with Reclaimed Materials for Use in Aggregates." *Presented at the International Road Federation Conference*, Calgary, Alberta, 1994.

Steward, J., Williamson, R., and Mohney, J. (1977), *Guidelines for use of fabrics in construction and maintenance of low-volume roads.*" Report No. FHWA-TS-78-205, U.S. Department of Transportation, Federal Highway Administration, Washington, D.C..

Taha, R., Ali, G., Basma, A. and Al-Turk, O. (1999). "Evaluation of reclaimed asphalt pavement aggregate in road bases and subbases." *Journal of Transportation Research Board,* 1 (1652), 264-269.

Thakur, J.K., Han, J., Leshchinky, D., Halahmi, I., and Parasons, R.L. (2011). "Creep deformation of unreinforced and geocell-reinforced recycled asphalt pavements." Accepted for publication at the *GeoFrontier International Conference 2010*, March 13-16, Dallas, Texas, USA.

Thakur, S.C. (2009). *Laboratory evaluation of characteristics of recycled asphalt pavement (RAP) in Kansas.* M.S. thesis, CEAE Department, the University of Kansas.

Thakur, S.C., Han, J., Chong, W.K., and Parsons, R.L. (2010). "Laboratory evaluation of physical and mechanical properties of recycled asphalt pavement as a base course material." *GeoShanghai International Conference 2010*, June 3 to 5, Shanghai, China.

Thakur, S.C., Han, J., Chong, W.K., and Parsons, R.L. (2011). "Comparison of Properties of RAP Aggregate Extracted by Ignition and Centrifuge Methods." Accepted for publication at the *GeoFrontier International Conference 2010,* March 13-16, Dallas, Texas, USA.

The benefit of using recycled asphalt pavement (RAP). Retrieved December 12, 2010 from: http://www.co-asphalt.com/documents/RAP_Brochure_all.pdf.

Thompson, M.R. and Smith, K.L.(1990). "Repeated triaxial characterization of granular bases." *Transportation Research Record 1278,* TRB, National Research Council, Washington, D.C., 1990, 7-17.

Tingle, J.S. and Webster, S.L. (2003). "Corps of engineers design of geosynthetic-reinforced unpaved roads." *Transportation Research Record 1849,* National Research Council, 193-201.

Tingle, J.S. and Jersey, S.R. (2007). "Empirical design methods for geosynthetic-reinforced low-volume roads." *Journal of the Transportation Research Board*, 1989 (2), 91-101.

Townsend, T. G., and Brantley, (1998). *Leaching Characteristics of Asphalt Road Waste*. Final Report, Florida Center for Solid and Hazardous Waste Management, University of Florida, Gainesville, Fl., 90p.

*User Guidelines for Byproducts and Secondary Use Materials in Pavement Construction (2008). FHWA publication, FHWA-RD-97-148, r*etrieved June 17, 2010 *from:* http://www.rmrc.unh.edu/tools/uguidelines/rap134.asp.

Viyanant, C., Rathje, E.M., and Rauch, A.F. (2007). "Creep of compacted recycled asphalt pavement." *Canadian Geotechnical Journal,* National Research Council of Canada, 44(6), 687-697.

Wang, Y.M., Chen, Y.K., and Liu, W. (2008). "Large-scale direct shear testing of geocell-reinforced soil." *Journal of Central South University of Technology,* 15 (6), 895-900.

Webster, S. L., R. H. Grau, and T. P Williams (1992). *Description and Application of Dual Mass Dynamic Cone Penetrometer*. Instruction Report GL-92-3, Department of the Army, US Army Corp of Engineers, Washington, DC.

Yang, X.M. (2010). *Numerical Analyses of Geocell-Reinforced Granular Soils under Static and Repeated Loads*. Ph.D. dissertation, CEAE Department, the University of Kansas.

Yuu, J., Han, J., Rosen, A., Parsons, R.L., and Leshchinsky, D. (2008). “Technical review of geocell-reinforced base courses over weak subgrade,” *Proceedings of the First Pan American Geosynthetics Conference & Exhibition*, Cancún, Mexico, 2-5 March 2008, 1022-1030.